

# Low-frequency fluctuation and large-scale network integration of brain activity support memory encoding in humans

by

Ruedeerat Keerativittayayut

Student ID Number: 1196003

A dissertation submitted to the  
Engineering Course, Department of Engineering,  
Graduate School of Engineering,  
Kochi University of Technology,  
Kochi, Japan

in partial fulfillment of the requirements for the degree of  
Doctor of Philosophy

## Assessment Committee:

Supervisor: Kiyoshi Nakahara

Co-Supervisor: Hiroaki Shigemasu, Kochi University of Technology

Co-Supervisor: Hiroshi Kadota, Kochi University of Technology

Makoto Iwata, Kochi University of Technology

Nobuhiro Mifune, Kochi University of Technology

March 2018

## ABSTRACT

Memory encoding have been one of the central topics in cognitive neuroscience. We experience many events in everyday life, some of which are remembered, while others are forgotten. What neural mechanisms underlie this process? To answer this question, this dissertation provides two sub topics with a complementary goal to investigate the cognition and neural mechanisms underlying the memory encoding system. We focused on two of considerably current topics in neuroscience research including the role of intrinsic fluctuations or low frequency fluctuations (LFFs) of neural signal lower than 0.1 Hz in the brain and dynamic aspects of functional connectivity across whole brain, during memory encoding.

Growing evidence suggests that LFFs can account for much of the variability in task-evoked activation, and variability in behavioral performances. Thus, we hypothesized that LFFs may affect memory encoding processes and contribute to variability of memory performances. If so, LFFs of neural activity during experience encoding would predict either that experience will be later remembered or forgotten. In the present study, twenty-five participants performed an incidental encoding task in a magnetic resonance imaging scanner, and their memory encoding performance was assessed by a subsequent surprise memory test. The encoding trials were classified into successful encoding and unsuccessful encoding trials based on answers from the memory test. To investigate the role of LFFs in encoding process, in the first sub topic, LFFs independent from task-related signal were extracted and tested whether these residual LFFs can predict subsequent memory performances. We found that LFFs amplitudes/functional connectivity at the time periods before the stimulus onset can predict whether the upcoming trial will be remembered. Specifically, higher amplitude of LFFs in the right fusiform gyrus, the left parahippocampal gyrus, the left middle frontal gyrus, and the left superior parietal lobule was

observed before the stimulus later remembered (vs. later forgotten). In contrast, LFFs functional connectivity from the fusiform gyrus to brain regions inside cingulo-opercular (CO) network was stronger before the stimulus later forgotten. Our results lend new insight into the role of LFFs in memory encoding processes suggesting that LFFs was modulated with task-evoked responses and related to variability of memory performances. Remarkably, LFFs in the specific brain regions potentially facilitate memory encoding whereas the functional connectivity involving the CO network may bias toward bad memory.

Previous neuroimaging studies revealed that local activation/deactivation of specific brain regions predicts successful memory encoding. However, research on large-scale functional organization in the brain emphasizes a network view of the brain rather than local activation/deactivation, showing that patterns of functional connectivity across the brain are organized in specific ways and are relevant to behavior and cognition. Notably, recent studies have revealed that large-scale brain networks dynamically fluctuate in relatively short time periods, typically within a timescale of 30-40 s. Furthermore, these studies have shown that dynamic fluctuations of large-scale functional connectivity patterns are associated with a variety of cognitive processes.

In the second topics, we employed recently developed time-varying functional connectivity analysis to examine large-scale functional connectivity patterns during memory encoding processes. We found that a dynamic reconfiguration of large-scale brain networks in a short timescale ( $< 1$  min) is related to memory encoding performance. A graph analysis revealed that network integration rather than segregation is a hallmark of successful memory encoding. This effect was primarily driven by increased integration of the subcortical, default-mode, and visual subnetworks with other subnetworks. Moreover, multivariate analysis using the graph

metrics of integration showed that functional brain networks could be reliably classified into the period of high (vs. low) memory encoding performance. Our findings suggest that a diverse set of brain systems dynamically interact to support successful memory encoding.

Together, this dissertation provides a better understanding of the neural mechanisms of memory encoding, emphasizing the effect of LFFs to memory encoding and highlighting the importance of orchestration across many distinct brain systems to support better memory encoding.

## ACKNOWLEDGEMENT

I would like to express my gratitude to a number of people without whom the study would not have been possible.

Firstly, I would like to express my sincere gratitude to my advisor Prof. Kiyoshi Nakahara for the continuous support of my Ph.D. study and related research, for his patience, motivation, and immense knowledge. His guidance helped me in all the time of research and writing of this thesis. I could not have imagined having a better advisor and mentor for my Ph.D. study.

Besides my advisor, I would like to express my deep thank to Dr. Ryuta Aoki for insightful suggestions and encouragement, for the stimulating discussions, for the valuable time we were working together before deadlines. This greatly contributed to the success of this thesis.

My sincere thanks also goes to Prof. Koji Jimura, who provided useful discussions on my thesis. Moreover, I would like to thank the rest of my co-advisors and also my thesis committee: Assoc. Prof. Hiroaki Shigemasu, Assoc. Prof. Hiroshi Kadota, Prof. Makoto Iwata, and Assoc. Prof. Nobuhiro Mifune for not only their insightful comments and encouragement, but also for the hard questions which incited me to widen my research from various perspectives.

A very special gratitude goes out to the Special Scholarship Program (SSP), Kochi University of Technology (KUT) for financial support along my Ph.D. Study. Nevertheless, I am also grateful to International Relation Division (IRD) staffs for all warm supports and suggestions since I came to Japan until now.

I would like to thank my Thai friends for accepting nothing less than excellence from me and for spending precious moments of life in Japan.

Last but not the least, I would like to thank my family: my parents, my sister, and Mr. Chanapai, who always encourage and stand by me when things look bleak. I also would like to thank other people who helped me in one way or another.

Ruedeerat Keerativittayayut

2018

## **DEDICATION**

This dissertation are dedicated to my advisors: Prof. Kiyoshi Nakahara and Asst. Prof. Ryuta Aoki, whose examples will forever inspire me to be a good researcher. Moreover, all of my academic achievements are dedicated to my beloved family, the symbol of endless love and giving.

# TABLE OF CONTENTS

	<b>Page</b>
<b>ABSTRACT</b>	ii
<b>ACKNOWLEDGEMENT</b>	v
<b>LIST OF TABLES</b>	vi
<b>LIST OF FIGURES</b>	vii
<b>CHAPTER 1 INTRODUCTION</b>	
1.1 Structure of dissertation	1-1
1.2 Motivation and literature review	1-2
1.3 Objectives	1-7
1.4 Reference for chapter 1	1-9
<b>CHAPTER 2 TOPIC 1: Low frequency fluctuations and its functional connectivity before memory encoding predict subsequent memory performances</b>	
2.1 Abstract	2-1
2.2 Methodology	2-2
2.2.1 Participants	2-2
2.2.2 Stimuli	2-2
2.2.3 Experimental paradigm	2-3
2.2.4 Image acquisition and preprocessing	2-4
2.2.5 Subsequent memory/forgetting effects	2-5
2.2.6 Prestimulus LFFs amplitude analysis	2-6



	<b>Page</b>
2.2.7 Possible effect from the preceding trial to the encoding performance of following trial	2-7
2.2.8 Trial-to-trial variability analysis	2-8
2.2.9 Prestimulus LFFs functional connectivity analysis	2-9
2.3 Results	2-10
2.3.1 Behavioral results	2-10
2.3.2 Subsequent memory/forgetting effects	2-11
2.3.3 Prestimulus LFFs amplitude predicts subsequent memory performances	2-15
2.3.4 LFFs Accounts for trial-to-trial variability in task-evoked activity	2-18
2.3.5 Prestimulus LFFs functional connectivity predicts subsequent memory performances	2-18
2.4 Discussion	2-22
2.5 References for chapter 2	2-26

## **CHAPTER 3 TOPIC 2: Large-scale Network Integration in the Human**

### **Brain Tracks Temporal Fluctuations in Memory Encoding Performance**

3.1 Abstract	3-1
3.2 Methodology	3-2
3.2.1 Participants	3-2
3.2.2 Stimuli	3-2
3.2.3 Experimental paradigm	3-2

	<b>Page</b>
3.2.4 Image acquisition and preprocessing	3-2
3.2.5 Regions of interest	3-3
3.2.6 Trial-related activation analysis	3-2
3.2.7 Extraction of fMRI time series	3-4
3.2.8 Definition of time windows	3-5
3.2.9 Functional connectivity analysis	3-6
3.2.10 Graph analysis	3-6
3.2.11 Multivariate pattern analysis	3-11
3.3 Results	3-12
3.3.1 Behavioral results	3-12
3.3.2 Classification of time windows based on encoding performance	3-13
3.3.3 Functional connectivity patterns among memory-encoding- related regions	3-16
3.3.4 Functional connectivity patterns across large-scale brain networks	3-19
3.3.5 Graph analysis on large-scale brain network	3-21
3.3.6 Multivariate pattern classification using graph metrics as features	3-25
3.3.7 Robustness check	3-27
3.3.8 Possible effects of overall functional connectivity strength	3-28
3.3.9 Addressing possible concerns about motion confounds	3-30
3.4 Discussion	3-32

	<b>Page</b>
3.5 References for chapter 3	3-41
3.6 Supplementary information for chapter 3	3-53
3.6.1 Supplementary figures	3-53
3.6.2 Supplementary files	3-64
<b>CHAPTER 4 CONCLUSIONS</b>	4-1
<b>LISTS OF PUBLICATIONS AND CONFERENCES</b>	P-1
<b>BIOGRAPHY</b>	B-1

## LIST OF TABLES

<b>Tables</b>		<b>Page</b>
2.1	Details of brain regions associated with subsequent memory effect (SME) and subsequent forgetting effect (SFE)	2-13
2.2	Detail of brain regions resulted from the PPI analysis	2-20

## LIST OF FIGURES OF CHAPTER 2

<b>Figures</b>		<b>Page</b>
2.1	Task design	2-3
2.2	Brain regions associated with the subsequent memory effect (SME) and subsequent forgetting effect (SFE)	2-12
2.3	Prestimulus LFFs amplitude analysis	2-15
2.4	Low frequency fluctuations (LFFs) functional connectivity map derived from the right fusiform gyrus (rtFuG) seed	2-19

## LIST OF FIGURES OF CHAPTER 3

<b>Figures</b>		<b>Page</b>
3.1	Analysis overview	3-14
3.2	Distributions of time windows classified as high and low encoding states	3-15
3.3	Functional connectivity patterns among memory-related brain regions	3-17
3.4	Functional connectivity patterns across large-scale brain network	3-20
3.5	Differences in integration/segregation of large-scale network between high and low encoding states	3-23
3.6	Differences in inter-subnetwork efficiency between high and low encoding states	3-24
3.7	Multivariate classification analysis using graph metrics	3-26

# **CHAPTER 1**

## **INTRODUCTION**

### **1.1 Structure of this Dissertation**

<b>CHAPTER 1</b>	<b>Motivation, Literature Review, and Objectives</b>
<b>CHAPTER 2</b>	<b>TOPIC 1: Low frequency fluctuations and its functional connectivity before memory encoding predict subsequent memory performances</b>
	2.1 Abstract
	2.2 Methodology
	2.3 Results
	2.4 Discussion
	2.5 References
<b>CHAPTER 3</b>	<b>TOPIC 2: Large-scale network integration in the human brain tracks temporal fluctuations in memory encoding performance</b>
	3.1 Abstract
	3.2 Methodology
	3.3 Results
	3.4 Discussion
	3.5 References
	3.6 Supplementary information
<b>CHAPTER 4</b>	<b>CONCLUSIONS</b>

### 1.2 Motivation and Literature Review

In everyday life, new memories of events and episodes are constantly formed, sometimes incidentally. For instance, even when we do not explicitly try to memorize a scene, we are often able to vividly recall it later. Psychological studies have shown that cognitive operations engaged during initial experience encoding are important for memorability of that experience [1]. Although the mechanisms underlying memory encoding have extensively been investigated in cognitive psychology and neuroscience, it is still not fully understood.

Most previous fMRI studies have focused on task-evoked responses to answer how neural activity is changed due to manipulated external stimuli and how the evoked responses are correlated to subsequent behaviors. However, only 5% from 20% of brain energy consumption is dedicated for the task execution whereas the rest is used to maintain spontaneous neural activity, the neural activity that is intrinsically generated by the brain [2]. Thus, we may lose sight of the possibility that behavior performances and functional activity observed during our experiment may be modulated by the intrinsic fluctuations. Beginning with the study that showed spontaneous blood-oxygen-level dependent (BOLD) fluctuations measured in the left somatomotor cortex were specifically correlated with spontaneous fluctuations in the right somatomotor cortex [3] and these lateral fluctuations were related to press force during right-hand button presses [4]. These findings have since raised widespread interest about the relationship between intrinsic fluctuations and variability in behaviors. Accumulating evidences over the past decades have shown that rather than motor performances, intrinsic fluctuations accounted for variability in other domains such as memory recollection [5], perception [6], [7], and cognitive control [8]. However, to date there are no studies focused on the role of intrinsic fluctuations in memory encoding processes.



In the first part of this dissertation underlying the topic “**Low frequency fluctuations and its functional connectivity before memory encoding predict subsequent memory performances**”, we hypothesized that intrinsic fluctuations may affect memory encoding processes and contribute to variability of memory performances. If so, intrinsic fluctuations of neural activity during experience encoding would predict either that experience will be later remembered or forgotten. Most of memory encoding studies have investigated how the brain operates during successful encoding and less encoding [9], [10]. They demonstrated that greater activation in the medial temporal lobes (MTL) and the prefrontal cortex was exhibited to response to stimuli successfully remembered later (vs. forgotten), a phenomenon referred to as the subsequent memory effect (SME) [11]. On the other hand, brain regions that are part of the default-mode network (DMN) tend to show stronger activation (or weaker deactivation) in response to stimuli that are later forgotten (vs. remembered), referred to as the subsequent forgetting effect (SFE) [11]. So far we know that activation/deactivation of specific sets of brain regions are predictive of successful memory encoding [12]–[19], however whether intrinsic fluctuations of observed neural activity from these brain regions contribute to variability of subsequent memory performances (subsequent remembering and subsequent forgetting) remain uncovered.

To answer this question, here the intrinsic fluctuations or low frequency fluctuations (LFFs) in the range of 0.01–0.1 Hz [4] were extracted from task-evoked responses during experience encoding to test their effect on subsequent memory performances. We focused on the LFFs at the time periods before the stimulus onset (to make sure that the LFFs do not carry task-driven signal) and used them to predict memory performances of upcoming trials. We first performed subsequent memory procedure [10], [20] in which participants participated the incidental memory encoding scan and their memory performances were assessed by the

## Introduction

---

subsequent surprise memory test. In the incidental encoding scan, the participants were instructed to make semantic judgement (man-made or natural objects) to given pictorial stimuli without prior knowledge to memorize the pictures. After that, they were asked to view pictures presented on a computer screen and to judge if each picture had been studied during scanning (studied with high confidence, studied with low confidence, or unstudied). Based on their answers, encoding trials can be classified into those that would be remembered (here defined as HH) and those that would be forgotten (here defined as Miss). Comparing neural activation during HH to Miss trials and comparing neural activation during Miss to HH trials, it allowed us to identify SME and SFE related regions, respectively. Lastly, the LFFs independent from task-related signal were extracted from the obtained SME and SFE related regions and then tested whether these residual LFFs can predict subsequent memory performances.

Our results revealed that prestimulus LFFs amplitude in the SME related regions including the right fusiform gyrus (rtFuG), the left parahippocampal gyrus (ltPHG), the left middle frontal gyrus (ltMFG), and the left superior parietal lobule (ltSPL) can predict HH and Miss trials while the SFE related regions cannot. Beside the LFFs amplitude, stronger LFFs functional connectivity from the rtFuG to the brain regions inside CO network was observed before onset of the Miss trials. Our results may suggest that measured neural responses during memory encoding might be modulated by the intrinsic fluctuations which were reported here as a significant contributor to the variability of subsequent memory performances. Interestingly, not only the prestimulus LFFs amplitudes but also the prestimulus LFFs functional connectivity before stimuli encoding can predict subsequent memory performances. These findings emphasize an involvement of LFFs underlying memory encoding processes but in different aspects.

In the second part of this dissertation, we investigated mechanism of memory encoding in term of dynamic functional connectivity underlying the topic “**Large-scale network integration in the human brain tracks temporal fluctuations in memory encoding performance**”. Several studies have shown that successful memory encoding is related to enhanced functional connectivity between memory-related regions [21]–[24], such as between the hippocampus and other areas. However, memory encoding is thought to require orchestration among many brain systems beyond the so-called memory system, because encoding success depends on a range of factors (e.g., attention, arousal, and motivation) processed in distributed brain networks [25]–[27]. Most previous studies have examined functional connectivity from a few selected “seed” regions, providing little evidence about how the entire brain functions as a network to support memory encoding. Therefore, the role of large-scale brain networks in memory encoding processes remains to be elucidated.

Research on large-scale functional organization in the brain has advanced substantially in the past decade [28]–[32]. This line of research emphasizes a network view of the brain rather than local activation/deactivation, showing that patterns of functional connectivity across the brain are organized in specific ways and are relevant to behavior and cognition [30], [33], [34]. Notably, recent studies have revealed that large-scale brain networks dynamically fluctuate in relatively short time periods, typically within a timescale of 30-40 s [35]–[37]. Furthermore, these studies have shown that dynamic fluctuations of large-scale functional connectivity patterns are associated with a variety of cognitive processes [30], [35], [36], [38]–[40], and even exist during the resting state [41]–[45]. These findings have spurred emerging perspectives of dynamic brain networks, leading researchers to focus more on time-varying functional connectivity patterns in short time

windows, instead of the traditional “static” functional connectivity computed in periods of 6–10 min.

Integration and segregation are key concepts in characterizing dynamic brain networks [34], [46], [47]. Theoretically, integration of large-scale networks is important for efficient communication across entire systems, whereas segregation is critical for specialized functioning of particular modules without interference from the rest of the network [39], [40], [48]. Accumulating evidence suggests that the degrees of integration and segregation in the brain dynamically change over time [49]–[52]. For example, when the brain processes a cognitively demanding task (e.g., the N-back working memory task), the degree of integration tends to increase, which is suitable for efficient communication among the sensory, motor and cognitive control systems. On the other hand, the degree of segregation tends to increase over time as the brain learns specialized skills, which allows automatic processing of a habitual task without effortful cognitive control [35], [39]. Together, it is likely that the brain changes its large-scale network configurations (i.e., integration and segregation) in highly adaptive ways. However, research on dynamic reconfigurations of large-scale brain networks is still nascent, and the findings so far suggest that the relative importance between integration and segregation is strongly dependent on tasks and situations [51], [53], making it difficult to draw comprehensive conclusions at this stage. Thus, it remains an open question whether integration or segregation is important for memory encoding processes.

In the present work, we examined whether and how dynamic functional connectivity patterns in the brain are related to memory encoding with distinct but complementary aims. The first aim was to clarify dynamic functional connectivity patterns in well-established memory-related regions. For this, we constructed a network consisting of the brain regions associated with

the SME and those associated with the SFE (hereafter referred to as the SME/SFE regions, for simplicity). Capitalizing on previous research suggesting functional interactions among SME regions for successful memory encoding [11], we predicted that the SME regions would show greater functional connectivity during time periods of higher (vs. lower) memory encoding performance. The second aim was to explore whether and how dynamic fluctuations in large-scale networks across the brain are related to memory encoding performance. For this analysis, we used a functional atlas consisting of 224 nodes that cover the entire brain [29]. Using graph theory analysis [54], we quantified the degrees of integration and segregation in the large-scale network, and tested whether these graph metrics differed between the time periods of high encoding performance and those of low encoding performance. Our results revealed a dynamic reconfiguration of the large-scale brain network depending on memory encoding performance. Specifically, greater integration of the large-scale network is a hallmark of better encoding performance. This effect was particularly driven by increased inter-subnetwork integration of the subcortical, default-mode, and visual networks.

### 1.3 Objectives

#### **TOPIC 1: Low frequency fluctuations and its functional connectivity before memory encoding predict subsequent memory performances**

- To investigate whether intrinsic fluctuations (here we defined as LFFs) can account for subsequent memory performance. We hypothesized that LFFs may be a significant contributing factor in successful memory encoding and account for trial-to-trial variability in encoding performance.

**TOPIC 2: Large-scale network integration in the human brain tracks temporal fluctuations in memory encoding performance**

- To explore whether and how dynamic fluctuations in large-scale networks across the brain are related to memory encoding performance.
- To investigate whether integration or segregation of large-scale brain networks is benefit for memory encoding processes.

## 1.4 References for Chapter 1

- [1] J. F. I. M. Craik and R. S. Lockhart, “Levels of processing: A framework for memory research,” *J. Verbal Learning Verbal Behav.*, vol. 11, no. 6, pp. 671–684, 1972.
- [2] M. E. Raichle and M. A. Mintun, “Brain Work and Brain Imaging,” *Annu. Rev. Neurosci.*, vol. 29, no. 1, pp. 449–476, 2006.
- [3] B. Biswal, F. Z. Yetkin, V. M. Haughton, and J. S. Hyde, “Functional connectivity in the motor cortex of resting human brain using echo-planar MRI,” *Magn. Reson. Med.*, vol. 34, no. 4, pp. 537–41, 1995.
- [4] M. D. Fox, A. Z. Snyder, J. L. Vincent, and M. E. Raichle, “Intrinsic fluctuations within cortical systems account for intertrial variability in human behavior.,” *Neuron*, vol. 56, no. 1, pp. 171–84, 2007.
- [5] J. L. Vincent, A. Z. Snyder, M. D. Fox, B. J. Shannon, J. R. Andrews, M. E. Raichle, and R. L. Buckner, “Coherent Spontaneous Activity Identifies a Hippocampal-Parietal Memory Network,” *J. Neurophysiol.*, vol. 96, no. 6, pp. 3517–3531, 2006.
- [6] M. Boly, E. Balteau, C. Schnakers, C. Degueldre, G. Moonen, A. Luxen, C. Phillips, P. Peigneux, P. Maquet, and S. Laureys, “Baseline brain activity fluctuations predict somatosensory perception in humans.,” *Proc. Natl. Acad. Sci. U. S. A.*, vol. 104, no. 29, pp. 12187–92, 2007.
- [7] S. Sadaghiani, G. Hesselmann, and A. Kleinschmidt, “Distributed and antagonistic contributions of ongoing activity fluctuations to auditory stimulus detection.,” *J. Neurosci.*, vol. 29, no. 42, pp. 13410–13417, 2009.
- [8] C. P. Coste, S. Sadaghiani, K. J. Friston, and A. Kleinschmidt, “Ongoing brain activity

- fluctuations directly account for intertrial and indirectly for intersubject variability in stroop task performance,” *Cereb. Cortex*, vol. 21, no. 11, pp. 2612–2619, 2011.
- [9] a D. Wagner, R. a Poldrack, L. L. Eldridge, J. E. Desmond, G. H. Glover, and J. D. Gabrieli, “Material-specific lateralization of prefrontal activation during episodic encoding and retrieval.,” *Neuroreport*, vol. 9, no. 16, pp. 3711–3717, 1998.
- [10] J. B. Brewer, Z. Zhao, J. E. Desmond, G. H. Glover, and J. D. Gabrieli, “Making memories: brain activity that predicts how well visual experience will be remembered.,” *Science*, vol. 281, no. 5380, pp. 1185–1187, 1998.
- [11] H. Kim, “Neural activity that predicts subsequent memory and forgetting: A meta-analysis of 74 fMRI studies,” *Neuroimage*, vol. 54, no. 3, pp. 2446–2461, 2011.
- [12] R. L. Buckner and D. C. Carroll, “Self-projection and the brain,” *Trends Cogn. Sci.*, vol. 11, no. 2, pp. 49–57, 2007.
- [13] G. Fernández and I. Tendolkar, “Integrated brain activity in medial temporal and prefrontal areas predicts subsequent memory performance: Human declarative memory formation at the system level,” *Brain Res. Bull.*, vol. 55, no. 1, pp. 1–9, 2001.
- [14] A. M. Morcom, C. D. Good, R. S. J. Frackowiak, and M. D. Rugg, “Age effects on the neural correlates of successful memory encoding,” *Brain*, vol. 126, no. 1, pp. 213–229, 2003.
- [15] J. S. Simons and H. J. Spiers, “Prefrontal and medial temporal lobe interactions in long-term memory.,” *Nat. Rev. Neurosci.*, vol. 4, no. 8, pp. 637–48, 2003.
- [16] T. Sommer, M. Rose, J. Gläscher, T. Wolbers, and C. Büchel, “Dissociable contributions within the medial temporal lobe to encoding of object-location associations,” *Learn. Mem.*, vol. 12, no. 3, pp. 343–351, 2005.



- [17] T. Sommer, M. Rose, C. Weiller, and C. Büchel, “Contributions of occipital, parietal and parahippocampal cortex to encoding of object-location associations,” *Neuropsychologia*, vol. 43, no. 5, pp. 732–743, 2005.
- [18] M. R. Uncapher and M. D. Rugg, “Selecting for memory? The influence of selective attention on the mnemonic binding of contextual information.,” *J. Neurosci.*, vol. 29, no. 25, pp. 8270–9, 2009.
- [19] N. Cohen, L. Pell, M. G. Edelson, A. Ben-Yakov, A. Pine, and Y. Dudai, “Peri-encoding predictors of memory encoding and consolidation,” *Neurosci. Biobehav. Rev.*, vol. 50, pp. 128–142, 2015.
- [20] a D. Wagner, D. L. Schacter, M. Rotte, W. Koutstaal, A. Maril, a M. Dale, B. R. Rosen, and R. L. Buckner, “Building memories: remembering and forgetting of verbal experiences as predicted by brain activity.,” *Science*, vol. 281, no. 5380, pp. 1188–1191, 1998.
- [21] B. H. Schott, T. Wüstenberg, M. Wimber, D. B. Fenker, K. C. Zierhut, C. I. Seidenbecher, H. J. Heinze, H. Walter, E. Düzel, and A. Richardson-Klavehn, “The relationship between level of processing and hippocampal-cortical functional connectivity during episodic memory formation in humans,” *Hum. Brain Mapp.*, vol. 34, no. 2, pp. 407–424, 2013.
- [22] C. Ranganath, A. Heller, M. X. Cohen, C. J. Brozinsky, and J. Rissman, “Functional connectivity with the hippocampus during successful memory formation,” *Hippocampus*, vol. 15, no. 8, pp. 997–1005, 2005.
- [23] C. Summerfield, M. Greene, T. Wager, T. Egner, J. Hirsch, and J. Mangels, “Neocortical connectivity during episodic memory formation,” *PLoS Biol.*, vol. 4, no. 5, pp. 855–864, 2006.

- [24] X. Liu and J. H. Duyn, “Time-varying functional network information extracted from brief instances of spontaneous brain activity.,” *Proc. Natl. Acad. Sci. U. S. A.*, vol. 110, no. 11, pp. 4392–7, 2013.
- [25] M. M. Chun and N. B. Turk-Browne, “Interactions between attention and memory,” *Curr. Opin. Neurobiol.*, vol. 17, no. 2, pp. 177–184, 2007.
- [26] M. J. Gruber, B. D. Gelman, and C. Ranganath, “States of Curiosity Modulate Hippocampus-Dependent Learning via the Dopaminergic Circuit,” *Neuron*, vol. 84, no. 2, pp. 486–496, 2014.
- [27] A. Tambini, U. Rimmele, E. A. Phelps, and L. Davachi, “Emotional brain states carry over and enhance future memory formation,” *Nat. Neurosci.*, vol. 20, no. 2, pp. 271–278, 2016.
- [28] E. T. Bullmore and O. Sporns, “Complex brain networks: graph theoretical analysis of structural and functional systems.,” *Nat. Rev. Neurosci.*, vol. 10, no. 3, pp. 186–98, 2009.
- [29] J. D. Power, A. L. Cohen, S. M. Nelson, G. S. Wig, K. A. Barnes, J. A. Church, A. C. Vogel, T. O. Laumann, F. M. Miezin, B. L. Schlaggar, and S. E. Petersen, “Article Functional Network Organization of the Human Brain,” *Neuron*, vol. 72, pp. 665–678, 2011.
- [30] M. W. Cole, D. S. Bassett, J. D. Power, T. S. Braver, and S. E. Petersen, “Intrinsic and Task-Evoked Network Architectures of the Human Brain,” *Neuron*, vol. 83, no. 1, pp. 238–251, 2014.
- [31] O. Sporns and R. F. Betzel, “Modular Brain Networks,” *Annu Rev Psychol.*, vol. 67, pp. 613–640, 2016.
- [32] D. S. Bassett and O. Sporns, “Network neuroscience,” *Nat. Neurosci.*, vol. 20, no. 3, pp.

- 353–364, 2017.
- [33] L. Cocchi, A. Zalesky, A. Fornito, and J. B. Mattingley, “Dynamic cooperation and competition between brain systems during cognitive control,” *Trends Cogn. Sci.*, vol. 17, no. 10, pp. 493–501, 2013.
- [34] J. M. Shine and R. A. Poldrack, “Principles of Dynamic Network Reconfiguration across Diverse Brain States,” *Neuroimage*, 2017.
- [35] H. Mohr, U. Wolfensteller, R. F. Betzel, B. Mis, O. Sporns, J. Richiardi, and H. Ruge, “Integration and segregation of large-scale brain networks during short-term task automatization,” *Nat. Commun.*, vol. 7, no. 13217, 2016.
- [36] C. Wang, J. L. Ong, A. Patanaik, J. Zhou, and M. W. L. Chee, “Spontaneous eyelid closures link vigilance fluctuation with fMRI dynamic connectivity states,” *Proc. Natl. Acad. Sci. U. S. A.*, vol. 113, no. 34, pp. 9653–9658, 2016.
- [37] U. Braun, A. Schäfer, H. Walter, S. Erk, N. Romanczuk-Seiferth, L. Haddad, J. I. Schweiger, O. Grimm, A. Heinz, H. Tost, A. Meyer-Lindenberg, and D. S. Bassett, “Dynamic reconfiguration of frontal brain networks during executive cognition in humans,” *Proc. Natl. Acad. Sci. U. S. A.*, vol. 112, no. 37, pp. 11678–11683, 2015.
- [38] D. S. Bassett, N. F. Wymbs, M. A. Porter, P. J. Mucha, J. M. Carlson, and S. T. Grafton, “Dynamic reconfiguration of human brain networks during learning,” *Proc. Natl. Acad. Sci. U. S. A.*, vol. 108, no. 18, pp. 7641–46, 2011.
- [39] D. S. Bassett, M. Yang, N. F. Wymbs, and S. T. Grafton, “Learning-induced autonomy of sensorimotor systems,” *Nat. Neurosci.*, vol. 18, no. 5, pp. 744–754, 2015.
- [40] S. Sadaghiani, J.-B. Poline, A. Kleinschmidt, and M. D’Esposito, “Ongoing dynamics in large-scale functional connectivity predict perception,” *Proc. Natl. Acad. Sci.*, vol. 112,

- no. 27, pp. 8463–8468, 2015.
- [41] A. Zalesky, A. Fornito, L. Cocchi, L. L. Gollo, and M. Breakspear, “Time-resolved resting-state brain networks,” *Proc. Natl. Acad. Sci. U. S. A.*, vol. 111, no. 28, pp. 10341–46, 2014.
- [42] M. R. Brier, J. B. Thomas, A. Z. Snyder, T. L. Benzinger, D. Zhang, M. E. Raichle, D. M. Holtzman, J. C. Morris, and B. M. Ances, “Loss of intranetwork and internetwork resting state functional connections with Alzheimer’s disease progression,” *J Neurosci*, vol. 32, no. 26, pp. 8890–8899, 2012.
- [43] V. D. Calhoun, R. Miller, G. Pearlson, and T. Adali, “The Chronnectome: Time-Varying Connectivity Networks as the Next Frontier in fMRI Data Discovery,” *Neuron*, vol. 84, no. 2, pp. 262–274, 2014.
- [44] E. A. Allen, E. Damaraju, S. M. Plis, E. B. Erhardt, T. Eichele, and V. D. Calhoun, “Tracking whole-brain connectivity dynamics in the resting state,” *Cereb. Cortex*, vol. 24, no. 3, pp. 663–676, 2014.
- [45] R. F. Betzel, M. Fukushima, Y. He, X. N. Zuo, and O. Sporns, “Dynamic fluctuations coincide with periods of high and low modularity in resting-state functional brain networks,” *Neuroimage*, vol. 127, pp. 287–297, 2016.
- [46] K. J. Friston, “Modalities, Modes, and Models in Functional Neuroimaging,” *Science (80-. ),*, vol. 362, pp. 399–403, 2009.
- [47] O. Sporns, “Network attributes for segregation and integration in the human brain Olaf Sporns,” *Curr. Opin. Neurobiol.*, vol. 23, no. 2, pp. 162–171, 2013.
- [48] D. S. Bassett, N. F. Wymbs, M. P. Rombach, M. A. Porter, P. J. Mucha, and S. T. Grafton, “Task-Based Core-Periphery Organization of Human Brain Dynamics,” *PLoS Comput.*

- Biol.*, vol. 9, no. 9, pp. 1–16, 2013.
- [49] J. M. Shine, P. G. Bissett, P. T. Bell, O. Koyejo, J. H. Balsters, K. J. Gorgolewski, C. A. Moodie, and R. A. Poldrack, “The Dynamics of Functional Brain Networks: Integrated Network States during Cognitive Task Performance,” *Neuron*, vol. 92, no. 2, pp. 544–554, 2016.
- [50] G. Deco, G. Tononi, M. Boly, and M. L. Kringelbach, “Rethinking segregation and integration : contributions of whole-brain modelling,” *Nat. Rev. Neurosci.*, vol. 16, pp. 430–439, 2015.
- [51] J. R. Cohen and M. D. Esposito, “The Segregation and Integration of Distinct Brain Networks and Their Relationship to Cognition,” *J. Neurosci.*, vol. 36, no. 48, pp. 12083–12094, 2016.
- [52] L.-D. Lord, A. B. Stevner, G. Deco, and M. L. Kringelbach, “Understanding principles of integration and segregation using whole-brain computational connectomics: implications for neuropsychiatric disorders.,” *Philos. Trans. R. Soc. A Math. Phys. Eng. Sci.*, vol. 376, no. 2096, pp. 1–21, 2017.
- [53] J. Gonzalez-Castillo, C. W. Hoy, D. a. Handwerker, M. E. Robinson, L. C. Buchanan, Z. S. Saad, and P. a. Bandettini, “Tracking ongoing cognition in individuals using brief, whole-brain functional connectivity patterns,” *Proc. Natl. Acad. Sci.*, vol. 112, no. 28, pp. 8762–8767, 2015.
- [54] M. Rubinov and O. Sporns, “NeuroImage Complex network measures of brain connectivity : Uses and interpretations,” *Neuroimage*, vol. 52, no. 3, pp. 1059–1069, 2010.

## CHAPTER 2

### **TOPIC 1: Low frequency fluctuations and its functional connectivity before memory encoding predict subsequent memory performances**

#### **2.1 Abstract**

Previous studies suggest that ongoing activity fluctuations or low frequency fluctuations (LFFs) in the brain contribute to variability in task-evoked responses and behaviors however little is known its effect on memory encoding. In the present study, we used event-related functional magnetic resonance imaging (fMRI) paradigm to investigate whether the LFFs during memory encoding task can predict subsequent memory performances. Participants underwent incidental memory encoding scan and their memory performances were assessed by later surprise memory test. We found that LFFs occurring before the onset of a stimulus can predict whether the stimulus was remembered or forgotten. Higher amplitude of LFFs in the right fusiform gyrus, the left parahippocampal gyrus, the left middle frontal gyrus, and the left superior parietal lobule was observed before the stimulus later remembered (vs. later forgotten). In contrast, LFFs functional connectivity from the fusiform gyrus to brain regions inside cingulo-opercular (CO) network was stronger before the stimulus later forgotten. Our results lend new insight into the role of LFFs in memory encoding processes suggesting that LFFs was modulated with task-evoked responses and related with variability of memory performances. Remarkably, LFFs in the specific brain regions potentially facilitate memory encoding and subsequent memory performances whereas the functional connectivity involving the CO network may bias toward bad memory.

## **2.2 Methodology**

### **2.2.1 Participants**

A total of 30 university students (20 males; age 18–22 years, mean  $\pm$  SD = 20.0  $\pm$  1.2) participated in the study. Four participants who fell asleep in the scanner and did not respond in more than 20 trials were excluded from the analysis. One additional participant who did not follow the instructions (not making any “low confidence” responses in the surprise memory test) was also excluded. The remaining 25 participants (17 males; age 18–22 years, mean  $\pm$  SD = 20.1  $\pm$  1.1) were therefore available for the analysis. All experimental procedures were approved by the Ethics Committee of Kochi University of Technology.

### **2.2.2 Stimuli**

Stimuli consisted of color pictures (sized  $8^\circ \times 6^\circ$ ) and a white fixation cross (sized  $0.8^\circ \times 0.8^\circ$ ). The pictorial stimuli included 360 pictures showing man-made objects (e.g. commodities, stationery, musical instruments, and appliances) and 360 pictures showing natural objects (e.g. animals, plants, fruits, and natural scenes). These pictures were selected from the Bank of Standardized Stimuli (BOSS) [1] and a commercially available image database. All color pictures underwent luminance, contrast, and spatial frequency equalizing by in-house MATLAB (MathWorks, Natick, MA) code adapted from the SHINE toolbox [2]. Half of the pictures (180 man-made and 180 natural pictures) were randomly selected for use in the incidental memory encoding task. The remaining 360 pictures were used as unstudied pictures in the surprise memory test. The tasks were programmed and administered using Presentation software (Neurobehavioral

Systems, Berkeley, CA). We projected the visual stimuli on a screen located behind the scanner. Participants viewed the projected visual stimuli through a mirror attached to a head coil.

### 2.2.3 Experimental paradigm

The experimental paradigm (Fig. 2.1) was based on the subsequent memory approach, which has been widely used in previous research [3]. Participants took part in a two-stage experiment: an incidental memory encoding task followed by a surprise memory test. During the incidental memory encoding scans, participants studied the pictorial stimuli. Twenty minutes later, memory for the studied pictures was assessed by the surprise memory test outside the scanner.

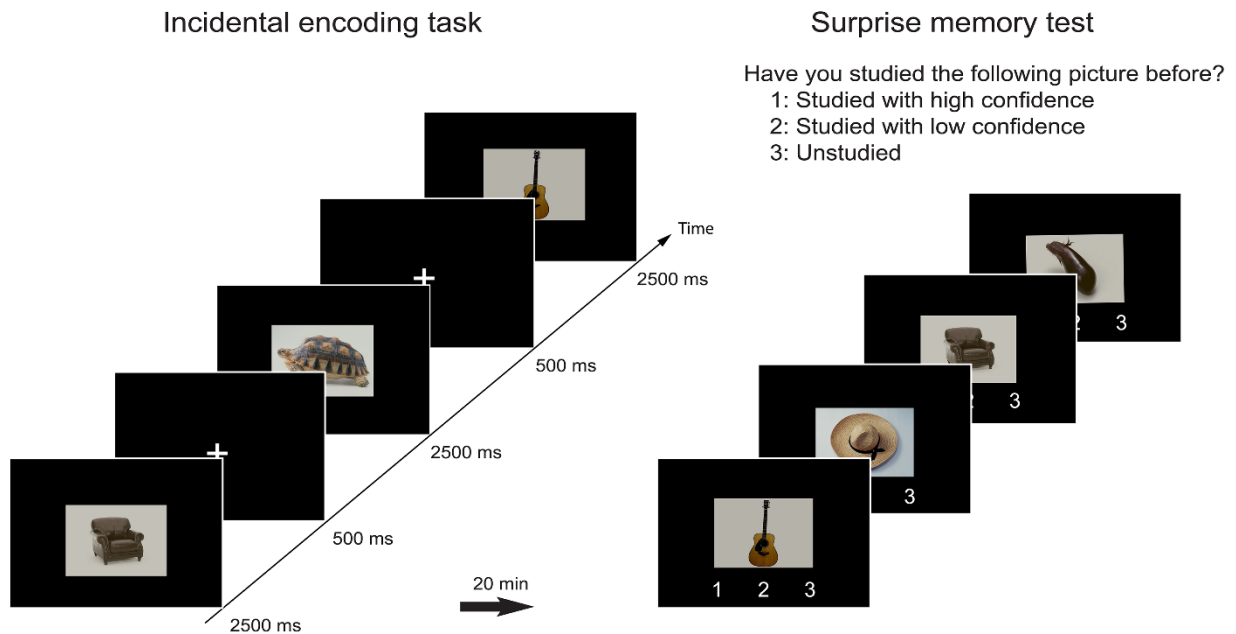


**Figure 2.1 Task design.** Participants performed 3 sessions of incidental memory encoding task inside the scanner. Participants judged whether a picture contains man-made or natural object. Twenty minute later, they were asked to view pictures presented on a computer screen and to judge if each picture had been studied during scanning (studied with high confidence, studied with low confidence, or unstudied). Encoding trials can be classified into those that



## **TOPIC 1: Low frequency fluctuations and its functional connectivity before memory encoding predict subsequent memory performances**

---

would be remembered (here defined as HH) and those that would be forgotten (here defined as Miss) based on memory test's answers.

In the incidental memory encoding task, participants studied 360 pictures in three runs. Each run began with a central fixation cross for 15 s, followed by a continuous series of 180 rapidly intermixed trials. Sixty man-made picture trials, 60 natural-made picture trials, and 60 fixation trials were pseudo-randomly presented with counterbalancing (each trial type followed every other trial type equally often). Each run ended with an additional fixation period of 20 s. For a picture trial, a pictorial stimulus was presented on the screen for 2500 ms, followed by a 500-ms presentation of a fixation cross. For a fixation trial, only a fixation cross was presented for 3 s. During the picture trials, participants were instructed to make a semantic judgment (man-made or natural) by right-handed button press as soon as possible after the picture onset. The total time for performing the incidental encoding task was approximately 30 minutes.

In the surprise memory test, participants were presented with the 360 studied pictures from the incidental memory encoding task, as well as 360 unstudied pictures. They were asked to indicate whether they recognized each picture as studied with high confidence, studied with low confidence, or unstudied. Each picture was displayed individually with self-paced timing. Participants responded by right-handed keyboard press.

### **2.2.4 Image acquisition and preprocessing**

All scanning was performed using a 3T Siemens Verio MRI scanner (Siemens, Erlangen, Germany) equipped with a 32-channel head coil. A high-resolution T1-weighted anatomical image was collected for each participant (MPRAGE; repetition time [TR] = 2500 ms; echo time [TE] =

4.32 ms; flip angle [FA] = 8°; field of view [FOV] = 230 mm; matrix = 256 × 256; in-plane resolution = 0.9 × 0.9 mm<sup>2</sup>; slice thickness = 1 mm; 192 slices; acceleration factor = 2). Functional data were collected using a multiband echo planar imaging (EPI) pulse sequence (TR = 720 ms; TE = 33 ms; FA = 52°; FOV = 192 mm; matrix = 64 × 64; in-plane resolution = 3 × 3 mm<sup>2</sup>; slice thickness = 3 mm; slice gap = 0.75 mm; 45 slices; multi-band acceleration factor = 5), which afforded whole-brain coverage. Preprocessing was carried out using SPM12 (Wellcome Department of Cognitive Neurology, London, UK). The first five volumes of each run were discarded before preprocessing. The remaining functional volumes were spatially realigned, coregistered to the individual high-resolution anatomical image, normalized to Montreal Neurological Institute (MNI) space, spatially smoothed with 8 mm full width at half maximum (FWHM) Gaussian kernel, and resampled to a spatial resolution of 2 × 2 × 2 mm<sup>3</sup>.

### **2.2.5 Subsequent memory/forgetting effects**

The 360 encoding trials in the incidental encoding task were classified into either remembered with high confidence (HH), remembered with low confidence (LH), or forgotten (Miss) based on participants' performances on the surprise memory test. We used a general linear model (GLM) to identify brain regions showing the subsequent memory effect (SME, i.e., greater activation in HH than Miss) and the subsequent forgetting effect (SFE, i.e., greater activation in Miss than HH). For the first-level GLM, we defined four task-related regressors (HH, LH, Miss, and Fixation). For each regressor, trials were modelled using a boxcar function (initiating at stimulus onset with the duration of 2500 ms) convolved with a canonical hemodynamic response function (HRF). The model also included six motion parameters as well as mean time series in the cerebral spinal fluid (CSF) and white matter (WM) as nuisance regressors. To obtain the mean time series in the CSF

and WM, we averaged time series of all voxels within the CSF and WM masks, each of which was derived from each individual's segmented structural image (binarized with a threshold of tissue probability  $> 0.8$ ) [4], [5]. The second-level random-effect analysis (one-sample t-tests) was performed using contrast images derived from individual participants (i.e., HH minus Miss for SME and Miss minus HH for SFE). The statistical threshold was set at voxel-wise  $P < 0.05$ , family-wise error corrected across voxels with the gray matter (defined by "TPM.nii" implemented in SPM12, thresholded at 0.5).

### **2.2.6 Prestimulus LFFs amplitude analysis**

The main purpose of this study is to investigate whether LFFs of task-evoked signal can account for encoding performances and subsequent memorability. To do so, we extracted the LFFs (independent of task-related components) from selected ROIs and test whether LFFs amplitude can predict HH and Miss trials. We first extracted fMRI signal time courses from four areas which showed peak-activation SME and SFE. Each ROI was defined by a sphere (radius = 5 mm) centered at the peak coordinates (Table 2.1). We removed trial-evoked and nuisance signals using a voxelwise GLM, in accordance with previous studies [6], [7]. Each trial was modeled as a 2.5 s boxcar convolved with the HRF and its temporal and dispersion derivatives with trials binned (HH, LH, and Miss). We included the six motion parameters and the mean time series in the CSF and WM as separate regressors. After removing trial-evoked signal, as well as nuisance signals, the residual signal time courses were bandpass filtered, leaving only signal between 0.01 and 0.1 Hz [8]. Critically, this frequency band is outside the task frequency (0.33 Hz), filtering out responses that were consistently elicited by the task. To prepare the signal time courses for the present main analysis, each LFFs was re-sampled at 1 s.

After obtaining LFFs, we reconstructed peritrial LFFs signal time courses separately for each trial condition (HH, LH, and Miss). To do so, we defined a 20-s time window around each trial, starting from 10 s before the stimulus onset to 10 s after the stimulus onset. The signal time courses were averaged within this time window across trials, separately for each trial condition. In our study, we used LFFs at the prestimulus time period (-1.5 s to 0 s relative to the stimulus onset of each trial resulting in pre-HH and pre Miss) to predict upcoming stimuli. The LFFs during this period is close to the stimulus but do not carry stimulus- or task-driven signal. This specific time period has been used in previous studies [9]–[12] which predicted subsequent responses using ongoing prestimulus activity. In our work, the prestimulus time period included two time points immediately before the stimulus onset, and we averaged the LFFs amplitudes over these time points for HH, LH, and Miss trials separately. We performed one-way ANOVA (HH, LH, and Miss as factors) and t-tests (HH versus Miss) across participants to examine statistical differences in the mean LFFs amplitude among HH, LH, and Miss trials.

### **2.2.7 Possible effect from the preceding trial to the encoding performance of following trial.**

Are trials more likely to identify as HH if they come after HH trial rather than Miss trial? To rule out the possibility of lingering effect of preceding trial to the performance of following trial, we performed generalized linear model regression using memory performance at trial  $t-1$ ,  $t-2$ , and  $t-3$  as predictors and memory performance at trial  $t$  as observations. By using binomial distribution, memory performance were defined as binary values (HH and LH trials = “1”; Miss trials = “0”). Moreover, we classified encoding trials into the trials following HH trial (preceding HH) and the trials following Miss trial (preceding Miss) and then test whether prestimulus LFFs amplitude of preceding HH is likely to higher compared with those of the preceding Miss trials. The LFFs at

the time period -1.5 s to 0 s relative to the stimulus onset were averaged separately for the preceding HH and the preceding Miss trials. The averaged prestimulus LFFs amplitude of two trial types were then compared across 25 participants using pair t-test.

### **2.2.8 Trial-to-trial variability analysis**

To investigate whether LFFs affect trial-to-trial variability in encoding performances during memory encoding task, we quantified this effect by regressing out LFFs from task-evoked responses and investigated a change in signal-to-noise ratio (SNR) after subtraction. To obtain task-evoked response time courses, we extracted BOLD response time courses containing task-related component, and excluded the six motion parameters and the mean activity in CSF and WM. The extracted time courses were baseline corrected so that the averaged value across all time points was set to zero. To obtain LFFs, we extracted LFFs from the same ROI, and then excluded the task-related component and nuisance signals as described in the aforementioned prestimulus LFFs amplitude analysis. To quantify the effect of this regression, we compared the SNR for the task-evoked responses before versus after LFFs regression as done in the previous study [13]. To compute the SNR, we decomposed each of the time courses (before and after LFFs regression, respectively) into “signal” time course and “noise” time course. The former was the time course explained by the task-related regressors (which was reconstructed from the HRF-convolved regressors multiplied by individual beta estimates resulting from the GLM), and the latter was the time course not explained by the task-related regressors (i.e., the residual after removing the reconstructed task-related time course). The signal power was calculated as the mean squared deviation from the baseline of the “signal” time course, and the noise power was calculated as the

mean square deviation of the “noise” time course. The significance of changes in these measures was assessed using t-tests.

### **2.2.9 Prestimulus LFFs functional connectivity analysis**

Rather than LFFs amplitude, we next asked whether prestimulus LFFs functional connectivity before trials (pre-HH and pre-Miss) predicts subsequent memory performances. We applied psychophysiological interactions (PPIs) analysis [14] using SPM12 to investigate LFFs functional connectivity from seed ROI to other regions separately for pre-HH and pre-Miss conditions. First, we chose the right fusiform gyrus (rtFuG), the region showing the greatest SME at the group level (Figure 2.2A, Table 2.1), as a seed ROI. The LFFs time courses of the rtFuG ROI were extracted as described above (*Prestimulus Low Frequency Fluctuations Amplitude Analysis*), and was used as a physiological factor. This time courses were deconvolved using the canonical HRF before making PPI interaction term [15]. Second, we defined a psychological variable using a boxcar function that denotes prestimulus time points (-2.88 s to 0 s, corresponding to four volumes [16] before the HH trials vs. Miss trials. Here, we used a dummy variable coding the prestimulus time points for the HH trials with value 1 and those for the Miss trials with value -1. Third, we multiplied the deconvolved LFFs time courses with the psychological variable, and reconvolved it with the canonical HRF to make a PPI interaction term. Finally, we estimated a new GLM, which included the PPI interaction term, the LFFs time courses (before deconvolution), and the psychological variable convolved with the canonical HRF as PPI-related regressors. The model also included six motion parameters, mean time series in CSF and WM as regressors of no interest. The second-level random-effect analysis (one-sample t-tests) was performed using the single participant contrast values associated with the PPI interaction term.

## **2.3 Results**

The main purpose of this work was to investigate the effect of LFFs in memory encoding processes. As mentioned previously, we hypothesized that the LFFs of neural activity during encoding would affect encoding processes and cause variability of subsequent memory performances. To test this, we asked the participants to participate the incidental encoding scan in order to localize brain regions which are related to encoding processes. They were presented with pictorial stimuli and instructed to make a semantic judgment about the content of each image (man-made or natural), without prior information about the subsequent memory test. In the memory test, participants indicated whether given pictures are studied pictures (reporting their confidence “high confidence studied” or “low confidence studied” or “unstudied”). Based on their answers, all encoding trials could be categorized into subsequently remembered or subsequently forgotten trials. We looked for an evidence that LFFs of neural activity during encoding can predict whether the picture will be remembered or forgotten.

### **2.3.1 Behavioral results**

Although participants were not informed about the surprise memory test after the fMRI scan, they were able to correctly distinguish between studied and unstudied pictures with accuracy of  $74.2 \pm 6.3\%$  (mean  $\pm$  SD across participants).  $67.7 \pm 15.9\%$  of the studied pictures were judged as studied (i.e., hit), whereas  $80.8 \pm 14.6\%$  of the unstudied pictures were judged as unstudied (i.e., correct rejection). Based on the individual participants' responses in the surprise memory test, the picture trials of the incidental encoding task were categorized into high-confidence hit (HH, the pictures later remembered with high confidence;  $48.9 \pm 15.4\%$ ), low-confidence hit (LH, the pictures later

remembered with low confidence;  $18.8 \pm 8.9\%$ ), or Miss (the picture later forgotten;  $32.3 \pm 15.9\%$ ) trials.

Data obtained in previous study [17] using verbal stimuli indicated participants took longer reaction times (RTs) to make the semantic judgement for HH compared with LH and Miss trials respectively. In our study using pictorial stimuli, RTs were different across 3 trial types ( $F(2, 48) = 4.08$ ,  $P = 0.0230$ , ANOVA). An averaged RTs for HH trials ( $1,204.34 \pm 275.20$  ms) was significantly longer when compared to LH trials ( $1143.86 \pm 295.03$  ms) ( $P < 0.001$ , post-hoc t-test) and Miss trials ( $1,156.07 \pm 294.10$  ms) ( $P < 0.001$ , post-hoc t-test). However, the RTs for LH trials were no longer compared to Miss trials ( $P < 0.001$ , post-hoc t-test), which is inconsistent with results obtained in the previous study [17]. The slightly differences were noted because of the different types of stimuli.

### **2.3.2 Subsequent memory/forgetting effects**

In order to identify brain regions related to memory encoding processes, we compared neural activation during HH to Miss trials. The SME indicated fMRI signal that is greater for the successfully encoded stimuli than for unsuccessfully one was noted in the bilateral fusiform gyrus, the bilateral medial temporal lobe (MTL), the left superior parietal lobe, and the left middle frontal cortex ( $P < 0.05$ , FWE corrected; Figure 2.2A, Table 2.1).



**TOPIC 1: Low frequency fluctuations and its functional connectivity before memory encoding predict subsequent memory performances**

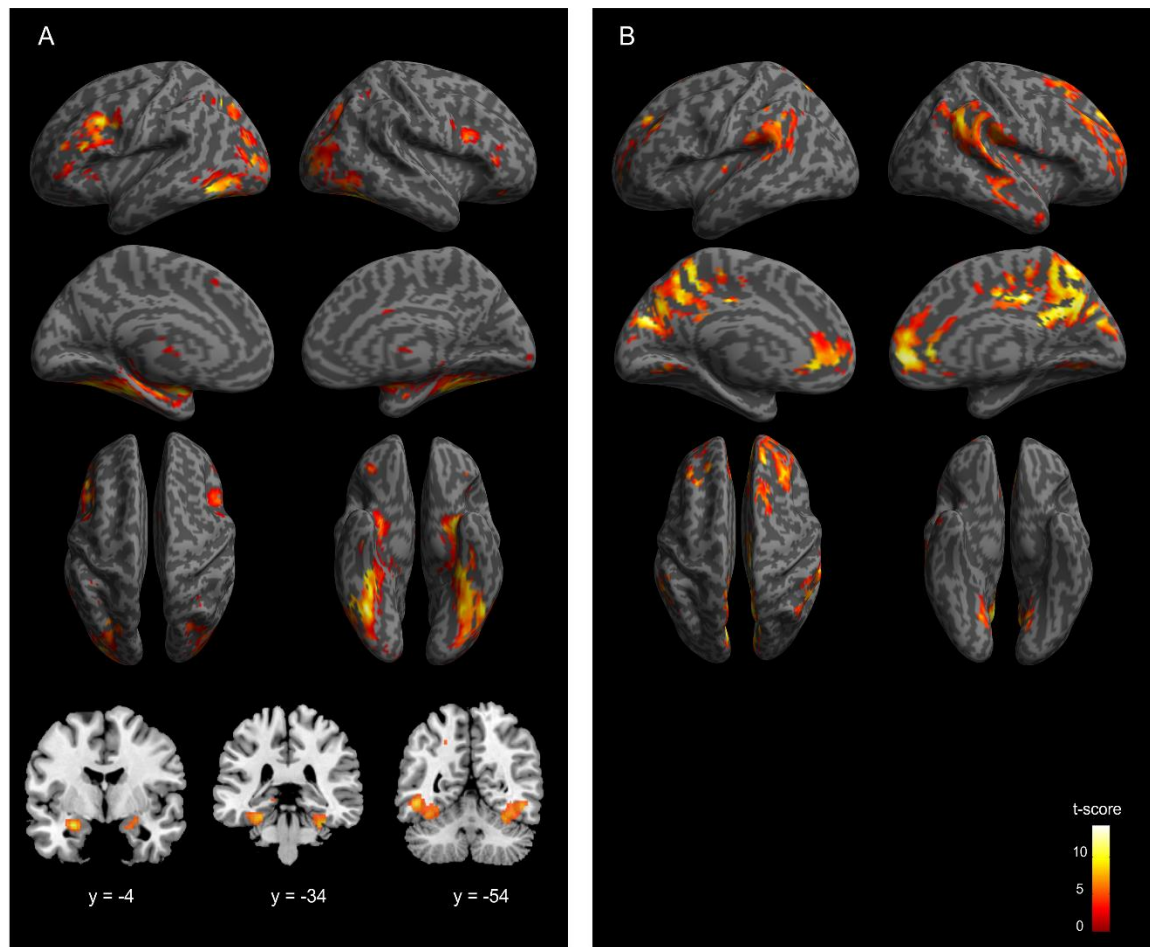


**Figure 2.2 Brain regions associated with the subsequent memory effect (SME) and subsequent forgetting effect (SFE)** (A) SME related regions. Statistical map showing voxels that are significantly correlated with HH relative to Miss conditions and (B) SFE related regions. Statistical map showing voxels that are significantly correlated with Miss relative to HH condition (SFE). Color bar indicates t value. Results are overlain onto the lateral and medial aspects of a cortical surface of a canonical template. Activations in medial temporal area are overlain onto coronal slices of the canonical template. All activations are thresholded at  $P < 0.05$ , FWE corrected.

**Table 2.1.** Details of brain regions associated with subsequent memory effect (SME) and subsequent forgetting effect (SFE).

	Region	H	MNI			$k_E$	$P_{FWE-corr}$
			x	y	z		
SME							
	Fusiform gyrus	R	36	-60	-20	1106	< 0.001
	Amygdala/Hippocampus	L	-26	-4	-18	155	< 0.001
	Inferior temporal gyrus	L	-48	-54	-10	1303	< 0.001
	parahippocampal gyrus	L	-26	-34	-20	1303	< 0.001
	Superior parietal lobule	L	-24	-68	46	241	< 0.001
	Middle frontal gyrus	L	-44	12	32	519	< 0.001
	Cerebellum exterior	L	-6	-76	-36	49	< 0.001
	Cerebellum exterior	R	8	-76	-28	77	< 0.001
	Inferior occipital gyrus	L	-36	-84	4	299	< 0.001
	Fusiform gyrus	L	-40	-18	-24	25	< 0.001
	Amygdala	R	26	-2	-16	68	< 0.001
	Inferior occipital gyrus	R	28	-88	0	124	< 0.001
SFE							
	Middle cingulate gyrus	R	4	-26	44	1408	< 0.001
	Superior frontal gyrus medial segment	R	10	46	-2	621	< 0.001
	Precuneus	L	-8	-72	26	219	< 0.001
	Superior frontal gyrus	R	24	46	36	129	< 0.001
	Middle frontal gyrus	L	-32	34	36	93	< 0.001
	Planum temporale	R	62	-30	16	50	< 0.001

**TOPIC 1: Low frequency fluctuations and its functional connectivity before memory encoding predict subsequent memory performances**

	Angular gyrus	R	58	-50	34	153	< 0.001
	Middle frontal gyrus	R	28	30	40	40	< 0.001
	Superior temporal gyrus	L	-66	-38	16	5	0.013
	Middle temporal gyrus	R	68	-22	-4	9	0.007
	Supramarginal gyrus	L	-64	-28	20	2	0.024

The MTL cluster included the amygdala/hippocampus and the parahippocampal gyrus. The left superior parietal lobe cluster included the left superior parietal lobe and extended into both middle and inferior extent of the occipital gyrus. The left middle frontal cortex cluster included the middle frontal gyrus and extended into the prefrontal gyrus and the inferior frontal gyrus. It is evident that our findings are consistent with previous studies [18]–[25] that reported many brain regions (e.g. prefrontal cortex, the MTL, fusiform cortex, the posterior parietal cortex, and the premotor cortex) involved in successful encoding.

In the other hand which brain regions activate against this successful encoding? To examine this, we compared neural activation during Miss to HH trials. Greater activation was observed in the right middle cingulate gyrus, the right inferior frontal gyrus medial segment, the left precuneus and the right superior frontal gyrus ( $P < 0.05$ , FWE corrected; Figure 2.2B, Table 2.1), which is consistent with results obtained in previous studies [26]–[28] (for meta-analysis, see [25]). It appears that the SFE observed here were noted as parts of default-mode network (DMN), known as task-negative network.

### 2.3.3 Prestimulus LFFs amplitude predicts subsequent memory performances

Although previous studies have reported that neural activity in the SME related regions can predict how well stimuli will be remembered [18], [19], [23], [29]–[32], however whether intrinsic fluctuations of observed neural activity from these brain regions contribute to variability of subsequent memory performances remain uncovered.

The results described above (Figure 2.2) strongly identified the neural activity that supports successful and unsuccessful memory encodings. Next, we asked whether LFFs of neural activity at the time points before stimulus onset (pre-HH and pre-Miss) observed in the SME and SFE related areas (Figure 2.2) can predict subsequent memory performances (HH trials or Miss trials).

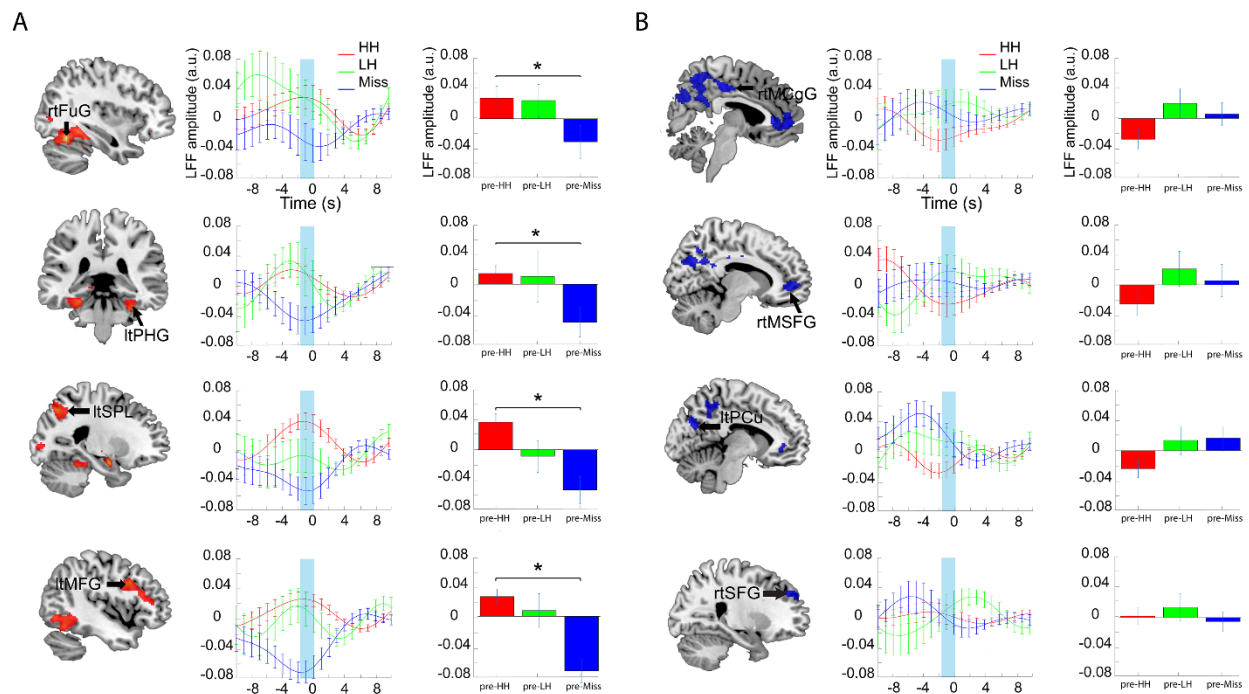


**Figure 2.3 Prestimulus LFFs amplitude analysis.** (A) Prestimulus LFFs amplitude analysis on the representative ROIs of subsequent memory effect (SME). The first column shows cross-sectional view of the representative ROIs

**TOPIC 1: Low frequency fluctuations and its functional connectivity before memory encoding predict subsequent memory performances**

---

for SME related regions. The second column illustrates LFFs time courses at the time period from -10 s to 10 s relative to the stimulus onset. The third column shows mean LFFs amplitude at the time period from -1.5 s to 0 s relative to the stimulus onset of each trial (pre-HH, pre-LH, and pre-Miss) (time period that is marked with blue rectangle in the second column). Mean LFFs amplitudes of pre-HH, pre-LH, and pre-Miss conditions are calculated and represented in red, green, and blue, respectively. (B) Prestimulus LFFs amplitude analysis on the representative ROIs of subsequent forgetting effect (SFE). Error bars indicate  $\pm$  standard error of the mean. Time courses are resampled at 1s. \* Significant at  $P < 0.05$ .

Based on the aforementioned SME results, we chose the rtFuG, the ltPHG, the ltMFG, and the ltSPL (Figure 2.3A, column 1) as representative ROIs of the SME. We selected the right middle cingulate gyrus (rtMCgG), the right superior frontal gyrus medial segment (rtMSFG), the left precuneus (ltPCu) and the right superior frontal gyrus (rtSFG) (Figure 2.3B, column 1) as representative ROIs of the SFE. We extracted signal time courses from these representative ROIs and then removed task-related signals and nuisance signals, and applied bandpass filter to obtain LFFs signal in a frequency range of 0.01-0.1 Hz [8] (Figure 2.1B, see Methods for details). By comparing LFFs amplitudes (at the time period -1.5 s to 0 s relative to the stimulus onset) [12] during pre-HH to pre-Miss, we observed significant differences between them in all 4 SME ROIs (the rtFuG:  $P = 0.0480$ ; the ltPHG:  $P = 0.0077$ ; the ltMFG:  $P = 0.0008$ ; the ltSPL:  $P = 0.0012$ , *ttest*) (Figure 2.3A). Results of one-way ANOVA comparing the prestimulus LFFs amplitudes among HH, LH, and Miss trials also confirmed these differences (the rtFuG: ( $F(2, 48) = 2.26$ ,  $P = 0.1158$ ); the ltPHG: ( $F(2, 48) = 2.07$ ,  $P = 0.1374$ ); the ltMFG: ( $F(2, 48) = 7.76$ ,  $P = 0.0012$ ); the ltSPL: ( $F(2, 48) = 5.81$ ,  $P = 0.0055$ , ANOVA).

We performed the same analysis to the SFE ROIs. Unlike the SME ROIs, we observed no significant differences in the LFFs amplitudes between pre-HH and pre-Miss in all SFE regions

---

(the rtMCgG:  $P = 0.1588$ ; the rtMSFG:  $P = 0.3469$ ; the ltPCu:  $P = 0.0684$ ; the rtSFG:  $P = 0.6894$ , ttest) (Figure 2.3B). No significant differences were also observed when applying one-way ANOVA to compare HH, LH, and Miss conditions (the rtMCgG: ( $F(2, 48) = 1.81, P = 0.1745$ ); the rtMSFG:  $F(2, 48) = 1.01, P = 0.3723$ ; the ltPCu:  $F(2, 48) = 1.47, P = 0.2396$ ; the rtSFG:  $F(2, 48) = 0.38, P = 0.6841$ , ANOVA). Thus, our results suggest that the LFFs in the brain regions demonstrating SME can predicts subsequent behavior, whereas the regions demonstrating SFE cannot.

For the prestimulus LFFs amplitude analysis described above, we used LFFs at the prestimulus time period which is close as much as possible to the stimuli but do not carry task-driven signal. Although this method has been used in many previous studies [9]–[12] but one may concern about the effect of preceding trial which may drive LFFs and encoding performance of its following trial. If there were some history-dependent effect, encoding trials would be more likely to identify as HH if they follow HH trials rather than Miss trials. To test this, we performed generalized linear model regression to test whether memory performance at trial  $t$  was influenced by memory performance at trial  $t-1$ ,  $t-2$ , and  $t-3$ , however we didn't observe significant relationship between them ( $P = 0.3744$ , t-test). Moreover, by classifying all encoding trials into the trials following HH trial (preceding HH) and the trials following Miss trial (preceding Miss), we observed no significant differences ( $P = 0.7200$ , t-test) between averaged prestimulus LFFs amplitude of preceding HH ( $-0.006 \pm 0.16$ ) and preceding Miss trials ( $-0.0243 \pm 0.17$ ). It indicated that higher amplitude of LFFs is not likely caused by prior HH trial. These results ruled out the possibility that encoding performance and LFFs at current trial may be influenced and driven by lingering effect of preceding trial.

### **2.3.4 LFFs accounts for trial-to-trial variability in task-evoked activity**

Previous study [13] showed an improvement of signal-to-noise ratio (SNR) after subtracting ongoing activity fluctuations from task-evoked neural activity indicating the superposition between them. In our study, we tested whether LFFs account for trial-to-trial variability in task-evoked activity. By simply regressed out LFFs from task-evoked response time courses and compared task-evoked response time courses before and after removal of the LFFs, we observed significant increase in SNR were substantially observed in 4 SME ROIs. There were a well 35.37% increase in SNR, 25.13% decrease in noise, and 1.73% increase in signal in the rtFuG ( $P < 0.001$ , t-test). The same trend was observed in the ltPHG (42.40% increase in SNR; 18.04% decrease in noise; 4.27% increase in signal;  $P < 0.001$ , t-test). As many as 122.09% and 145.58% increase in SNR were observed in the ltSPL (50.54% decrease in noise; 5.19% increase in signal) and the ltMFG (54.20% decrease in noise; 6.76% increase in signal;  $P < 0.001$ , t-test). Although this was not much increase in signal compare to large amount of decrease in noise, it still indicates an influence of LFFs to task-evoked activity.

### **2.3.5 Prestimulus LFFs connectivity predicts subsequent memory performances**

So far we showed that the prestimulus LFFs amplitude can predict whether the stimuli will be remembered. However, many previous studies [11], [16], [33], [34] revealed that in addition to the prestimulus intrinsic fluctuations amplitude, functional connectivity of intrinsic fluctuations also correlated with evoked neural response strength and subsequent behavior. Therefore, we next performed the functional connectivity analysis to test whether LFFs functional connectivity before the stimulus onset can predict subsequent memory performances. To do so, we performed a

psychophysiological interaction analysis (PPI) to investigate LFFs functional connectivity during pre-HH and pre-Miss. We hypothesized that LFFs functional connectivity within the SME related regions may impact encoding performances. Thus, In PPI analysis, the rtFuG, the brain region which exhibit highest peak activation of SME, was used as a seed region for PPI model. We aimed to identify brain regions whose activity was influenced by an interaction between the prestimulus LFFs in the rtFuG seed and conditions (HH or Miss).

Surprisingly, by comparing pre-Miss to pre-HH, as can be seen in Figure 2.4 and Table 2.2, the rtFuG seed positively connected to other regions (e.g. the bilateral anterior insular, the middle cingulate gyrus, the bilateral middle frontal gyrus, the thalamus proper, the cerebellum exterior, and the supramarginal gyrus which were not related with SME).

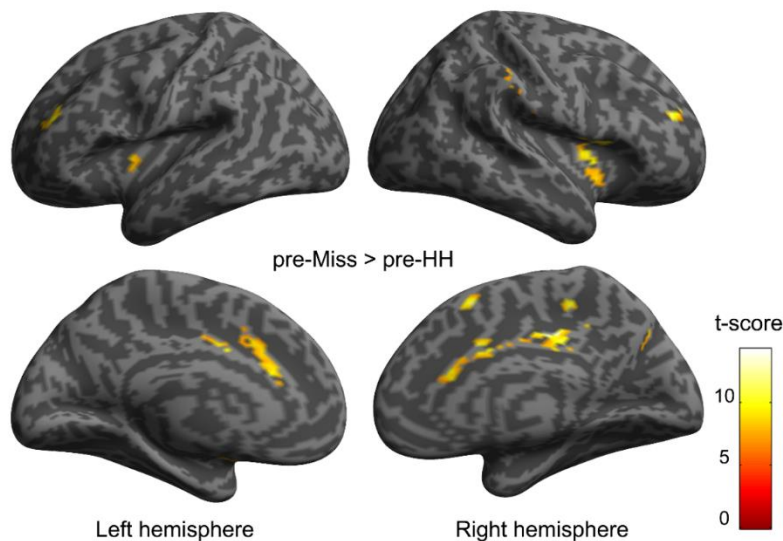


**Figure 2.4** Low frequency fluctuations (LFFs) functional connectivity map derived from the right fusiform gyrus (rtFuG) seed. The right fusiform seed showed greater LFFs functional connectivity to the following regions during pre-Miss compared to pre-HH conditions. Activations are shown at a threshold level of  $P < 0.001$ , uncorrected.



**TOPIC 1: Low frequency fluctuations and its functional connectivity before memory encoding predict subsequent memory performances**

---

**Table 2.** Detail of brain regions resulted from the PPI analysis. The LFFs from these brain areas were connected with LFFs from the right fusiform seed before Miss trials (pre-Miss) compared to before HH trials (pre-HH).

Region	H	MNI			k <sub>E</sub>	P <sub>FWE-corr</sub>
		x	y	z		
Anterior insular	R	40	12	6	469	< 0.001
Middle cingulate gyrus	R	6	-22	40	874	<0.001
Middle frontal gyrus	R	34	48	24	117	0.073
Middle frontal gyrus	L	-34	42	26	92	0.107
Cerebella Vermal Lobules	R	0	-74	-36	12	0.969
Cerebella Vermal Lobules	R	4	-60	-26	9	0.976
Anterior insular	L	-42	4	2	44	0.644
Cerebellum exterior	L	-6	-64	-16	13	0.954
Supramarginal gyrus	R	58	-34	46	66	0.429
Thalamus proper	R	8	-16	2	12	0.960
Precuneus	R	14	-70	38	29	0.811
Posterior insular	L	-38	-16	-6	14	0.948
Thalamus proper	L	-8	-20	4	8	0.980
Temporal pole	R	52	12	-8	4	0.993
Precuneus	R	16	-62	28	5	0.990
Inferior frontal gyrus	R	48	38	0	10	0.971

These areas are a part of cinguloopercular (CO) network, which known to maintain tonic alertness [35]. These results seem to indicate that at the time period before Miss trials (pre-Miss), the LFFs in the rtFuG disconnected with SME related regions but co-activated with the LFFs in the CO network. This phenomenon may benefits for maintaining the current task (semantic judgement task) but not good for memory encoding.

## **2.4 Discussion**

We demonstrated that LFFs amplitude before the stimulus onset can predict whether the stimulus will be later remembered. Higher prestimulus LFFs amplitude was observed in many brain regions including the right fusiform gyrus (rtFuG), the left parahippocampal gyrus (ltPHG), the left middle frontal gyrus (ltMFG), and the left superior parietal lobule (ltSPL) before the stimulus later remembered (vs. later forgotten). Furthermore, besides its amplitude, we demonstrated that the prestimulus LFFs functional connectivity can predict later memory performances of the upcoming stimuli. The stronger prestimulus LFFs functional connectivity from the rtFuG to the remote brain regions inside CO network was observed before the stimulus later forgotten (vs. later forgotten).

After ongoing intrinsic fluctuations were found to relate with task-evoked responses during motor task and motor performances [13], many studies have replicated this investigation into other domains demonstrating that intrinsic fluctuations amplitude in memory recollection [36], perception [9]–[11], and cognitive control [12] regions correlate with evoked neural response strength, subsequent behavior, and variability in behaviors (for review see [37]). Moreover, several studies [38]–[40] revealed a coherence between spontaneous intrinsic fluctuations and brain functionality by showing that brain regions inside the same network are likely to exhibit highly correlation in their spontaneous intrinsic fluctuations for example visual, auditory, default mode, episodic memory, language, and attention systems. It became more likely that intrinsic fluctuations may reflect functionality of brain system and predict task performances however relationship between intrinsic fluctuations and memory encoding system and memory performances remain unclear.

By employing the incidental memory encoding task, we replicated the previous studies (for review see [25]) by showing the brain regions related with memory encoding processes including both the SME related regions (including the medial temporal lobe and prefrontal cortex) and SFE related regions (including the DMN). The rtFuG exhibited the strongest SME related to successful encoding. A study by [12] showed that the prestimulus LFFs at time points -1.5 and 0s predict subsequent response speed in a stroop task. In our study, the LFFs of brain signal extracted from the rtFuG and other SME related regions showed the differences in their amplitudes comparing between conditions (pre-HH and pre-Miss). We observed higher LFFs amplitudes in pre-HH compared to pre-Miss in all 4 SME ROIs (Figure 2.3A) but not in all 4 SFE ROIs (Figure 2.3B). Previous studies have shown that prestimulus neural activity localized to the medial temporal lobe (MTL) and sub-cortical structures can predict later memory performances [18], [41]–[44]. Our results support previous study by showing consistency between task-evoked responses and their spontaneous intrinsic fluctuations in the SME related regions and providing an evidence that higher LFFs benefit for memory encoding processes.

To test whether the task-evoked responses observed in the SME related regions was modulated by LFFs, we subtracted LFFs from task-evoked activity and expected to see a change in SNR after the subtraction. As expected, comparing task-evoked response time courses before and after removal of the LFFs, the significant increased SNR was observed in all SME ROIs. This results confirm our hypothesis that the task-related responses in the experiment were modulated with ongoing intrinsic fluctuations and these fluctuations impact behavior in a significant way.

Many previous studies [11], [16], [33], [34] revealed that in addition to prestimulus intrinsic fluctuations amplitude, functional connectivity of intrinsic fluctuations and fluctuations

**TOPIC 1: Low frequency fluctuations and its functional connectivity before memory encoding predict subsequent memory performances**

---

across large-scale network regions also correlated with evoked neural response strength and subsequent behavior. For example there was an evidence that prestimulus functional connectivity of intrinsic fluctuations in and across large-scale brain networks correlates with perception performances in an auditory perception task, showing functional connectivity before the target predicts whether it would heard or missed [16]. In our study, we showed that the stronger prestimulus LFFs functional connectivity from the rtFuG to the brain regions inside CO network was the predictor of subsequent memory performances. Due to our first finding showed higher LFFs amplitude in the SME related regions during pre-HH condition, therefore we hypothesized that we would also observe stronger LFFs functional connectivity within these related network. However, it appears that there was no stronger connection from the rtFuG to other SME related regions during pre-HH condition. Interestingly, increased positive LFFs functional connectivity from the rtFuG seed to the brain regions inside CO network was observed during pre-Miss rather than pre-HH condition. The CO network, was known to maintain tonic alertness [35]. Greater functional connectivity between the CO network and FuG during the prestimulus period might facilitate visual processing of upcoming stimuli. However in turn this might be disadvantageous for memory encoding, because participants would spent less time and pay less effort for visual scrutiny. These results are in line with previous studies [35], [45], [46] which characterized the role of CO network as to maintain current brain state and to prepare for response. It is noteworthy that for participants the goal of the task is to make semantic judgments (“task-relevant) and not to memorize the pictures (“task-irrelevant”). To date it is still unclear that functional connectivity of intrinsic fluctuations in the CO network benefit or deteriorates the perception [11], [34]. In our study, we indicate that intrinsic fluctuations in the CO network may facilitate the semantic

judgement task but may take neural resource from encoding processes and bias toward bad memory encoding.

Together, our study demonstrates that the intrinsic fluctuations in SME related region benefit for memory encoding whereas its functional connectivity to the CO network is disadvantage. Our findings obtained here provide compelling evidence to support the view that LFFs are modulated with task-evoked responses during task and account for the variability in task performances.

## 2.5 References for chapter 2

- [1] M. B. Brodeur, E. Dionne-Dostie, T. Montreuil, and M. Lepage, “The Bank of Standardized Stimuli (BOSS), a New Set of 480 Normative Photos of Objects to Be Used as Visual Stimuli in Cognitive Research,” *PLoS One*, vol. 5, no. 5, p. e10773, 2010.
- [2] V. Willenbockel, J. Sadr, D. Fiset, G. O. Horne, F. Gosselin, and J. W. Tanaka, “Controlling low-level image properties: The SHINE toolbox,” *Behav. Res. Methods*, vol. 42, no. 3, pp. 671–684, 2010.
- [3] a D. Wagner, D. L. Schacter, M. Rotte, W. Koutstaal, A. Maril, a M. Dale, B. R. Rosen, and R. L. Buckner, “Building memories: remembering and forgetting of verbal experiences as predicted by brain activity.,” *Science (80-. )*, vol. 281, pp. 1188–1191, 1998.
- [4] B. B. Biswal, M. Mennes, X. N. Zuo, S. Gohel, C. Kelly, S. M. Smith, C. F. Beckmann, J. S. Adelstein, R. L. Buckner, S. Colcombe, A. M. Dogonowski, M. Ernst, D. Fair, M. Hampson, M. J. Hoptman, J. S. Hyde, V. J. Kiviniemi, R. Kotter, S. J. Li, C. P. Lin, M. J. Lowe, C. Mackay, D. J. Madden, K. H. Madsen, D. S. Margulies, H. S. Mayberg, K. McMahon, C. S. Monk, S. H. Mostofsky, B. J. Nagel, J. J. Pekar, S. J. Peltier, S. E. Petersen, V. Riedl, S. A. Rombouts, B. Rypma, B. L. Schlaggar, S. Schmidt, R. D. Seidler, G. J. Siegle, C. Sorg, G. J. Teng, J. Veijola, A. Villringer, M. Walter, L. Wang, X. C. Weng, S. Whitfield-Gabrieli, P. Williamson, C. Windischberger, Y. F. Zang, H. Y. Zhang, F. X. Castellanos, and M. P. Milham, “Toward discovery science of human brain

- function,” *Proc.Natl.Acad.Sci.U.S.A*, vol. 107, no. 10, pp. 4734–4739, 2010.
- [5] S. Vahdat, M. Darainy, T. E. Milner, and D. J. Ostry, “Functionally Specific Changes in Resting-State Sensorimotor Networks after Motor Learning,” *J. Neurosci.*, vol. 31, no. 47, pp. 16907–16915, 2011.
- [6] K. Duncan, A. Tompary, and L. Davachi, “Associative Encoding and Retrieval Are Predicted by Functional Connectivity in Distinct Hippocampal Area CA1 Pathways,” *J. Neurosci.*, vol. 34, no. 34, pp. 11188–98, 2014.
- [7] A. Tompary, K. Duncan, and L. Davachi, “Consolidation of Associative and Item Memory Is Related to Post-Encoding Functional Connectivity between the Ventral Tegmental Area and Different Medial Temporal Lobe Subregions during an Unrelated Task,” *J. Neurosci.*, vol. 35, no. 19, pp. 7326–31, 2015.
- [8] D. Cordes, V. M. Haughton, K. Arfanakis, J. D. Carew, P. A. Turski, C. H. Moritz, M. A. Quigley, and M. E. Meyerand, “Frequencies contributing to functional connectivity in the cerebral cortex in ‘resting-state’ data,” *Am. J. Neuroradiol.*, vol. 22, no. 7, pp. 1326–1333, 2001.
- [9] G. Hesselmann, C. a Kell, E. Eger, and A. Kleinschmidt, “Spontaneous local variations in ongoing neural activity bias perceptual decisions,” *Proc. Natl. Acad. Sci. U. S. A.*, vol. 105, no. 31, pp. 10984–10989, 2008.
- [10] G. Hesselmann, C. A. Kell, and A. Kleinschmidt, “Ongoing activity fluctuations in hMT+



- bias the perception of coherent visual motion.,” *J. Neurosci.*, vol. 28, no. 53, pp. 14481–5, 2008.
- [11] S. Sadaghiani, G. Hesselmann, and A. Kleinschmidt, “Distributed and antagonistic contributions of ongoing activity fluctuations to auditory stimulus detection.,” *J. Neurosci.*, vol. 29, no. 42, pp. 13410–13417, 2009.
- [12] C. P. Coste, S. Sadaghiani, K. J. Friston, and A. Kleinschmidt, “Ongoing brain activity fluctuations directly account for intertrial and indirectly for intersubject variability in stroop task performance,” *Cereb. Cortex*, vol. 21, no. 11, pp. 2612–2619, 2011.
- [13] M. D. Fox, A. Z. Snyder, J. L. Vincent, and M. E. Raichle, “Intrinsic fluctuations within cortical systems account for intertrial variability in human behavior.,” *Neuron*, vol. 56, no. 1, pp. 171–84, 2007.
- [14] K. J. Friston, C. Buechel, G. R. Fink, J. Morris, E. Rolls, and R. J. Dolan, “Psychophysiological and modulatory interactions in neuroimaging.,” *Neuroimage*, vol. 6, no. 3, pp. 218–229, 1997.
- [15] D. R. Gitelman, W. D. Penny, J. Ashburner, and K. J. Friston, “Modeling regional and psychophysiological interactions in fMRI: The importance of hemodynamic deconvolution,” *Neuroimage*, vol. 19, no. 1, pp. 200–207, 2003.
- [16] S. Sadaghiani, J.-B. Poline, A. Kleinschmidt, and M. D’Esposito, “Ongoing dynamics in large-scale functional connectivity predict perception,” *Proc. Natl. Acad. Sci.*, vol. 112,

- no. 27, p. 201420687, 2015.
- [17] a D. Wagner, D. L. Schacter, M. Rotte, W. Koutstaal, A. Maril, a M. Dale, B. R. Rosen, and R. L. Buckner, “Building memories: remembering and forgetting of verbal experiences as predicted by brain activity.,” *Science*, vol. 281, no. 5380, pp. 1188–1191, 1998.
- [18] G. Fernández and I. Tendolkar, “Integrated brain activity in medial temporal and prefrontal areas predicts subsequent memory performance: Human declarative memory formation at the system level,” *Brain Res. Bull.*, vol. 55, no. 1, pp. 1–9, 2001.
- [19] J. S. Simons and H. J. Spiers, “Prefrontal and medial temporal lobe interactions in long-term memory.,” *Nat. Rev. Neurosci.*, vol. 4, no. 8, pp. 637–48, 2003.
- [20] B. C. Dickerson, S. L. Miller, D. N. Greve, a M. Dale, M. S. Albert, D. L. Schacter, and R. a Sperling, “NIH Public Access,” vol. 17, no. 11, pp. 1060–1070, 2009.
- [21] R. J. Garoff, S. D. Slotnick, and D. L. Schacter, “The neural origins of specific and general memory: The role of the fusiform cortex,” *Neuropsychologia*, vol. 43, no. 6, pp. 847–859, 2005.
- [22] H. Kim and R. Cabeza, “Differential contributions of prefrontal, medial temporal, and sensory-perceptual regions to true and false memory formation,” *Cereb. Cortex*, vol. 17, no. 9, pp. 2143–2150, 2007.

**TOPIC 1: Low frequency fluctuations and its functional connectivity before memory encoding predict subsequent memory performances**

---

- [23] M. R. Uncapher and M. D. Rugg, "Selecting for memory? The influence of selective attention on the mnemonic binding of contextual information.," *J. Neurosci.*, vol. 29, no. 25, pp. 8270–9, 2009.
- [24] Y.-C. Kao, E. S. Davis, and J. D. E. Gabrieli, "Neural correlates of actual and predicted memory formation.," *Nat. Neurosci.*, vol. 8, no. 12, pp. 1776–1783, 2005.
- [25] H. Kim, "Neural activity that predicts subsequent memory and forgetting: A meta-analysis of 74 fMRI studies," *Neuroimage*, vol. 54, no. 3, pp. 2446–2461, 2011.
- [26] N. B. Turk-Browne, D. J. Yi, and M. M. Chun, "Linking implicit and explicit memory: Common encoding factors and shared representations," *Neuron*, vol. 49, no. 6, pp. 917–927, 2006.
- [27] S. M. Daselaar, S. E. Prince, and R. Cabeza, "When less means more: Deactivations during encoding that predict subsequent memory," *Neuroimage*, vol. 23, no. 3, pp. 921–927, 2004.
- [28] H. Kim, S. M. Daselaar, and R. Cabeza, "Overlapping brain activity between episodic memory encoding and retrieval: Roles of the task-positive and task-negative networks," *Neuroimage*, vol. 49, no. 1, pp. 1045–1054, 2010.
- [29] R. L. Buckner and D. C. Carroll, "Self-projection and the brain," *Trends Cogn. Sci.*, vol. 11, no. 2, pp. 49–57, 2007.

- [30] A. M. Morcom, C. D. Good, R. S. J. Frackowiak, and M. D. Rugg, “Age effects on the neural correlates of successful memory encoding,” *Brain*, vol. 126, no. 1, pp. 213–229, 2003.
- [31] T. Sommer, M. Rose, C. Weiller, and C. Büchel, “Contributions of occipital, parietal and parahippocampal cortex to encoding of object-location associations,” *Neuropsychologia*, vol. 43, no. 5, pp. 732–743, 2005.
- [32] T. Sommer, M. Rose, J. Gläscher, T. Wolbers, and C. Büchel, “Dissociable contributions within the medial temporal lobe to encoding of object-location associations,” *Learn. Mem.*, vol. 12, no. 3, pp. 343–351, 2005.
- [33] M. D. Fox, A. Z. Snyder, J. L. Vincent, M. Corbetta, D. C. Van Essen, and M. E. Raichle, “The human brain is intrinsically organized into dynamic, anticorrelated functional networks,” *Proc. Natl. Acad. Sci. U. S. A.*, vol. 102, no. 27, pp. 9673–8, 2005.
- [34] M. Boly, E. Balteau, C. Schnakers, C. Degueldre, G. Moonen, A. Luxen, C. Phillips, P. Peigneux, P. Maquet, and S. Laureys, “Baseline brain activity fluctuations predict somatosensory perception in humans,” *Proc. Natl. Acad. Sci. U. S. A.*, vol. 104, no. 29, pp. 12187–92, 2007.
- [35] M. I. Posner, “Measuring alertness,” *Ann. N. Y. Acad. Sci.*, vol. 1129, pp. 193–199, 2008.
- [36] J. L. Vincent, A. Z. Snyder, M. D. Fox, B. J. Shannon, J. R. Andrews, M. E. Raichle, and R. L. Buckner, “Coherent Spontaneous Activity Identifies a Hippocampal-Parietal

- Memory Network,” *J. Neurophysiol.*, vol. 96, no. 6, pp. 3517–3531, 2006.
- [37] M. D. Fox and M. E. Raichle, “Spontaneous fluctuations in brain activity observed with functional magnetic resonance imaging,” *Nature*, vol. 8, pp. 700–711, 2007.
- [38] S. M. Smith, P. T. Fox, K. L. Miller, D. C. Glahn, P. M. Fox, C. E. Mackay, N. Filippini, K. E. Watkins, R. Toro, A. R. Laird, and C. F. Beckmann, “Correspondence of the brain’s functional architecture during activation and rest,” *Proc. Natl. Acad. Sci. U. S. A.*, vol. 106, no. 31, pp. 13040–5, 2009.
- [39] S. Sadaghiani, “The relation of ongoing brain activity, evoked neural responses, and cognition,” *Front. Syst. Neurosci.*, vol. 4, no. June, pp. 1–14, 2010.
- [40] M. W. Cole, D. S. Bassett, J. D. Power, T. S. Braver, and S. E. Petersen, “Intrinsic and Task-Evoked Network Architectures of the Human Brain,” *Neuron*, vol. 83, no. 1, pp. 238–251, 2014.
- [41] H. Park and M. D. Rugg, “Pre stimulus hippocampal activity predicts later recollection,” *Hippocampus*, vol. 20, no. 1, pp. 24–28, 2010.
- [42] J. J. Yoo, O. Hinds, N. Ofen, T. W. Thompson, S. Whitfield-Gabrieli, C. Triantafyllou, and J. D. E. Gabrieli, “When the brain is prepared to learn: Enhancing human learning using real-time fMRI,” *Neuroimage*, vol. 59, no. 1, pp. 846–852, 2012.
- [43] R. J. Addante, M. de Chastelaine, and M. D. Rugg, “Pre-stimulus neural activity predicts

- successful encoding of inter-item associations,” *Neuroimage*, vol. 105, pp. 21–31, 2015.
- [44] N. Cohen, L. Pell, M. G. Edelson, A. Ben-Yakov, A. Pine, and Y. Dudai, “Peri-encoding predictors of memory encoding and consolidation,” *Neurosci. Biobehav. Rev.*, vol. 50, pp. 128–142, 2015.
- [45] S. Sadaghiani and M. D’Esposito, “Functional characterization of the cingulo-opercular network in the maintenance of tonic alertness,” *Cereb. Cortex*, vol. 25, no. 9, pp. 2763–2773, 2015.
- [46] S. Sadaghiani, R. Scheeringa, K. Lehongre, B. Morillon, A.-L. Giraud, and A. Kleinschmidt, “Intrinsic Connectivity Networks, Alpha Oscillations, and Tonic Alertness: A Simultaneous Electroencephalography/Functional Magnetic Resonance Imaging Study,” *J. Neurosci.*, vol. 30, no. 30, pp. 10243–10250, 2010.

# CHAPTER 3

## TOPIC 2: Large-scale Network Integration in the Human Brain Tracks

### Temporal Fluctuations in Memory Encoding Performance

#### 3.1 Abstract

Although activation/deactivation of specific brain regions have been shown to be predictive of successful memory encoding, the relationship between time-varying large-scale brain networks and fluctuations of memory encoding performance remains unclear. To elucidate this issue, we investigated time-varying functional connectivity patterns across the human brain in periods of 30–40 s, which have recently been implicated in various cognitive functions. Participants performed a memory encoding task in a magnetic resonance imaging scanner, and their encoding performance was assessed with a subsequent surprise memory test. A graph analysis of functional connectivity patterns revealed that increased integration of the subcortical, default-mode, and visual subnetworks with other subnetworks are hallmarks of successful memory encoding. Moreover, multivariate analysis using the graph metrics reliably classified the brain network states into the period of high (vs. low) memory encoding performance. Our findings suggest that a diverse set of brain systems dynamically interact to support successful memory encoding.

## **3.2 Methodology**

### **3.2.1 Participants**

We used the same set of participants participated in topic 1. Please refer to page 2-2 for detail.

### **3.2.2 Stimuli**

We used the same type of stimuli. Please refer to page 2-2 for detail.

### **3.2.3 Experimental paradigm**

We used the same experimental paradigm. Please refer to page 2-2 for detail.

### **3.2.4 Image acquisition and preprocessing**

We used the same setting and preprocessing processes. Please refer to page 2-4 for detail.

### **3.2.5 Regions of interest**

In the current study, we used two different sets of ROIs. The first set of ROIs was used to investigate FC patterns among well-established memory-related brain regions. Therefore, we used a set of 21 ROIs derived from a recent meta-analysis of the SME/SFE [1]. The ROIs included 11 brain regions associated with the SME (e.g., the inferior frontal cortex, hippocampus, intraparietal sulcus, and middle occipital gyrus) and 10 brain regions associated with the SFE (e.g., the frontal pole, superior temporal gyrus, posterior cingulate cortex, and temporoparietal junction; see



Supplementary file 1A for the list of all 21 ROIs). The second set of ROIs was used to investigate FC patterns across a large-scale brain network. We used 224 ROIs consisting of 10 subnetworks from the Power atlas [2]. The subnetworks had the following labels: sensorimotor networks (SMN), cingulo-opercular network (CON), auditory network (AUD), default mode network (DMN), visual network (VIN), fronto-parietal network (FPN), salience network (SAN), subcortical nodes (SUB), ventral attention network (VAN), and dorsal attention network (DAN) (see supplementary file 1C for the list of the ROIs). Although the Power atlas was originally derived from resting-state fMRI data, the same set of ROIs and subnetwork labels have been repeatedly used in task-fMRI studies on large-scale functional brain networks [3]–[8]. To cross-validate our findings regarding large-scale networks, we also used 285 ROIs organized into 11 subnetworks derived from the Gordon atlas (Gordon et al. 2016; Supplementary file 1P).

### **3.2.6 Trial-related activation analysis**

To identify brain regions showing the SME (i.e., greater activation in HH than Miss trials) and the SFE (i.e., greater activation in Miss than HH trials), we performed trial-related activation/deactivation analysis using a general linear model (GLM). First, based on participants' responses in the surprise memory test, we categorized the 360 picture trials of the incidental encoding task into three types: high-confidence hit (HH, subsequently remembered with high confidence), low-confidence hit (LH, remembered with low confidence), and Miss (forgotten) trials. Second, we constructed a GLM that included trial-related regressors denoting: 1) the onsets of HH trials, 2) the onsets of LH trials, 3) the onsets of Miss trials, and 4) the onsets of fixation trials, following the conventions of the subsequent memory approach (Wagner et al. 1998). Each trial was modeled using a box-car function (initiating at picture onset, duration = 2500 ms)

convolved with a canonical hemodynamic function provided by SPM12. The GLM also included eight nuisance regressors per run: six motion parameters as well as mean time series in the white matter (WM) and cerebral spinal fluid (CSF). The mean time series in the WM and CSF were obtained by averaging time series of voxels within the WM and CSF masks, each of which was derived from an individual's segmented structural image (binarized at a threshold of tissue probability  $> 0.8$ ) [11], [12]. The second-level random-effects analysis (one-sample t-tests) was performed using contrast images derived from individual participants (i.e., HH minus Miss for the SME and Miss minus HH for the SFE). The statistical threshold was set at voxel-wise  $P < 0.05$ , family-wise error corrected across voxels with the gray matter (defined by "TPM.nii" implemented in SPM12, thresholded at 0.5). For a set of selected ROIs (Figure 3.1A), we extracted beta estimates of individual participants and contrasts from 5-mm radius spheres centered on the MNI coordinates derived from the meta-analysis of the SME/SFE [1].

### **3.2.7 Extraction of fMRI time series**

We extracted residual time series data from each ROI using a voxel-wise GLM, in accord with previous research [6], [13]–[15]. More specifically, we averaged time series across voxels within a 5-mm radius sphere around each ROI, after regressing out the trial-related (HH, LH, Miss, and fixation) and nuisance (six motion parameters as well as WM and CSF) signals defined by the regressors of the aforementioned GLM. The obtained residual time series were used for FC analysis described below. For the additional control analysis using trial-evoked time series (Supplementary file 1I), we regressed out only the nuisance signals (i.e., motion parameters and WM/CSF time series), while maintaining the trial-related signals. All other procedures were

identical to the main analysis. In an additional analysis, we used another denoising method (“32P+scrubbing” denoising) that included 32 nuisance regressors (the six motion parameters and WM and CSF time series, as well as their temporal derivatives and quadratic terms) combined with motion scrubbing [16]. Note that we did not include global signal regression because it could introduce spurious anti-correlations. For scrubbing, frames with  $FD > 0.2$  mm were censored [17]–[19], and ignored in computing FC. All other procedures were identical to the main analysis.

### **3.2.8 Definition of time windows**

We sought to examine time-varying FC patterns associated with incidental memory encoding performance. To do so, we first divided the extracted time series into 36-s (i.e., 50 TRs) time windows, resulting in 45 windows per participant. This window size was determined on the basis of recent studies showing dynamic changes in FC during relatively short periods (30–40 s) [5], [7], [20], [21]. Importantly, we confirmed that our findings were robust to a range of window sizes (7.2–60 s; see Supplementary file 1F). We also confirmed that our results were unchanged when we used overlapping sliding windows (sliding in steps of 1 TR, resulting in 2,100 windows per participant) or when we used time windows shifted by 5 s (with taking into account the hemodynamic delay; see Supplementary file 1G and 1H). Next, for each participant, we classified the time windows into either “high encoding” or “low encoding” states based on window-wise encoding performance: the proportion of HH trials (the number of HH trials divided by that of picture trials) computed within each window. We used participant-specific median values for the classification, ensuring roughly equal numbers of windows for the high and low encoding states at an individual level. When a window had the exactly the same value as the median, we classified the window into either the high or low encoding state, depending on each participant, so that we could maximally equate the number of windows between the two states. In additional analyses, we also used tertiles and quartiles (instead of medians) to classify the windows according to memory encoding performance (Supplementary file 1K and 1L). To examine history dependence in the encoding states, we computed the probability of state switching (i.e., high to low or low to high,

as opposed to high to high or low to low). We used a permutation test to determine statistical significance: the (group-averaged) probabilities of state switching for the empirical data were compared with a null distribution derived from 1,000 permutations (i.e., we permuted the order of 45 windows within each participant and computed the probability of state switching for the permuted sequences of windows).

To test the robustness and specificity of our findings, we repeated the classification analysis with several alternative inputs. First, we classified the windows based on the proportion of HH and LH trials (i.e., the number of HH plus LH trials divided by that of the picture trials). This analysis confirmed that our findings held true when we included the LH trials in computing the window-wise encoding performance (see Supplementary file 1J). Second, to rule out the possibility that our findings resulted from simple visual-related brain responses, we classified the windows into “more pic” and “fewer pic” periods, based on the proportion of the picture trials (i.e., the number of picture trials divided by the total number of trials including fixation trials) irrespective of encoding performance. Third, to assess the influence of window-to-window variability in RT for semantic judgment (possibly reflecting task difficulty or general arousal level not directly related to memory performance), we classified the windows into “longer RT” and “shorter RT” periods based on mean RT computed within each window. The RT of a trial was defined as the time from the picture onset to the participant’s button press ( $1167.1 \pm 240.8$  ms, mean  $\pm$  SD across participants). The results from the second and third analyses confirmed that our findings are specific to encoding performance (see Supplementary file 1N and 1O).

### **3.2.9 Functional connectivity analysis**

We examined how FC patterns among ROIs (either in the 21-node or 224-node networks) differed between the high and low encoding states. For each time window, we computed Pearson's correlation coefficients of the time series between all pairs of ROIs, which were Fisher Z-transformed to form a connectivity matrix. We then averaged the connectivity matrices across the windows, separately for the high and low encoding states. For statistical tests of the difference in FC patterns between the states, we used Wilcoxon's signed-rank tests across participants. The significance threshold was set at  $P = 0.05$ , with multiple comparison corrections controlling for FDR. To compute Euclidean distance, we used  $x$ ,  $y$ , and  $z$  of MNI coordinates for each ROI.

### 3.2.10 Graph analysis

We performed graph analysis to examine integration and segregation of the 224-node network, using the Brain Connectivity Toolbox [22]. Note that this analysis was not applied to the 21-node network because graph metrics estimated in small networks are not necessarily stable [5], [22]. To derive graph metrics from the 224-node network, we constructed an unweighted, undirected graph from a  $224 \times 224$  connectivity matrix by applying a proportional threshold of connection density = 0.15. To ensure that effects were not driven by the particular connection density, we checked robustness by varying the threshold values: 0.1, 0.15, 0.2, and 0.25 (Supplementary file 1F).

Network topologies were characterized using the following metrics: global efficiency ( $E_g$ ), local efficiency ( $E_{loc}$ ), inter-subnetwork efficiency ( $E_{is}$ ), and PC. In the present study,  $N$  is the set of all nodes in the network, and  $n$  is the number of nodes.  $(i, j)$  is a link between nodes  $i$  and  $j$ , ( $i, j \in N$ ).  $a_{ij}$  is the connection status between  $i$  and  $j$ :  $a_{ij} = 1$  when link  $(i, j)$  exists;  $a_{ij} = 0$  when no connection is present.  $d_{ij}$  is the shortest path length between nodes  $i$  and  $j$ .  $M$  is the set of subnetworks, and  $m$  is the number of subnetworks.

The global efficiency ( $E_g$ ) is a measure of integration. A network with high  $E_g$  is considered topologically integrated. The global efficiency of a network is the average of the inverse shortest path lengths across all pairs of nodes:

$$E_g = \frac{1}{n} \sum_{i \in N} \frac{\sum_{j \in N, j \neq i} d_{ij}^{-1}}{n-1}$$

The local efficiency ( $E_{loc}$ ) is a measure of segregation. The local efficiency of node  $i$  is the average of the inverse shortest path lengths defined in the subgraph consisting of  $i$  and its neighboring nodes

$$E_{loc} = \frac{1}{n} \sum_{i \in N} \frac{\sum_{j, h \in N, j \neq i} a_{ij} a_{ih} [d_{jh}(N_i)]^{-1}}{k_i(k_i - 1)}$$

where  $k_i$  is the number of links connected to  $i$ , and  $d_{jh}(N_i)$  is the shortest path length between  $j$  and  $h$ , that contains only neighbors of  $i$ . For a network- or subnetwork-level measure of segregation,  $E_{loc}$  is averaged across nodes within a network or subnetwork, respectively.

The participation coefficient ( $PC$ ) is an alternative measure of integration, which quantifies the diversity of inter-subnetwork connections of a node:

$$PC = \frac{1}{n} \sum_{i \in N} \left( 1 - \sum_{m \in M} \left( \frac{k_i(m)}{k_i} \right)^2 \right)$$

where  $k_i(m)$  is the number of links between  $i$  and all nodes in subnetwork  $m$ . For a subnetwork-level measure,  $PC$  is averaged across nodes within a subnetwork.

Furthermore, we defined “inter-subnetwork” efficiency ( $E_{is}$ ) as a measure of integration between a specific pair of subnetworks:

$$E_{is} = \frac{1}{s} \sum_{i \in S} \frac{\sum_{j \in T} d_{ij}^{-1}}{t}$$

where  $S$  and  $T$  are the (non-overlapping) sets of nodes in two subnetworks, and  $s$  and  $t$  are the numbers of nodes in them. Note that  $d_{ij}$  is defined over the entire network, and the shortest path may be mediated by nodes outside the subnetworks of interest.

We also computed modularity as an index of how well a network can be partitioned into distinct communities:

$$Q = \sum_{u \in M} \left[ e_{uu} - \left( \sum_{v \in M} e_{uv} \right)^2 \right]$$

where the network is partitioned into a set of non-overlapping modules  $M$  (identified by Newman's algorithm), and  $e_{uv}$  is the proportion of all edges that connect nodes in module  $u$  with nodes in module  $v$  [5], [22].

These graph metrics were calculated for each window, then averaged across the windows, separately for the high and low encoding states. Finally, the graph metrics were compared between the two states across 25 subjects using Wilcoxon signed-rank test. All statistical results were corrected for multiple comparisons using FDR correction.

To rule out the possible confounding effects of time, within and across sessions, we performed additional statistical analyses, as follows (Supplementary file 1M). First, to exclude the effects of the amount of time passed within each session, we define a 45-by-1 dummy vector denoting the order of windows within each session (i.e., [1, 2, 3, ... 15], repeated three times), and regressed out this effect on a window-by-window basis before averaging graph metrics within each state. Second, to exclude the effect of the amount of time passed across sessions, we defined another 45-by-1 vector denoting session (i.e., [1, 1, ... 2, 2, ... 3, 3, ...]), and regressed out this

effect from graph metrics of each window. We confirmed that neither linear nor quadratic effects of the amount of time passed explained our results.

It should be noted that a recent paper raised a concern about the possible influences of overall FC strength on graph metrics [23]. In short, the authors argued that weaker overall FC of a network may result in the inclusion of more random connections (particularly when a graph is constructed using proportional thresholding), which tends to give a higher value of global efficiency and a lower value of local efficiency. In other words, differences in graph-metric values between two networks may reflect differences in overall FC strength. To address this concern, we performed an additional analysis controlling for the effect of overall FC strength, as proposed in the paper [23]. Specifically, we first computed overall FC strength (the mean of all positive values across all elements of a connectivity matrix) for each window. We then regressed out the overall FC strength from all graph metrics to obtain “adjusted” graph metrics. We performed the statistical analysis using these adjusted graph metrics in the same manner as the main analysis (Supplementary file 1T).

We also analyzed “edge reliability” to confirm that the difference in the proportions of reliable edges between the high and low encoding states did not affect our results. Specifically, for each participant and state, we examined how often an edge appeared between a given node pair across time windows. An edge was defined as “reliable” if it consistently appeared across windows more than by chance. To determine the chance level, we created 100 randomized networks from each of the real networks per participant and state, while preserving degree distributions [22], and generated null distributions of the probability of edge appearance. The 95th percentile of this null distribution was used as a threshold to determine the reliable edges in the real networks. We compared the proportions of reliable edges (i.e., the number of reliable edges relative to all possible edges) between the high and low encoding states using a signed-rank test across participants.



### 3.2.11 Multivariate pattern analysis

For the multivariate analysis based on graph metrics, we performed across-participant binary classification (with leave-one-out cross validation) using a support vector machine (SVM) implemented in LIBSVM [24]. We used PCs and local efficiency of the 10 subnetworks (averaged across windows for each participant and state) as inputs for the classifier. The input variables were Z-score normalized (mean = 0, standard deviation = 1) within each participant as a method of feature scaling. The SVM was trained using 48 samples from 24 participants (i.e., the high and low encoding states) with the default parameters (kernel type = radial basis function, gamma = 1/the number of features;  $c = 1$ ), and tested using two samples from the left-out participant. The classification accuracy was averaged across the 25 folds of cross validation. The statistical significance of classification accuracy was evaluated using a permutation test, as proposed by Golland and Fischl (2003) [25]. In the permutation test, the class labels (i.e., the high or low encoding states) of the original data are reversed in randomly selected participants, and the same SVM classification was performed to obtain a null distribution of classification accuracy (10,000 permutations). The  $P$  value was calculated as the proportion of classification accuracies that are equal to or greater than the accuracy obtained by the original data. For control analyses, we repeated the same classification procedure, except we used different sets of input variables.

### **3.3 Results**

We used an incidental memory task (Wagner et al. 1998; Paller, Kutas, and Mayes 1987), in which participants ( $n = 25$ ) in a MRI scanner were presented with pictorial stimuli and instructed to make a semantic judgment about the content of each image (man-made or natural), without knowing about a subsequent surprise memory test. To investigate dynamic fluctuations in FC patterns associated with memory encoding performance, we examined time-varying FC within a period of 36 s (consisting of 50 time points, given our sampling rate of 0.72 s; Figure 3.1A, B).

#### **3.3.1 Behavioral results**

Although participants were not informed about the surprise memory test after the fMRI scan, they were able to correctly distinguish between studied and unstudied pictures with accuracy of  $74.2 \pm 6.3\%$  (mean  $\pm$  SD across participants).  $67.7 \pm 15.9\%$  of the studied pictures were judged as studied (i.e., hit), whereas  $80.8 \pm 14.6\%$  of the unstudied pictures were judged as unstudied (i.e., correct rejection). Based on the individual participants' responses in the surprise memory test, the picture trials of the incidental encoding task were categorized into high-confidence hit (HH, the pictures later remembered with high confidence;  $48.9 \pm 15.4\%$ ), low-confidence hit (LH, the pictures later remembered with low confidence;  $18.8 \pm 8.9\%$ ), or Miss (the picture later forgotten;  $32.3 \pm 15.9\%$ ) trials.

#### **3.3.2 Classification of time windows based on encoding performance**

---

To relate dynamic FC patterns to incidental memory encoding performance, we divided the fMRI time series into non-overlapping small time windows (each consisting of 50 repetition time (TR) or 36 s; 45 windows per participant), and classified them into two groups based on encoding performance defined for each window. Specifically, we first defined window-wise encoding performance by computing the proportion of HH trials (the number of HH trials divided by the number of picture trials) for each time window. We then classified the time windows into either high or low encoding states on the basis of the window-wise encoding performance, with median split at participant-specific cutoff points (see Methods for details). Figure 3.2 shows the distributions of the windows as a function of the window-wise encoding performance, pooled across all participants. We confirmed that the number of windows classified as the high encoding state ( $22.7 \pm 1.9$ , mean  $\pm$  SD across participants) and the low encoding state ( $22.3 \pm 1.9$ ) were closely matched (Wilcoxon signed-rank test,  $z_{(24)} = 1.0968$ ,  $P = 0.2727$ ). The proportion of HH trials was  $64.6 \pm 15.4\%$  ( $5.18 \pm 1.25$  trials per window) for the high encoding state and  $32.6 \pm 15.0\%$  ( $2.59 \pm 1.17$  trials per window) for the low encoding state, confirming a difference in encoding performance between the two states.

It should be noted that the proportion of the high encoding state was close to 50% in all three sessions (session 1:  $51.2 \pm 19.7\%$ , session 2:  $45.9 \pm 18.7\%$ , session 3:  $54.1 \pm 13.2\%$ , mean  $\pm$  SD across participants), with no increasing or decreasing trend over time ( $F_{(2,24)} = 1.020$ ,  $P = 0.367$ , one-way ANOVA). This ruled out the possibility that window-wise encoding performance is influenced by a mere effect of temporal proximity to the surprise memory test. In addition, we computed the probability of “state switching” (i.e., a window followed by the other type of window, such as high to low or low to high). If the state of each window was random and independent of the previous state, the probability of state switching would be approximately 50%. However, we found that the probability was significantly lower than the theoretical chance level of 50% ( $41.0\%$ ,  $P < 0.001$ , permutation test). This indicated a history dependence of window-wide

encoding performance, such that the state type of a window tended to be carried over to the next window.

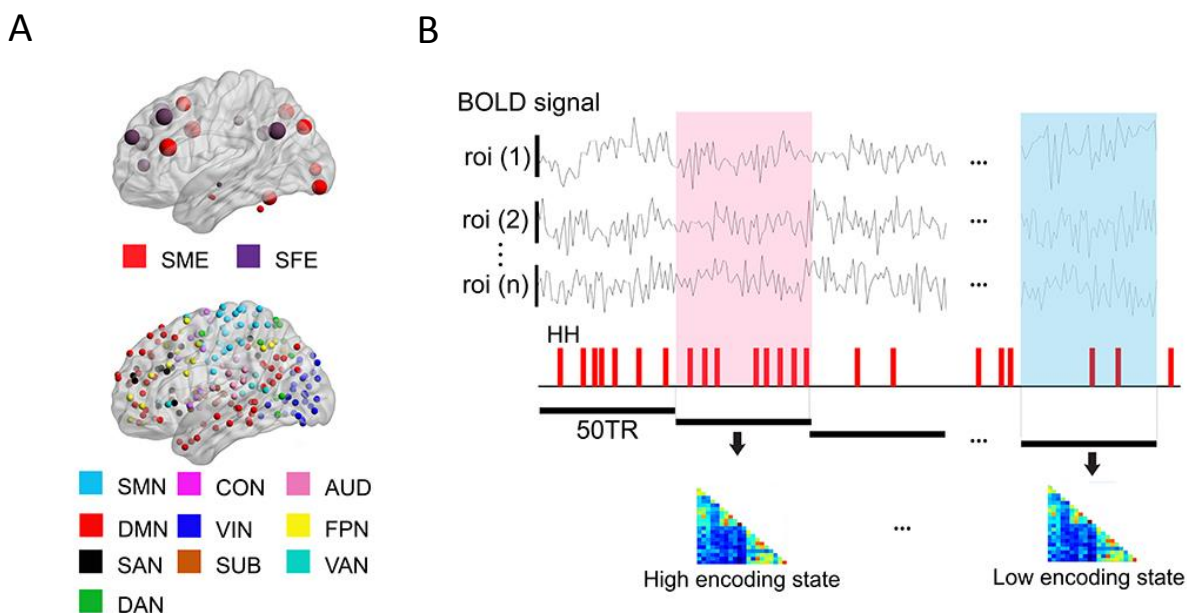


**Figure 3.1 Analysis overview.** (A) Regions of interest (ROI) used in connectivity analysis. We used two sets of ROIs: One consisting of 21 well-established memory-related brain regions derived from a recent meta-analysis (Kim et al., 2011) and the other consisting of 224 ROIs across the whole brain derived from a functional atlas (Power et al., 2010). (B) fMRI signal time series was extracted from each ROI and divided into 36-s time windows. Each window was classified as high or low encoding state based on encoding performance during that time window. Functional connectivity patterns and graph metrics were estimated within each window, then averaged within each state. SME, subsequent memory effect; SFE, subsequent forgotten effect; SMN, sensorimotor networks; CON, cingulo-opercular network; AUD, auditory network; DMN, default mode network; VIN, visual network; FPN, fronto-parietal network; SAN, salience network; SUB, subcortical network; VAN, ventral attention network; DAN, dorsal attention network.

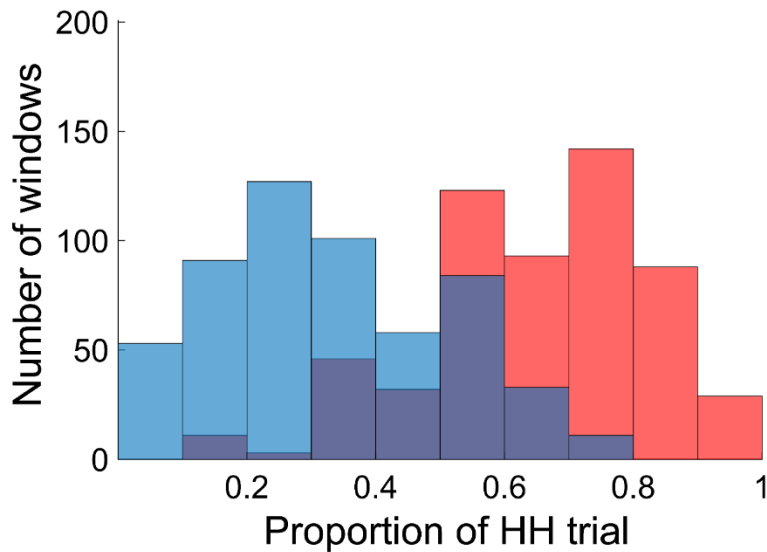


**Figure 3.2. Distributions of time windows classified as high and low encoding states.** The histogram shows distributions of the time windows with regard to the window-wise encoding performance, pooled across participants (red, high encoding state; blue, low encoding state). Note that the two distributions are overlapping because we used participant-specific median split to classify the high and low encoding states.

Figure 3.2 shows the distributions of the windows as a function of the window-wise encoding performance, pooled across all participants. The number of windows classified as the high encoding state ( $22.7 \pm 1.9$ , mean  $\pm$  SD across participants) and the low encoding state ( $22.3 \pm 1.9$ ) were closely matched (Wilcoxon signed-rank test,  $z_{24} = 1.0968$ ,  $P = 0.2727$ ).

It should be noted that the proportion of the high encoding state was close to 50% in all three sessions (session 1:  $51.2 \pm 19.7\%$ , session 2:  $45.9 \pm 18.7\%$ , session 3:  $54.1 \pm 13.2\%$ , mean  $\pm$  SD across participants), with no increasing or decreasing trend over time ( $F_{(2,24)} = 1.020$ ,  $P = 0.367$ , one-way ANOVA). This ruled out the possibility that window-wise encoding performance is influenced by a mere effect of temporal proximity to the surprise memory test. In addition, we

computed the probability of “state switching” (i.e., a window followed by the other type of window, such as high to low or low to high). If the state of each window was random and independent of the previous state, the probability of state switching would be approximately 50%. However, we found that the probability was significantly lower than the theoretical chance level of 50% (41.0%,  $P < 0.001$ , permutation test). This indicated a history dependence of window-wide encoding performance, such that the state type of a window tended to be carried over to the next window.

### **3.3.3 Functional connectivity patterns among memory-encoding-related regions**

Do FC patterns differ between the high and low encoding states? To examine this issue, we first focused on well-established memory-encoding-related brain regions. Based on a recent meta-analysis (Kim 2011), we defined a brain network consisting of 11 SME regions and 10 SFE regions (Figure 3.1A; for the detail of the regions of interest (ROIs), see Supplementary file 1A). By focusing on functionally well-characterized regions, we were able to make clear predictions, and thereby confirm effectiveness of our approach based on FC in relatively short time windows (i.e., 50 TRs). Specifically, we predicted greater FC among the SME regions in the high encoding state relative to the low encoding state, given the proposed functional interactions among the SME regions for successful memory encoding (Kim 2011). Importantly, trial-related activation analysis of our own fMRI data confirmed the SME and SFE in these ROIs (Figure 3.3 A–C; Supplementary file 1B).

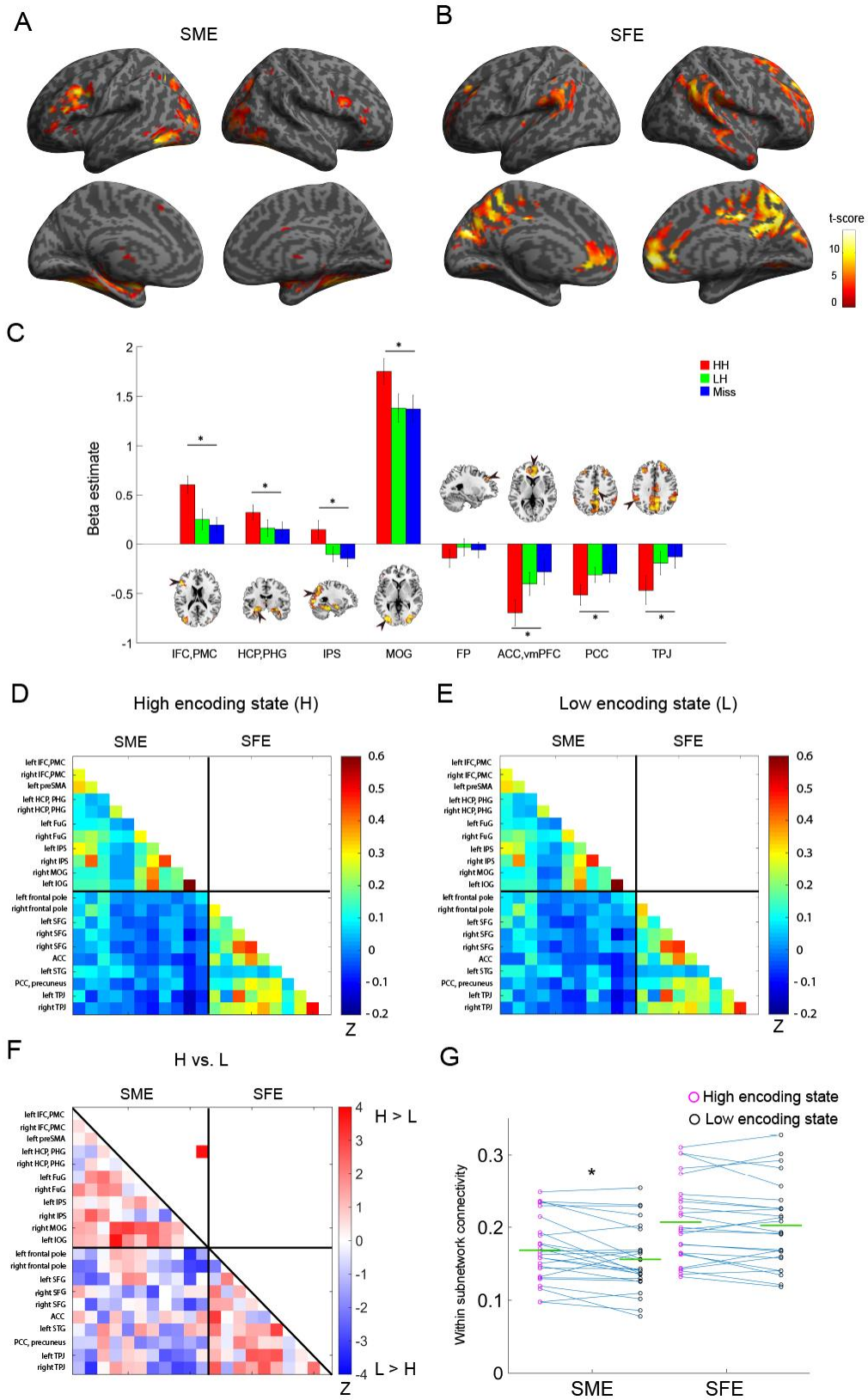


**Figure 3.3. Functional connectivity patterns among memory-related brain regions.** Functional connectivity patterns among memory-related brain regions. Trial-related activation analysis confirmed (A) the subsequent memory effect (SME, i.e., HH > Miss) and (B) subsequent forgetting effect (SFE, i.e., Miss > HH). Statistical parametric maps are thresholded at  $P < 0.05$ , FWE corrected across the whole brain. (C) Bar graph shows beta estimates (mean  $\pm$  SEM across participants) for high-confidence hit (HH), low-confidence hit (LH), and Miss trials in representative ROIs from the SME/SFE regions. (D) Connectivity matrix of the high encoding state, averaged across participants. (E) Connectivity matrix of the low encoding state, averaged across participants. Color bars indicate Fisher-Z transform of Pearson's correlation coefficients. (F) A matrix illustrating statistical differences in functional connectivity patterns between the high and low encoding states. Color bar indicates z values derived from Wilcoxon signed-rank test across participants. Connections showing significant differences ( $P < 0.05$ , FDR corrected) are marked in red in the upper triangle of the matrix. (G) Within-subnetwork connectivity for the SME and SFE regions (mean Fisher's Z value of connections within the SME and SFE regions, respectively). Magenta and black circles represent individual-participant data for the high and low encoding states, respectively. Green horizontal lines indicate across-participant means. Asterisk indicates a significant difference in within-subnetwork connectivity between the high and low encoding states (Wilcoxon signed-rank test,  $P < 0.05$ ). IFC, inferior frontal cortex; PMC, premotor cortex; HCP, hippocampus; PHG, parahippocampal gyrus; IPS, intraparietal sulcus; MOG, middle occipital gyrus; FP, frontal pole; ACC, anterior cingulate cortex; vmPFC, ventromedial prefrontal cortex; PCC, posterior cingulate cortex; TPJ, temporoparietal junction.

To examine FC patterns, we calculated Fisher's Z-transform of Pearson's correlation coefficients of the windowed time series between all pairs of ROIs. The connectivity matrices were then averaged across time windows separately for the high and low encoding states (Figure 3.3D and E). While the connectivity matrices of the two states looked similar to each other, direct comparison revealed a significant difference in a pair of ROIs within the SME regions: the connectivity between the hippocampus and occipital cortex (Wilcoxon signed-rank test,  $z_{(24)} = 3.7266$ ,  $P = 0.0002$ , surviving false-discovery-rate [FDR] correction among  ${}_{21}C_2 = 210$  tests; Figure 3.3F). We also computed "within-subnetwork" connectivity by averaging the values in the connectivity matrices only among the SME regions. The within-subnetwork connectivity for the



---

SME regions was significantly greater in the high vs. low encoding state (Wilcoxon signed-rank test,  $z_{(24)} = 2.4889$ ,  $P = 0.0128$ ; Figure 3.3G). On the other hand, within-subnetwork connectivity for the SFE regions was not significantly different between the high and low encoding states ( $z_{(24)} = 1.0897$ ,  $P = 0.2758$ ; Figure 3.3G). Overall, these results were consistent with our prediction of greater FC among the SME regions during the high encoding state (see Discussion for more details).

### 3.3.4 Functional connectivity patterns across large-scale brain networks

Next, to elucidate how a diverse set of brain systems are coordinated for successful memory encoding, we examined FC patterns across a large-scale brain network. In this analysis, we defined a brain-wide network consisting of 224 ROIs (organized into 10 subnetworks; Figure 3.1B; Supplementary file 1C). This network was derived from a well-established functional brain atlas [2], and the same ROIs and subnetwork labels have been used in many previous studies investigating dynamic/static FC during task fMRI (Cole et al. 2014; Cohen et al. 2014; Braun et al. 2015; Cohen and Esposito 2016; Mohr et al. 2016; Westphal, Wang, and Rissman 2017). To obtain FC patterns, we calculated pairwise correlations of the windowed time series among the 224 ROIs (Figure 3.4A and B), just as we did for the SME/SFE networks. By comparing the high and low encoding states, we found significant differences in FC associated with encoding performance: 72 connections showed significant increases in FC during the high encoding states, whereas 335 connections showed significant decreases (surviving FDR corrections among  ${}_{224}C_2 = 24,976$  tests; Figure 3.4C; Supplementary file 1D and 1E). Three-dimensional (3D) visualizations of differential FC patterns are shown in Figure 3.4D and E. Interestingly, the connections showing significant increases in FC during the high encoding state tended to be long range (Euclidean distance:  $86.1 \pm 27.3$ ; Figure 3.4D), whereas those showing significant decreases tended to be short range (Euclidean distance:  $67.3 \pm 28.6$ ; Figure 3.4E; increases vs. decreases:  $z_{(405)} = 5.0244$ ,  $P < 0.0001$ , Wilcoxon rank-sum test). These observations suggest a systematic reconfiguration of the large-scale network between the high and low encoding states, rather than a homogeneous, brain-wide increase or decrease in FC.

TOPIC 2: Large-scale Network Integration in the Human Brain  
Tracks Temporal Fluctuations in Memory Encoding Performance

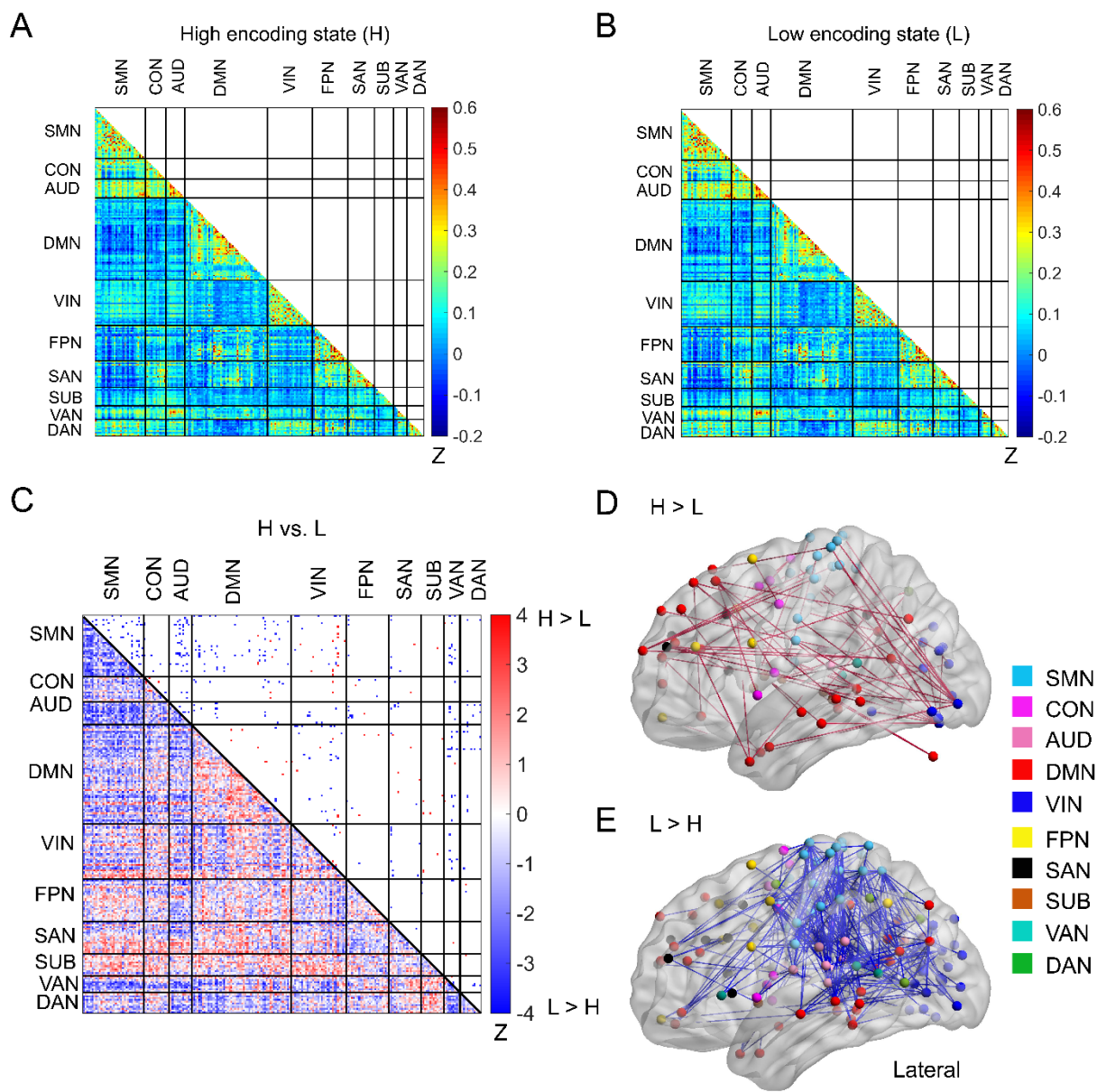


**Figure 3.4. Functional connectivity patterns across large-scale brain network.** (A) Connectivity matrix of the high encoding state, averaged across participants. (B) Connectivity matrix of the low encoding state, averaged across participants. Color bars indicate Fisher-Z transform of Pearson correlation coefficient. (C) A matrix illustrating statistical differences in functional connectivity patterns between the high and low encoding states. ROIs belonging to the same subnetwork were grouped together resulting in 10 subnetworks. Color bar indicates Z-value derived from Wilcoxon signed-rank test across participants. Connections showing significant differences ( $P < 0.05$ , FDR corrected)

---

are marked in color (red, high > low; blue, low > high) in the upper triangle of the matrix. (D) Three-dimensional (3D) visualizations of significantly greater functional connectivity during the high encoding state. (E) 3D visualizations of significantly greater functional connectivity during the low encoding state.

In light of the pivotal role of the hippocampus in memory encoding, we also examined the FC patterns between the hippocampus and the large-scale network. In this analysis, we considered a 226-node network that combined the bilateral hippocampus ROIs [1] with the 224 ROIs [2]. As expected, we observed increased FC between the hippocampus and occipital cortex during the high vs. low encoding state (right hippocampus-left inferior occipital gyrus:  $z_{(24)} = 3.9413$ ,  $P < 0.0001$ ; right hippocampus-left middle occipital gyrus:  $z_{(24)} = 4.0495$ ,  $P < 0.0001$ ; surviving FDR corrections among  ${}_{226}C_2 = 25,425$  tests; Supplementary figure S1). The right hippocampus also showed increased FC with the right superior temporal gyrus ( $z_{(24)} = 3.4575$ ,  $P = 0.0005$ ) and decreased FC with the right precentral gyrus ( $z_{(24)} = -3.3499$ ,  $P = 0.0008$ ), while the left hippocampus showed decreased FC with the left superior temporal gyrus ( $z_{(24)} = -3.6190$ ,  $P = 0.0003$ ).

### 3.3.5 Graph analysis on large-scale brain network

The results described above imply a dynamic reconfiguration of a large-scale brain network between the high and low encoding states. In particular, the high encoding state appears to be characterized by enhanced long-range FC among distant brain regions, whereas the low encoding state seems to be characterized by increased local connectivity among neighboring regions. This may indicate that the brain shows different levels of functional integration/segregation depending on encoding performance. To formally test this possibility, we applied graph theory to derive measures of integration and segregation from the 224-node network. First, we computed global efficiency, a measure of integration defined for the entire network, and local efficiency (averaged

across all nodes), a measure of segregation. We found that global efficiency was significantly higher during the high (vs. low) encoding state ( $z_{(24)} = 3.8611$ ,  $P = 0.0001$ ; Figure 3.5A), whereas local efficiency was significantly higher during the low (vs. high) encoding state ( $z_{(24)} = -3.0808$ ,  $P = 0.0021$ ; Figure 3.5C). This suggests that a higher integration of the large-scale brain network is a hallmark of a better window-wise encoding performance. Next, to examine the network architecture in more detail, we examined subnetwork-wise measures of integration and segregation. Specifically, we computed participation coefficients (PCs) and local efficiency averaged across nodes within each subnetwork, as measures of integration and segregation, respectively [15], [27], [28]. We found significantly higher PCs during the high (vs. low) encoding state in several subnetworks (SMN:  $z_{(24)} = 2.4082$ ,  $P = 0.0160$ ; DMN:  $z_{(24)} = 2.3005$ ,  $P = 0.0214$ ; visual network [VIN]:  $z_{(24)} = 2.5696$ ,  $P = 0.0102$ ; fronto-parietal network [FPN]:  $z_{(24)} = 2.4889$ ,  $P = 0.0128$ ; salience network [SAN]:  $z_{(24)} = 2.8925$ ,  $P = 0.0038$ ; subcortical nodes [SUB]:  $z_{(24)} = 3.2423$ ,  $P = 0.0012$ ; ventral attention network [VAN]:  $z_{(24)} = 2.2467$ ,  $P = 0.0247$ ; surviving FDR correction among 10 tests; Figure 3.5B). On the other hand, local efficiency was significantly higher during the low (vs. high) encoding state in many subnetworks (SMN:  $z_{(24)} = -2.7849$ ,  $P = 0.0054$ ; CON:  $z_{(24)} = -2.3274$ ,  $P = 0.0199$ ; AUD:  $z_{(24)} = -4.0226$ ,  $P = -0.0001$ ; VIN:  $z_{(24)} = -2.8387$ ,  $P = 0.0045$ ; SAN:  $z_{(24)} = -2.2467$ ,  $P = 0.0247$ ; DAN:  $z_{(24)} = -2.2736$ ,  $P = 0.023$ ; surviving FDR correction; Figure 3.5D). Only the SUB showed higher local efficiency during the high encoding state ( $z_{(24)} = 2.5696$ ,  $P = 0.0102$ ; surviving FDR correction; Figure 3.5D).

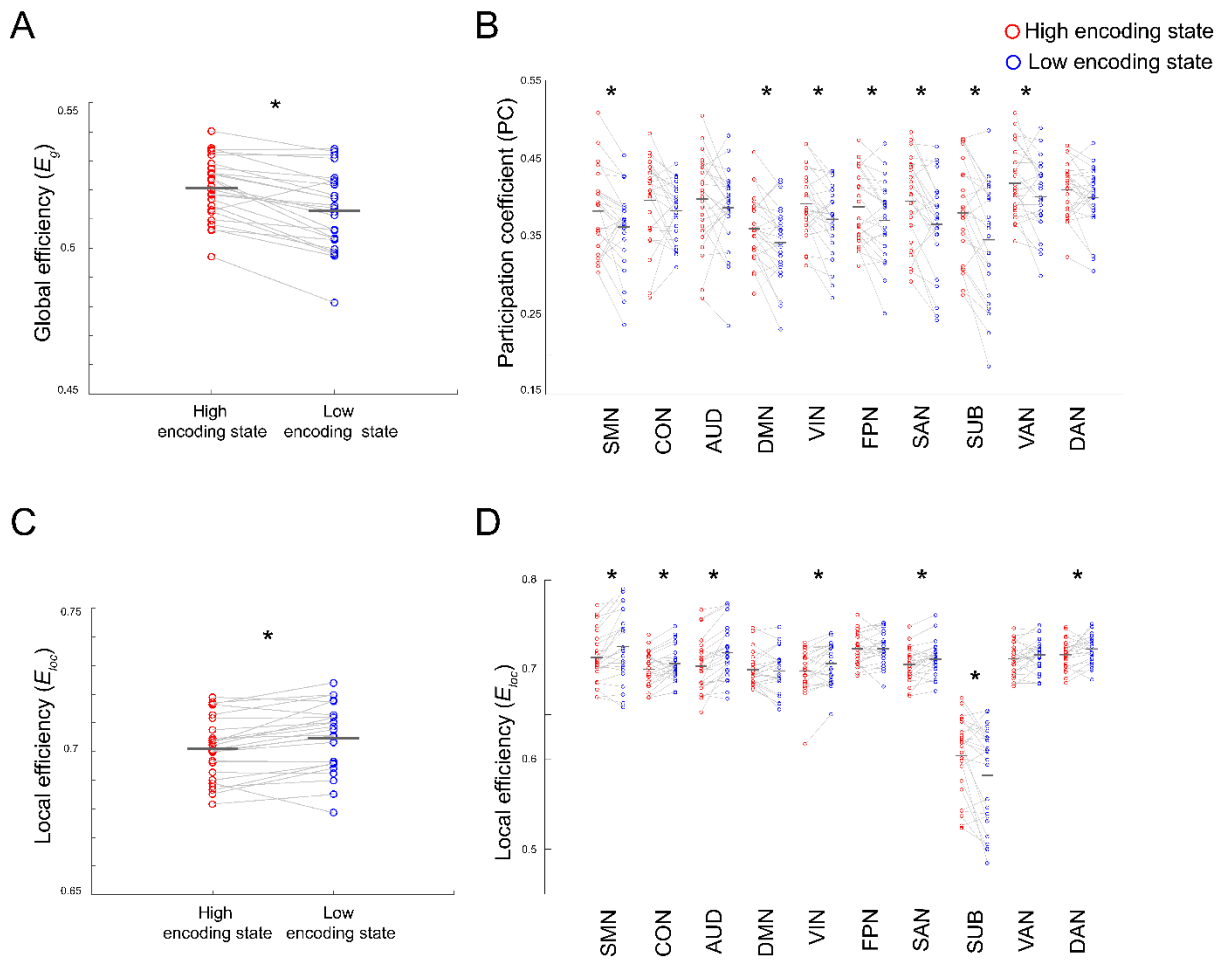


**Figure 3.5. Differences in integration/segregation of large-scale network between high and low encoding states.** (A) Global efficiency, a measure of network integration. (B) Participation coefficient (averaged across nodes within each subnetwork), a measure of integration defined at subnetwork level. (C) Local efficiency (averaged across all nodes), a measure of segregation. (D) Local efficiency (averaged across nodes within each subnetwork), a measure of segregation defined at the subnetwork level. Graph metrics were computed for each time window, then averaged across windows separately for each state. Dots represent individual-participant data. Black horizontal lines indicate across-participant means. Asterisks indicate a significant difference between the states ( $P < 0.05$ , FDR corrected for subnetwork-wise metrics).

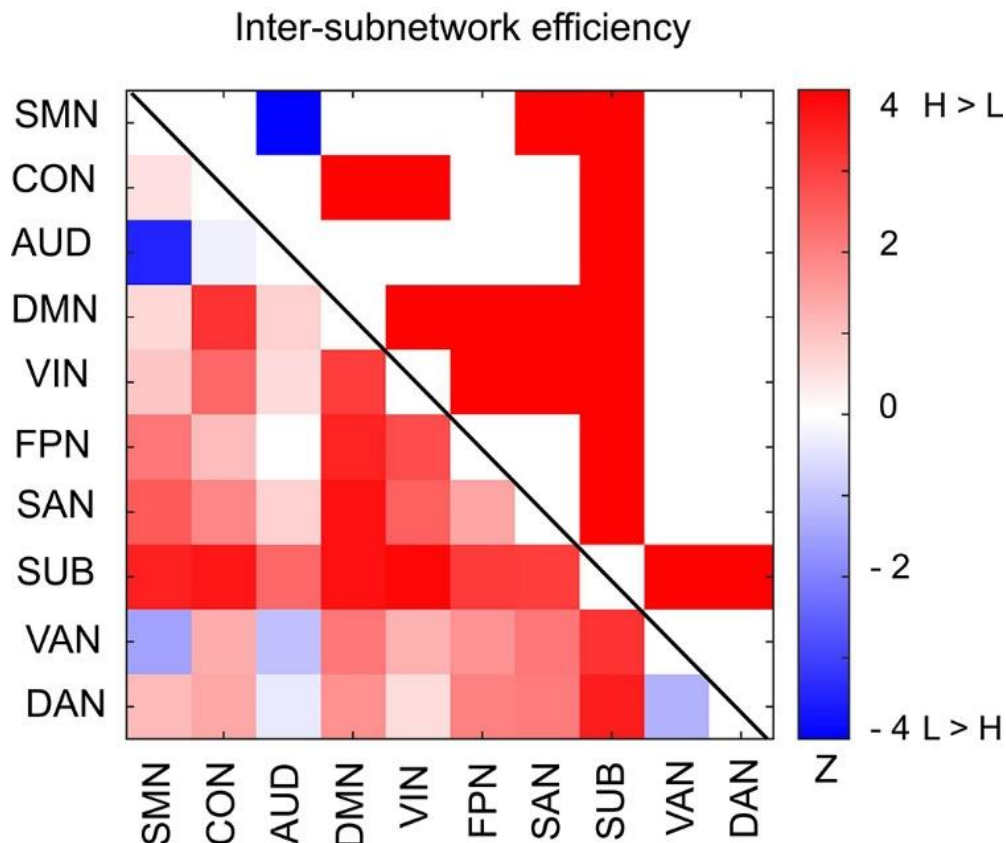


**Figure 3.6. Differences in inter-subnetwork efficiency between high and low encoding states.** Inter-subnetwork efficiency ( $E_{is}$ ) was computed for each pair of subnetworks. Color bar indicates Z-value derived from Wilcoxon signed-rank test across participants. Subnetwork pairs showing significant differences ( $P < 0.05$ , FDR corrected) are marked in color (red, high > low; blue, low > high) in the upper triangle of the matrix.

Furthermore, we asked whether functional integration between specific pairs of subnetworks differs between the high and low encoding states. For this aim, we defined “inter-subnetwork efficiency” ( $E_{is}$ ), which quantifies integration between each subnetwork pair. We found significant differences in inter-subnetwork efficiency between the high and low encoding states in many subnetwork pairs (surviving FDR correction among  $_{10}C_2 = 45$  tests; Figure 3.6). Specifically, higher inter-subnetwork efficiency for the high encoding state was observed among

---

some subnetworks, e.g., between the SUB, DMN, and VIN and the rest of the subnetworks ( $z_{(24)} > 2.3813$ ,  $P < 0.0173$ ). Only the SMN-AUD pair showed lower inter-subnetwork efficiency for the high encoding state ( $z_{(24)} = -3.4575$ ,  $P = 0.0005$ ).

We also examined modularity, an index of how well a network can be partitioned into distinct communities [8], [29]. However, we did not find a significant difference in modularity between the high and low encoding states ( $z_{(24)} = 0.1480$ ,  $P = 0.8824$ ; see Discussion for more details). Although modularity is a measure of segregation, it should be noted that high (or low) modularity does not necessarily indicate low (or high) global efficiency (Pan and Sinha 2009; Meunier, Lambiotte, and Bullmore 2010). When we examined the window-to-window correlation between modularity and global efficiency, we did not find a significant relationship between the two metrics (Pearson  $r = 0.059 \pm 0.410$ ;  $z_{(24)} = 0.7130$ ,  $P = 0.4758$ ).

### 3.3.6 Multivariate pattern classification using graph metrics as features

Graph analysis is considered an effective method for extracting a concise set of features from a large-scale network. If a set of graph metrics (e.g., participation coefficients computed at a subnetwork level) represent the large-scale network architecture well, one network state can be discriminated from another using multi-dimensional vectors of the graph metrics, instead of using the entire connectivity matrices. Building on this idea, we attempted to classify the high and low encoding states using the graph metrics of integration and segregation derived from the 224-node network. Specifically, we performed across-participant binary classification using support vector machine (SVM) with leave-one-out cross validation. When we used the subnetwork-wise PCs (i.e., 10 features) as the input of the SVM classifier, we were able to reliably distinguish the high from low encoding states with 84% classification accuracy ( $P = 0.0015$ , permutation test; Figure 3.7A). Likewise, when we used subnetwork-wise local efficiency, we obtained a classification accuracy of 78% ( $P = 0.0013$ , permutation test; Figure 3.7B). Notably, when we used the entire FC patterns (i.e., Fisher Z-transform of Pearson's correlation coefficients,  ${}_{224}C_2 = 24,976$  features) as the input,

classification accuracy dropped to chance levels (38%,  $P = 0.9865$ , permutation test), likely because of the curse of dimensionality.

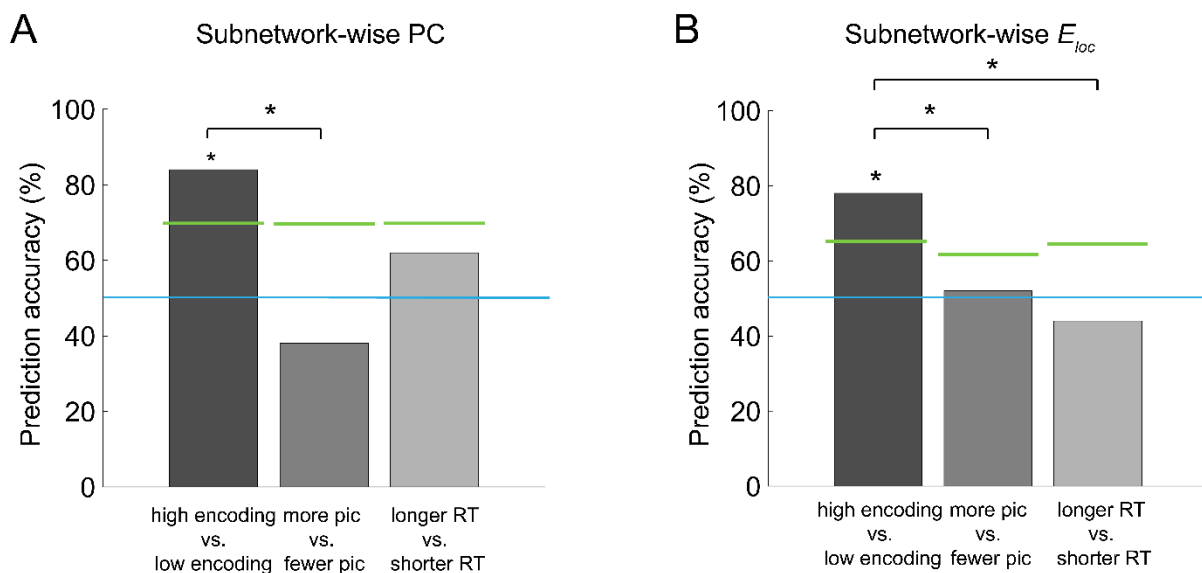


**Figure 3.7. Multivariate classification analysis using graph metrics.** (A) Prediction accuracy of support vector machine (SVM) classifier using subnetwork-wise PCs as the input. (B) Prediction accuracy of SVM classifier using subnetwork-wise local efficiency as the input. Bar graphs represent prediction accuracy obtained by different criteria for sorting time windows: encoding performance and two control criteria (proportion of picture trials and RT for semantic judgment). Asterisks indicate statistical significance ( $P < 0.05$ , permutation test). Green lines indicate significance threshold determined by permutation null distributions. The blue lines indicate the theoretical chance level (i.e., 50%).

To ensure that the observed differences in the functional network architecture associated with encoding performance were not caused by other confounding factors, such as visual responses to pictures or reaction times (RTs) for semantic judgment, we performed two control analyses, as follows. First, to assess the influence of simple visual stimulation on functional network architecture, we sorted the windows based on the proportion of picture trials (varied across



windows because of occasional fixation trials), instead of dividing the states based on encoding performance. We used the same SVM approach as above, but this time to classify the periods with more picture trials and those with fewer picture trials (“more pic” vs. “fewer pic”; split at the participant-specific medians). In this control analysis, we did not see significant classification accuracy either with the subnetwork-wise PCs (38%,  $P = 0.8296$ , permutation test; Figure 3.7A) nor with the subnetwork-wise local efficiency (52%,  $P = 0.4511$ , permutation test; Figure 3.7B). Second, to examine the influence of RT for semantic judgment, we sorted the windows based on average RT computed within each window. We ran the SVM analysis to classify the periods of longer average RT and those of shorter average RT (“longer RT” vs. “shorter RT”; split at the participant-specific medians). Again, we did not observe significant classification accuracy either with the subnetwork-wise PCs (62%,  $P = 0.2122$ , permutation test; Figure 3.7A) or with the subnetwork-wise local efficiency (44%,  $P = 0.8040$ , permutation test; Figure 3.7B). Furthermore, we confirmed that classification based on encoding performance generally resulted in higher accuracy than that based on the proportion of pictures or RT, either with PCs (encoding vs. pictures:  $P = 0.0076$ ; encoding vs. RT:  $P = 0.1448$ ; Figure 3.7A) or with local efficiency (encoding vs. pictures:  $P = 0.0192$ ; encoding vs. RT:  $P = 0.0098$ ; Figure 3.7B). Overall, these results suggest that the observed differences in functional network architecture were specifically related to encoding performance, not to simple visual stimulation or RT for semantic judgment.

### **3.3.7 Robustness check**

To check the robustness of our findings (particularly the graph analysis applied to the large-scale network; Figure 3.5), we performed a number of additional analyses. First, we confirmed that our results were robust across a range of window sizes and proportional thresholds (Supplementary

file 1F). Importantly, our finding of higher global efficiency during the high encoding state was maintained even for much shorter window sizes (at a minimum of 7.2 s). Second, the results did not change when we used overlapping sliding windows (in a steps of 1 TR; Supplementary file 1G). Third, the results were unchanged when we shifted the time series by 5 s to take hemodynamic delay into account (Supplementary file 1H), or when we used task fMRI time series instead of residuals (see Methods; Supplementary file 1I). Fourth, we confirmed that our results were unchanged when we used both high- and low-confidence hit trials to define the window-wise encoding performance (Supplementary file 1J). Fifth, the results remained the same when we used the top and bottom tertiles or quartiles instead of median split to classify the time windows based on encoding performance (Supplementary file 1K and 1L; Supplementary figure S2). Finally, the results did not change after controlling for the effect of time passed within each session or across sessions (see Methods; Supplementary file 1M), ruling out the possibility that our findings were simply driven by gradual changes in psychological states over time (e.g., a decrease in concentration/motivation) or by primacy/recency effects. It should be emphasized that the significant differences in graph metrics were observed only in association with encoding performance, not with the proportion of picture trials or with RT for semantic judgment (Supplementary file 1N and 1O).

To cross-validate our findings regarding large-scale network characteristics, we repeated the same analyses using an independent atlas [9], which consisted of 285 nodes (see Supplementary file 1P). The results were consistent across the two atlases (Supplementary file 1Q; Supplementary figures S3–S5), further demonstrating the robustness of the findings. Likewise, the graph metrics computed on the 226-node network (i.e., the bilateral hippocampus combined with the Power atlas) also showed consistent results (Supplementary file 1R).

### **3.3.8 Possible effects of overall functional connectivity strength**

For the graph analysis described above, we applied proportional thresholding to obtain unweighted graphs. Although this method has been widely used in previous research [5], [6], a recent study raised a concern [23], suggesting a possible influence of overall FC strength on graph metrics

computed by this method (it should be noted that the use of absolute thresholding or unthresholded weighted graphs may not effectively circumvent this issue, as discussed in the paper mentioned above). Specifically, if overall FC strength of a given connectivity matrix is weaker, the graph constructed from that connectivity matrix by proportional thresholding can include less-reliable (or false-positive) edges more frequently. This may confound graph metrics. In other words, differences in the reliability of edges between two graphs could result in spurious differences in graph metrics.

To refute this possibility, we examined the “edge reliability” of large-scale graphs separately for the high and low encoding states. Here, edges were defined as reliable if they existed consistently across time windows more than by chance (see Methods). We found that the proportions of reliable edges were significantly high in both high and low encoding states (relative to randomized networks; Supplementary file 1S), and that they were not statistically different from each other ( $z_{(24)} = 1.6817$ ,  $P = 0.0926$ ; Supplementary figure S6). In theory, a lower proportion of reliable edges (i.e., a higher proportion of false-positive edges) may result in a higher value of global efficiency, because it can introduce random connections between unrelated nodes [23]. In our case, the proportion of reliable edges was numerically higher for the high encoding state across a range of proportional thresholds (Supplementary file 1S). Therefore, if differences in edge reliability between the two states confounded our results, we would have found higher global efficiency during the low encoding state. However, this is the opposite of what we observed, ruling out the possibility that our findings were mere artifacts arising from less reliable edges.

To further examine potential effects of overall FC strength, we performed an additional analysis using “adjusted” graph metrics, in which we regressed out the effect of overall FC strength estimated for each time window (see Methods). When we compared the high and low encoding states, we found no significant differences in these adjusted graph metrics (see Supplementary file 1T). This suggests that overall FC strength shared a considerable amount of variance (on a window-by-window basis) with the graph metrics of integration/segregation. Importantly, however, the multivariate analysis using the adjusted subnetwork-wise PC resulted in a significant

classification accuracy (84%,  $P = 0.0203$ , permutation test), indicating that the subnetwork-wise measure of integration still contains sufficient information for distinguishing between the high and low encoding states. On the other hand, the multivariate analysis using the adjusted subnetwork-wise  $E_{loc}$  did not provide significant classification accuracy (38%,  $P = 0.7194$ , permutation test). This may imply that the result for the subnetwork-wise segregation associated with encoding performance is difficult to disentangle from the effect of overall FC strength, at least in this case.

### 3.3.9 Addressing possible concerns about motion confounds

Another issue is the potential effects of motion confounds on graph metrics. To examine this issue, we computed framewise displacement (FD) as an index of head motion [17]–[19]. We found a subtle but significant difference in mean FD between the high and low encoding states (high:  $0.1324 \pm 0.0242$ , low:  $0.1395 \pm 0.0314$ ;  $z_{(24)} = -3.0270$ ,  $P = 0.0025$ ), and the window-wise FD was correlated with window-wise memory encoding performance (Pearson's  $r = -0.0904 \pm 0.1635$ ;  $z_{(24)} = -2.3005$ ,  $P = 0.0214$ ) and global efficiency (Pearson's  $r = -0.1743 \pm 0.2701$ ;  $z_{(24)} = -2.5696$ ,  $P = 0.0102$ ). This raises the concern that our results could have been affected by motion artifacts. To address this issue, we performed a set of supplement analyses as below.

First, we repeated the analysis with including only half of the participants ( $n = 13$ ) such that the difference in mean FD between the high and low encoding states became minimal in the subsample. In this subset of participants, mean FD was closely matched between the two states (high:  $0.1265 \pm 0.0142$ , low:  $0.1265 \pm 0.0129$ ; signed rank = 39,  $P = 0.6848$ ), and the window-wise FD was not correlated with either memory encoding performance (Pearson's  $r = 0.0032 \pm 0.1077$ ; signed rank = 47,  $P = 0.9460$ ) or global efficiency (Pearson's  $r = -0.0778 \pm 0.2716$ ; signed rank = 33,  $P = 0.4143$ ). The difference in global efficiency between the two states remained significant (signed rank = 89,  $P = 0.0007$ ; Supplementary file 1U), indicating that the findings with this subset could not be explained by motion-derived confounds.

Second, to minimize potential impacts of motion confounds on graph metrics, we repeated the analyses using another denoising method that included an extended set of nuisance regressors and motion scrubbing (hereafter referred to as “32P+scrubbing” denoising; see Methods). This denoising method was effective for reducing the difference in mean FD between the high and low encoding states (high:  $0.1078 \pm 0.0096$ , low:  $0.1093 \pm 0.0086$ ;  $z_{(24)} = -1.9238$ ,  $P = 0.0544$ ) and the correlations of the window-wise FD with memory encoding performance (Pearson’s  $r = -0.0742 \pm 0.1794$ ;  $z_{(24)} = -1.8700$ ,  $P = 0.0615$ ) and global efficiency (Pearson’s  $r = -0.0429 \pm 0.2557$ ;  $z_{(24)} = -0.9014$ ,  $P = 0.3674$ ). The results based on 32P+scrubbing denoising revealed a significant difference in global efficiency between the high and low encoding states ( $z_{(24)} = 4.0495$ ,  $P = 0.0001$ ; Supplementary file 1V). The SVM classification analysis using the subnetwork-wise PCs also showed significant classification accuracy (74%,  $P = 0.0260$ ; for more details, see Supplementary figures S7-S10 and Discussion).

Third, we performed multivariate classification analysis using the graph metrics adjusted for the window-wise FD. The results revealed significant classification accuracy with the subnetwork-wise PCs adjusted for the window-wise FD (92%,  $P = 0.0049$ , permutation test), indicating that the graph metrics retained information about the encoding states even after controlling for window-wise FD. This result held true for the graph metrics based on 32P+scrubbing denoising (84%,  $P = 0.0244$ , permutation test).

Taken together, the results of these analyses indicate that our finding of large-scale integration associated with memory encoding performance cannot be accounted for by motion confounds.

### **3.4 Discussion**

We demonstrated dynamic reconfiguration of a large-scale functional brain network associated with moment-to-moment fluctuations in encoding performance. Importantly, we observed a higher level of network integration during periods of high (vs. low) encoding performance. This effect was mainly driven by increased inter-subnetwork integration of the subcortical, default mode, and visual networks with other subnetworks. Furthermore, dynamic reconfiguration of functional brain network architecture was uniquely related to encoding performance, and not accounted for by the effect of simple visual stimulation or RT for semantic judgment.

#### **Time-varying FC among memory-related brain regions**

Previous neuroimaging studies have repeatedly shown that successful memory encoding is associated with activation/deactivation of specific brain regions, particularly the SME regions (including the medial temporal lobe and prefrontal cortex) (Wagner et al. 1998; Brewer et al. 1998; Paller and Wagner 2002; Reber et al. 2002; Uncapher and Rugg 2005; Kim 2011) and SFE regions (including the posterior cingulate cortex and temporoparietal junction) (Wagner and Davachi 2001; Otten and Rugg 2001; Daselaar, Prince, and Cabeza 2004; Kim 2011). However, the ways in which the dynamic interaction among these regions supports successful memory encoding remain unclear. By analyzing time-varying FC within short time windows (~36 s), we showed that FC among SME regions, particularly between the hippocampus and occipital cortex, was higher during periods of high (vs. low) encoding performance. This may indicate that successful encoding of visual information is supported by functional interaction between the visual area and the hippocampus, a key structure for memory formation [39].

#### **Dynamic reconfiguration of a large-scale functional brain network**

Successful memory encoding is likely to be influenced by many state factors, such as arousal, attention to external stimuli, and motivation to perform a task [40]–[42]. Therefore, moment-to-moment fluctuations in encoding performance may be associated with dynamic interactions among

a diverse set of brain systems, beyond the so-called memory system. In the current study, we observed differential FC patterns between the high and low encoding states, both within and across many subnetworks. Importantly, during the periods of high (vs. low) encoding performance, FC was increased between specific brain regions, whereas it was decreased between another specific set of regions. For instance, we observed significant FC increases within the DMN, such as among the superior frontal gyrus, angular gyrus, and precuneus. This finding is in line with a recent study reporting increased within-network connectivity in the DMN associated with successful memory encoding [43]. On the other hand, we observed significant FC decreases between the SMN and AUD, such as between the postcentral gyrus and superior temporal gyrus. This observation is in accord with the notion that neither auditory perception nor motor execution is required for incidental encoding of visual stimuli. In addition, we observed a marked increase in FC between distant brain regions, whereas FC decreases were prominent (but not limited to) between neighboring regions. These findings suggest a systematic reconfiguration of the large-scale functional brain network related to incidental encoding performance, rather than a uniform increase/decrease in FC across the entire network.

Recent studies have shown the dynamic nature of FC patterns in the brain and their contributions to a variety of cognitive functions [3], [5], [7], [21], [44], [45]. For example, one study reported that dynamic FC in a time window of 40 s reflected moment-to-moment fluctuations in arousal level as indicated by RTs on a continuous performance task, and spontaneous eyelid closure [21]. Other studies have also shown that dynamic reconfigurations of FC patterns are observed across many situations, from performance of cognitively demanding tasks (e.g., working memory and Stroop tasks) to simple perceptual detection of visual and auditory stimuli [5], [6], [46]–[48]. Our findings extend previous studies by showing that temporal fluctuations in FC across a large-scale brain network are related to incidental memory encoding.

Although our finding of large-scale integration associated with memory encoding is novel, several previous studies investigated FC changes during memory encoding. For example, a previous study reported increased FC between the hippocampus and neocortical regions including the occipital cortex during successful (vs. unsuccessful) memory encoding [49]. It should be noted that FC between the hippocampus and cortical areas is also considered to be important for memory

retrieval [50], [51]. One recent study examining FC patterns during memory retrieval reported greater FC among many brain regions during correct (vs. incorrect) retrieval [52]. This finding may suggest that successful memory encoding and retrieval are at least partially supported by common patterns of network dynamics. However, it has also been reported that functional coupling between specific regions (e.g., the hippocampus and other regions in the DMN) are different between memory encoding and retrieval [53]. Future studies should directly compare large-scale network configurations during encoding and retrieval in a single experiment.

### **Network integration and segregation associated with incidental encoding performance**

Using graph analysis, we tested whether dynamic changes in network integration/segregation are associated with encoding performance. At the entire-network level, we found a higher degree of integration (as measured by global efficiency) during periods of high encoding performance. When we examined individual subnetworks, we generally observed greater integration and weaker segregation during the high encoding state. A notable exception was the SUB, which showed both higher PCs and local efficiency during the high encoding state. This indicates that the subcortical nodes (specifically the thalamus and putamen) are more interconnected with other nodes in the same subnetwork, as well as the nodes belonging to other subnetworks. Therefore, the subcortical nodes may play a unique role in incidental memory encoding, contributing to both within- and across-subnetwork functional interactions and serving as a hub to support large-scale network integration [54].

When we examined inter-subnetwork graph metrics, we found that the SUB and DMN, among others, showed higher inter-subnetwork integration with many other subnetworks during the high encoding state. In addition to the aforementioned hub-like characteristics of the SUB, the increased inter-subnetwork integration between the DMN and other subnetworks should also be noted. Previous studies have shown the involvement of the DMN in episodic memory [55]–[57]. It has also been reported that FC within the DMN is associated with subsequent memory performance [43], [58]. Our results, on the other hand, revealed that inter-subnetwork integration between the DMN and other subnetworks was related to within-individual time-to-time



fluctuations of memory performance, providing further evidence of a central role of the DMN in successful memory encoding. Notably, some regions within the DMN (e.g., the posterior cingulate cortex and temporoparietal junction) exhibited the SFE (i.e., decreased trial-related activation for successful [vs. unsuccessful] memory encoding). This highlights the importance of examining both trial-related activation changes and FC changes to understand the role of specific brain systems in certain cognitive functions.

### **Multivariate pattern classification using graph metrics**

Our multivariate analysis using graph metrics demonstrated that functional network architecture during the high and low encoding states can be reliably classified using subnetwork-wise metrics of integration. That is, the graph metrics defined at the subnetwork level contain sufficient information to distinguish the high from low encoding states. When we used the entire connectivity patterns as the input, the classification accuracy dropped to chance levels. This suggests that the use of graph metrics can efficiently reduce the number of features and achieve more accurate predictions. The method employed here could be useful for many other applications, such as comparing large-scale brain networks between specific disease groups and normal controls. In addition to other methods of connectivity pattern classification [5], [59], [60], multivariate analysis using graph metrics could facilitate future research on large-scale brain network architecture.

### **Methodological considerations for graph analysis**

Several details of the analysis should be noted. First, recent studies have suggested that motion confounds may affect temporal fluctuations in FC patterns [19]. To address this concern, we performed three supplement analyses, all of which supported our main findings. As suggested by recent reports [16], [19], we found that a denoising method that included an extended set of nuisance regressors combined with motion scrubbing was effective for reducing FD and its correlation with graph metrics. Notably, our finding of large-scale integration associated with memory encoding was maintained regardless of the choice of denoising method. Another strategy, which was more effective for reducing the influence of FD on graph metrics, was to focus on a subset of participants whose FD was less dependent on memory performance. One possible

explanation for the significant correlation we observed between FD and memory performance in the full sample is that some individuals may have exhibited a fluctuating level of arousal over the course of the task, which could be positively correlated with window-wise memory performance and negatively correlated with mean FD [19]. Such momentary fluctuations in arousal level would be inevitable for some individuals, particularly during tasks that require continuous performance (like the one we used). The fact that we observed a significant difference in global efficiency between the high and low encoding states even after excluding such participants provides strong support for our finding. Although motion confounds would be expected to influence both momentary encoding performance and dynamic FC patterns, our supplement analyses suggest that the finding of large-scale integration associated with encoding performance was above and beyond the effect of motion confounds.

Second, our measure of inter-subnetwork integration ( $E_{is}$ ) and PCs characterize different aspects of a network: the former quantifies integration between a specific pair of subnetworks, whereas the latter quantifies the diversity of inter-subnetwork connections of a particular subnetwork/node to all other subnetworks [15], [22], [27], [28]. In our case, the results from these two metrics convergently suggested the core roles of the subcortical, default-mode, and visual systems in incidental encoding of visual stimuli. The present results concerning global efficiency and modularity should also be considered. Although we observed increased global efficiency during the high encoding state, this was not accompanied by decreased modularity. Unlike global efficiency, modularity is a metric based on the community structure of a network (Rubinov and Sporns 2010; Wig 2017). Thus, the current results may suggest that the number of long-range connections across modules was increased, rather than indicating that the network became less modular.

Third, our additional analysis controlling for overall FC strength suggested that window-to-window fluctuations in the graph metrics substantially covaried with overall FC strength. This makes it difficult to disentangle the effects of network integration/segregation from those of overall FC strength in examining dynamic changes in functional brain networks. However, this does not necessarily undermine the usefulness of graph analysis, for the following reasons. First, correcting

for overall FC strength would be overly strict: although it rules out the possibility that observed differences in graph metrics result from artifacts of spurious weak connections, it could also remove real differences in network architecture [23]. Second, even if graph metrics and overall FC strength are highly correlated, subnetwork-wise graph metrics may provide additional insight into detailed network organization (e.g., specificity and heterogeneity among subnetworks), which may not be captured by overall FC strength. Importantly, we examined the reliability of edges across time windows, and confirmed that our findings are not attributable to differential proportions of false-positive edges (Zalesky et al. 2014; van den Heuvel et al. 2017). In addition, the dynamic reconfiguration of the large-scale network associated with encoding performance was also supported by an analysis that did not rely on graph metrics. Overall, it is unlikely that our findings were solely due to temporal fluctuations in overall FC strength.

### **The effects of denoising methods**

To remove possible motion confounds, we used six motion regressors together with nuisance signals derived from WM and CSF in the first place (hereafter “8P denoising”). We further repeated our main analyses using a more stringent denoising method that included an extended set of nuisance regressors and motion scrubbing (“32P+scrubbing” denoising). Notably, the results were largely consistent across the two denoising methods, especially for large-scale network integration. However, we also observed a few differences in the results between the two denoising methods. Below we discuss possible reasons for these differences.

First, when we used 32P+scrubbing denoising, FC differences in the memory-related regions between the high and low encoding states did not survive at the FDR-corrected statistical threshold (Supplementary figure S7). However, we did observe similar trends, to those we observed in 8P denoising, particularly for FC between the hippocampus and occipital cortex ( $z_{(24)} = 2.6503$ ,  $P = 0.0080$ ). Meanwhile, the within-subnetwork connectivity among the SME regions was not significantly different between the two states ( $z_{(24)} = 0.6861$ ,  $P = 0.4926$ ). This may suggest that FC did not necessarily increase among all nodes of the SME regions, but specifically increased between the hippocampus and occipital cortex. It should also be noted that the SME ROIs were defined on the basis of a meta-analysis of task activation, not FC. This may explain why the results

of FC patterns among the SME regions were less robust than those of the 224-node large-scale network. Importantly, in our additional analysis using the 226-node network (i.e., the bilateral hippocampus ROIs from the SME regions plus the 224 nodes from the Power atlas), the increase in FC between the hippocampus and occipital cortex during the high (vs. low) encoding state was also significant when 32P+scrubbing denoising was used (right hippocampus-left middle occipital gyrus:  $z_{(24)} = 3.5652$ ,  $P = 0.0004$ ). Overall, the finding of increased FC between the hippocampus and occipital cortex during the high encoding state was found in both 8P and 32P+scrubbing denoising.

Second, in 32P+scrubbing denoising, the multivariate classification result for the subnetwork-wise PCs remained significant (classification accuracy = 74%,  $P = 0.0260$ ), which is consistent with the results of the analysis using 8P denoising. On the other hand, the classification accuracy was not significant (28%,  $P = 0.8228$ ) when we used the subnetwork-wise PCs adjusted for overall FC strength. This may indicate that the strategy of adjusting for overall FC strength would be too strict because it could remove potentially true information about network organization, as mentioned in previous studies [23]. In an attempt to at least control for potential effects of motion confounds, we performed the multivariate classification analysis using the subnetwork-wise PCs adjusting for window-wise FD, instead of adjusting for overall FC strength. This analysis resulted in significant classification accuracy (92%,  $P = 0.0049$ ), ruling out the possibility that the successful classification of the high and low encoding states was merely due to motion confounds.

Third, when we used 32P+scrubbing denoising, we observed a significant difference in modularity between the high and low encoding states (Supplementary file 1V). Interestingly, modularity was higher in the high (vs. low) encoding states. It is important to distinguish between different graph metrics: unlike global efficiency and local efficiency, modularity is computed based on the community structure of a network. Theoretically, a highly modular network can simultaneously exhibit a high level of functional integration through sparse long-range connections across communities [30], [31]. One interesting possibility is that during the high encoding state, the large-scale functional networks may have been reconfigured to co-express high levels of

integration and segregation [62], [63]. However, the results of modularity difference associated with memory encoding performance were not robust compared with those of global efficiency (e.g., Supplementary file 1F), making it difficult to draw a conclusion at this stage. Future research should investigate this possibility by examining multiple metrics of integration and segregation to clarify how dynamic changes in network complexity are related to cognition and behavior.

### **Limitations and future perspectives**

Although our study provides a number of novel findings about the dynamic FC associated with incidental memory encoding, several limitations should be considered. First, the current study was unable to determine the causal directions between dynamic FC and temporal fluctuations in encoding performance. Recent studies have shown that large-scale FC patterns during short time periods (e.g., 30–40 s) show dynamic fluctuation even in the resting state [15], [61], [64]–[66]. Given these previous findings, it could be hypothesized that intrinsic, spontaneous dynamics of FC patterns underlie moment-to-moment fluctuations in encoding performance. However, we cannot rule out the possibility that different levels of encoding performance across the time windows induce time-varying FC patterns. Future research should be conducted to test these two possibilities using methods that can causally manipulate large-scale FC patterns [67], [68].

Second, to examine dynamic changes in FC patterns, we divided the fMRI time series into short time windows, and sorted the windows in reference to behavioral data (i.e., encoding performance). As a result, we sorted the FC patterns into two “states.” However, this does not necessarily mean that there are only two dynamic FC states; it is possible that there are more than two dissociable states and only some of them are truly related to encoding performance. Some recent studies have employed other approaches, first identifying distinct dynamic FC states based solely on neural data, then relating individual states to behavioral measures [15], [21], [64]. Such approaches could provide further detail about the relationships between dynamic network architecture and memory encoding. Meanwhile, in the current study, comparison of the FC patterns of high and low encoding states revealed very similar patterns. This implies that approaches attempting to identify distinct dynamic states solely using neural data may not work for our data. However, approaches using behavioral data as references for classification may be particularly

useful when behavioral performance is associated with very subtle differences in network states, as in the current study.

Third, although our study demonstrated large-scale integration associated with moment-to-moment memory performance within individuals, we did not examine how the network characteristics are related to inter-individual variations in memory performance. To further clarify the role of large-scale networks in memory encoding, future studies should investigate how these networks are related to individual differences in memory performance in both healthy and clinical populations.

### 3.5 References for chapter 3

- [1] H. Kim, “Neural activity that predicts subsequent memory and forgetting: A meta-analysis of 74 fMRI studies,” *Neuroimage*, vol. 54, no. 3, pp. 2446–2461, 2011.
  
- [2] J. D. Power, A. L. Cohen, S. M. Nelson, G. S. Wig, K. A. Barnes, J. A. Church, A. C. Vogel, T. O. Laumann, F. M. Miezin, B. L. Schlaggar, and S. E. Petersen, “Functional Network Organization of the Human Brain,” *Neuron*, vol. 72, pp. 665–678, 2011.
  
- [3] M. W. Cole, D. S. Bassett, J. D. Power, T. S. Braver, and S. E. Petersen, “Intrinsic and Task-Evoked Network Architectures of the Human Brain,” *Neuron*, vol. 83, no. 1, pp. 238–251, 2014.
  
- [4] J. R. Cohen, C. L. Gallen, E. G. Jacobs, T. G. Lee, and M. D. Esposito, “Quantifying the Reconfiguration of Intrinsic Networks during Working Memory,” *PLoS One*, vol. 9, no. 9, pp. 1–8, 2014.
  
- [5] S. Sadaghiani, J.-B. Poline, A. Kleinschmidt, and M. D’Esposito, “Ongoing dynamics in large-scale functional connectivity predict perception,” *Proc. Natl. Acad. Sci.*, vol. 112, no. 27, pp. 8463–8468, 2015.
  
- [6] J. R. Cohen and M. D. Esposito, “The Segregation and Integration of Distinct Brain Networks and Their Relationship to Cognition,” *J. Neurosci.*, vol. 36, no. 48, pp. 12083–12094, 2016.

- [7] H. Mohr, U. Wolfensteller, R. F. Betzel, B. Mis, O. Sporns, J. Richiardi, and H. Ruge, “Integration and segregation of large-scale brain networks during short-term task automatization,” *Nat. Commun.*, vol. 7, no. 13217, 2016.
- [8] A. J. Westphal, S. Wang, and J. Rissman, “Episodic Memory Retrieval Benefits from a Less Modular Brain Network Organization,” *J. Neurosci.*, vol. 37, no. 13, pp. 3523–3531, 2017.
- [9] E. M. Gordon, T. O. Laumann, B. Adeyemo, J. F. Huckins, W. M. Kelley, and S. E. Petersen, “Generation and Evaluation of a Cortical Area Parcellation from Resting-State Correlations,” *Cereb. Cortex*, vol. 26, no. 1, pp. 288–303, 2016.
- [10] A. D. Wagner, D. L. Schacter, M. Rotte, W. Koutstaal, A. Maril, a M. Dale, B. R. Rosen, and R. L. Buckner, “Building memories: remembering and forgetting of verbal experiences as predicted by brain activity.,” *Science (80-. )*, vol. 281, pp. 1188–1191, 1998.
- [11] B. B. Biswal, M. Mennes, X. N. Zuo, S. Gohel, C. Kelly, S. M. Smith, C. F. Beckmann, J. S. Adelstein, R. L. Buckner, S. Colcombe, A. M. Dogonowski, M. Ernst, D. Fair, M. Hampson, M. J. Hoptman, J. S. Hyde, V. J. Kiviniemi, R. Kotter, S. J. Li, C. P. Lin, M. J. Lowe, C. Mackay, D. J. Madden, K. H. Madsen, D. S. Margulies, H. S. Mayberg, K. McMahon, C. S. Monk, S. H. Mostofsky, B. J. Nagel, J. J. Pekar, S. J. Peltier, S. E. Petersen, V. Riedl, S. A. Rombouts, B. Rypma, B. L. Schlaggar, S. Schmidt, R. D. Seidler, G. J. Siegle, C. Sorg, G. J. Teng, J. Veijola, A. Villringer, M. Walter, L. Wang, X.



- C. Weng, S. Whitfield-Gabrieli, P. Williamson, C. Windischberger, Y. F. Zang, H. Y. Zhang, F. X. Castellanos, and M. P. Milham, “Toward discovery science of human brain function,” *Proc.Natl.Acad.Sci.U.S.A*, vol. 107, no. 10, pp. 4734–4739, 2010.
- [12] S. Vahdat, M. Darainy, T. E. Milner, and D. J. Ostry, “Functionally Specific Changes in Resting-State Sensorimotor Networks after Motor Learning,” *J. Neurosci.*, vol. 31, no. 47, pp. 16907–16915, 2011.
- [13] H. Cao, M. M. Plichta, A. Schäfer, L. Haddad, O. Grimm, M. Schneider, C. Esslinger, P. Kirsch, A. Meyer-Lindenberg, and H. Tost, “Test-retest reliability of fMRI-based graph theoretical properties during working memory, emotion processing, and resting state,” *Neuroimage*, vol. 84, pp. 888–900, 2014.
- [14] A. Tompariy, K. Duncan, and L. Davachi, “Consolidation of Associative and Item Memory Is Related to Post-Encoding Functional Connectivity between the Ventral Tegmental Area and Different Medial Temporal Lobe Subregions during an Unrelated Task,” *J. Neurosci.*, vol. 35, no. 19, pp. 7326–31, 2015.
- [15] J. M. Shine, P. G. Bissett, P. T. Bell, O. Koyejo, J. H. Balsters, K. J. Gorgolewski, C. A. Moodie, and R. A. Poldrack, “The Dynamics of Functional Brain Networks: Integrated Network States during Cognitive Task Performance,” *Neuron*, vol. 92, no. 2, pp. 544–554, 2016.
- [16] R. Ciric, D. H. Wolf, J. D. Power, D. R. Roalf, G. L. Baum, K. Ruparel, R. T. Shinohara,

- M. A. Elliott, S. B. Eickhoff, C. Davatzikos, R. C. Gur, R. E. Gur, D. S. Bassett, and T. D. Satterthwaite, “Benchmarking of participant-level confound regression strategies for the control of motion artifact in studies of functional connectivity,” *Neuroimage*, vol. 154, no. March, pp. 174–187, 2017.
- [17] J. D. Power, K. A. Barnes, A. Z. Snyder, B. L. Schlaggar, and S. E. Petersen, “Spurious but systematic correlations in functional connectivity MRI networks arise from subject motion,” *Neuroimage*, vol. 59, no. 3, pp. 2142–2154, 2012.
- [18] J. D. Power, A. Mitra, T. O. Laumann, A. Z. Snyder, B. L. Schlaggar, and S. E. Petersen, “Methods to detect, characterize, and remove motion artifact in resting state fMRI,” *Neuroimage*, vol. 84, pp. 320–341, 2014.
- [19] T. O. Laumann, A. Z. Snyder, A. Mitra, E. M. Gordon, C. Gratton, B. Adeyemo, A. W. Gilmore, S. M. Nelson, J. J. Berg, D. J. Greene, J. E. McCarthy, E. Tagliazucchi, H. Laufs, B. L. Schlaggar, N. U. F. Dosenbach, and S. E. Petersen, “On the Stability of BOLD fMRI Correlations,” *Cereb. Cortex*, vol. 27, no. 10, pp. 4719–4732, 2017.
- [20] U. Braun, A. Schäfer, H. Walter, S. Erk, N. Romanczuk-Seiferth, L. Haddad, J. I. Schweiger, O. Grimm, A. Heinz, H. Tost, A. Meyer-Lindenberg, and D. S. Bassett, “Dynamic reconfiguration of frontal brain networks during executive cognition in humans,” *Proc. Natl. Acad. Sci. U. S. A.*, vol. 112, no. 37, pp. 11678–11683, 2015.
- [21] C. Wang, J. L. Ong, A. Patanaik, J. Zhou, and M. W. L. Chee, “Spontaneous eyelid

- closures link vigilance fluctuation with fMRI dynamic connectivity states.,” *Proc. Natl. Acad. Sci. U. S. A.*, vol. 113, no. 34, pp. 9653–9658, 2016.
- [22] M. Rubinov and O. Sporns, “NeuroImage Complex network measures of brain connectivity : Uses and interpretations,” *Neuroimage*, vol. 52, no. 3, pp. 1059–1069, 2010.
- [23] M. P. van den Heuvel, S. C. de Lange, A. Zalesky, C. Seguin, B. T. T. Yeo, and R. Schmidt, “Proportional thresholding in resting-state fMRI functional connectivity networks and consequences for patient-control connectome studies: Issues and recommendations,” *Neuroimage*, vol. 152, pp. 437–449, 2017.
- [24] C. Chang and C. Lin, “LIBSVM : A Library for Support Vector Machines,” *ACM Trans. Intell. Syst. Technol.*, vol. 2, no. 27, pp. 1–27, 2011.
- [25] P. Golland and B. Fischl, *Permutation Tests for Classification: Towards Statistical Significance in Image-Based Studies*. Berlin, Heidelberg: Springer, 2003.
- [26] K. A. Paller, M. Kutas, and A. R. Mayes, “Neural correlates of encoding in an incidental learning paradigm.,” *Electroencephalogr. Clin. Neurophysiol.*, vol. 67, no. 4, pp. 360–371, 1987.
- [27] J. D. Power, B. L. Schlaggar, C. N. Lessov-Schlaggar, and S. E. Petersen, “Evidence for hubs in human functional brain networks,” *Neuron*, vol. 79, no. 4, pp. 798–813, 2013.
- [28] S. Marek, K. Hwang, W. Foran, M. N. Hallquist, and B. Luna, “The Contribution of

- Network Organization and Integration to the Development of Cognitive Control,” *PLoS Biol.*, vol. 13, no. 12, pp. 1–25, 2015.
- [29] G. S. Wig, “Segregated Systems of Human Brain Networks,” *Trends Cogn. Sci.*, vol. 21, no. 12, pp. 981–996, 2017.
- [30] D. Meunier, R. Lambiotte, and E. T. Bullmore, “Modular and hierarchically modular organization of brain networks,” *Front. Neurosci.*, vol. 4, no. DEC, pp. 1–11, 2010.
- [31] R. K. Pan and S. Sinha, “Modularity produces small-world networks with dynamical time-scale separation,” *Epl*, vol. 85, no. 6, 2009.
- [32] J. B. Brewer, Z. Zhao, J. E. Desmond, G. H. Glover, and J. D. Gabrieli, “Making memories: brain activity that predicts how well visual experience will be remembered.” *Science (80-. )*, vol. 281, no. 5380, pp. 1185–1187, 1998.
- [33] K. A. Paller and A. D. Wagner, “Observing the transformation of experience into memory,” *Trends Cogn. Sci.*, vol. 6, no. 2, pp. 93–102, 2002.
- [34] P. J. Reber, R. M. Siwec, D. R. Gitleman, T. B. Parrish, M.-M. Mesulam, and K. A. Paller, “Neural correlates of successful encoding identified using functional magnetic resonance imaging,” *J. Neurosci.*, vol. 22, no. 21, pp. 9541–9548, 2002.
- [35] M. R. Uncapher and M. D. Rugg, “Encoding and the Durability of Episodic Memory: A Functional Magnetic Resonance Imaging Study,” *J. Neurosci.*, vol. 25, no. 31, pp. 7260–

7267, 2005.

- [36] A. D. Wagner and L. Davachi, “Cognitive neuroscience: Forgetting of things past,” *Curr. Biol.*, vol. 11, pp. 964–967, 2001.
- [37] L. J. Otten and M. D. Rugg, “When more means less: Neural activity related to unsuccessful memory encoding,” *Curr. Biol.*, vol. 11, no. 19, pp. 1528–1530, 2001.
- [38] S. M. Daselaar, S. E. Prince, and R. Cabeza, “When less means more: Deactivations during encoding that predict subsequent memory,” *Neuroimage*, vol. 23, no. 3, pp. 921–927, 2004.
- [39] H. Eichenbaum, A. P. Yonelinas, and C. Ranganath, “The Medial Temporal Lobe and Recognition Memory,” *Annu. Rev. Neurosci.*, vol. 30, no. 1, pp. 123–152, 2007.
- [40] M. M. Chun and N. B. Turk-Browne, “Interactions between attention and memory,” *Curr. Opin. Neurobiol.*, vol. 17, no. 2, pp. 177–184, 2007.
- [41] M. J. Gruber, B. D. Gelman, and C. Ranganath, “States of Curiosity Modulate Hippocampus-Dependent Learning via the Dopaminergic Circuit,” *Neuron*, vol. 84, no. 2, pp. 486–496, 2014.
- [42] A. Tambini, U. Rimmel, E. A. Phelps, and L. Davachi, “Emotional brain states carry over and enhance future memory formation,” *Nat. Neurosci.*, vol. 20, no. 2, pp. 271–278, 2016.

- [43] E. Simony, C. J. Honey, J. Chen, O. Lositsky, Y. Yeshurun, A. Wiesel, and U. Hasson, “Dynamical reconfiguration of the default mode network during narrative comprehension,” *Nat. Commun.*, vol. 7, no. May 2015, pp. 1–13, 2016.
- [44] D. S. Bassett, N. F. Wymbs, M. A. Porter, P. J. Mucha, J. M. Carlson, and S. T. Grafton, “Dynamic reconfiguration of human brain networks during learning,” *Proc. Natl. Acad. Sci. U. S. A.*, vol. 108, no. 18, pp. 7641–46, 2011.
- [45] D. S. Bassett, M. Yang, N. F. Wymbs, and S. T. Grafton, “Learning-induced autonomy of sensorimotor systems,” *Nat. Neurosci.*, vol. 18, no. 5, pp. 744–754, 2015.
- [46] J. Gonzalez-Castillo, C. W. Hoy, D. a. Handwerker, M. E. Robinson, L. C. Buchanan, Z. S. Saad, and P. a. Bandettini, “Tracking ongoing cognition in individuals using brief, whole-brain functional connectivity patterns,” *Proc. Natl. Acad. Sci.*, vol. 112, no. 28, pp. 8762–8767, 2015.
- [47] J. M. Spielberg, G. A. Miller, W. Heller, and M. T. Banich, “Flexible brain network reconfiguration supporting inhibitory control,” *Proc. Natl. Acad. Sci.*, vol. 112, no. 32, pp. 1–6, 2015.
- [48] D. Godwin, R. L. Barry, and R. Marois, “Breakdown of the brain’s functional network modularity with awareness,” *Proc Natl Acad Sci U S A*, vol. 112, no. 12, pp. 3799–3804, 2015.
- [49] C. Ranganath, A. Heller, M. X. Cohen, C. J. Brozinsky, and J. Rissman, “Functional

- connectivity with the hippocampus during successful memory formation,” *Hippocampus*, vol. 15, no. 8, pp. 997–1005, 2005.
- [50] D. R. King, M. de Chastelaine, R. L. Elward, T. H. Wang, and M. D. Rugg, “Recollection-Related Increases in Functional Connectivity Predict Individual Differences in Memory Accuracy,” *J. Neurosci.*, vol. 35, no. 4, pp. 1763–1772, 2015.
- [51] M. Ritchey, E. A. Wing, K. S. LaBar, and R. Cabeza, “Neural similarity between encoding and retrieval is related to memory via hippocampal interactions.,” *Cereb. Cortex*, vol. 23, no. 12, pp. 2818–2828, 2013.
- [52] A. M. Schedlbauer, M. S. Copara, A. J. Watrous, and A. D. Ekstrom, “Multiple interacting brain areas underlie successful spatiotemporal memory retrieval in humans,” *Sci. Rep.*, pp. 1–9, 2014.
- [53] W. Huijbers, C. M. A. Pennartz, R. Cabeza, and S. M. Daselaar, “The hippocampus is coupled with the default network during memory retrieval but not during memory encoding,” *PLoS One*, vol. 6, no. 4, 2011.
- [54] P. T. Bell and J. M. Shine, “Neuroscience and Biobehavioral Reviews Subcortical contributions to large-scale network communication,” *Neurosci. Biobehav. Rev.*, vol. 71, pp. 313–322, 2016.
- [55] M. D. Greicius and V. Menon, “Default-Mode Activity during a Passive Sensory Task : Uncoupled from Deactivation but Impacting Activation,” *J. Cogn. Neurosci.*, vol. 16, no.

- 9, pp. 1484–1492, 2004.
- [56] R. N. Spreng and C. L. Grady, “Patterns of Brain Activity Supporting Autobiographical Memory, Propection, and Theory of Mind, and Their Relationship to the Default Mode Network,” *J. Cogn. Neurosci.*, vol. 22, no. 6, pp. 1112–1123, 2009.
- [57] J. R. Andrews-hanna, J. S. Reidler, J. Sepulcre, R. Poulin, and R. L. Buckner, “Functional-Anatomic Fractionation of the Brain’s Default Network,” *Neuron*, vol. 65, no. 4, pp. 550–562, 2010.
- [58] U. Hasson, H. C. Nusbaum, and S. L. Small, “Task-dependent organization of brain regions active during rest.,” *Proc Natl Acad Sci U S A*, vol. 106, no. 26, pp. 10841–10846, 2009.
- [59] M. D. Rosenberg, E. S. Finn, D. Scheinost, X. Papademetris, X. Shen, R. T. Constable, and M. M. Chun, “A neuromarker of sustained attention from whole-brain functional connectivity.,” *Nat. Neurosci.*, vol. 19, no. 1, pp. 165–71, 2016.
- [60] G. Hein, Y. Morishima, S. Leiberg, S. Sul, and E. Fehr, “The brain’s functional network architecture reveals human motives,” *Science (80-. )*, vol. 351, no. 6277, pp. 1074–1078, 2016.
- [61] A. Zalesky, A. Fornito, L. Cocchi, L. L. Gollo, and M. Breakspear, “Time-resolved resting-state brain networks,” *Proc. Natl. Acad. Sci. U. S. A.*, vol. 111, no. 28, pp. 10341–46, 2014.



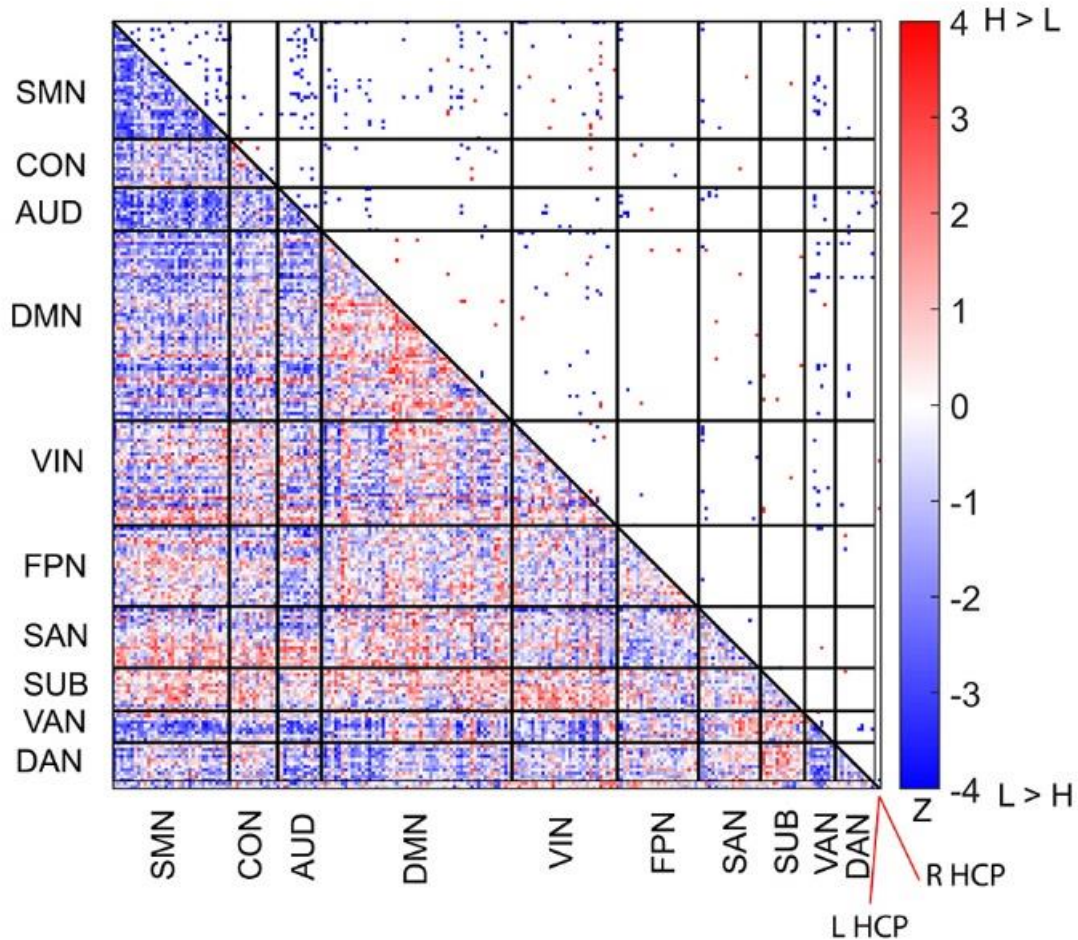
- [62] G. Tononi, O. Sporns, and G. M. Edelman, “A measure for brain complexity: relating functional segregation and integration in the nervous system.,” *Proc. Natl. Acad. Sci.*, vol. 91, no. 11, pp. 5033–5037, 1994.
- [63] D. J. Watts and S. H. Strogatz, “Collective dynamics of ‘small-world’ networks,” *Nature*, vol. 393, no. 6684, pp. 440–442, 1998.
- [64] V. D. Calhoun, R. Miller, G. Pearlson, and T. Adali, “The Chronnectome: Time-Varying Connectivity Networks as the Next Frontier in fMRI Data Discovery,” *Neuron*, vol. 84, no. 2, pp. 262–274, 2014.
- [65] E. A. Allen, E. Damaraju, S. M. Plis, E. B. Erhardt, T. Eichele, and V. D. Calhoun, “Tracking whole-brain connectivity dynamics in the resting state,” *Cereb. Cortex*, vol. 24, no. 3, pp. 663–676, 2014.
- [66] R. F. Betzel, M. Fukushima, Y. He, X. N. Zuo, and O. Sporns, “Dynamic fluctuations coincide with periods of high and low modularity in resting-state functional brain networks,” *Neuroimage*, vol. 127, pp. 287–297, 2016.
- [67] Y. Ezzyat, J. E. Kragel, J. F. Burke, D. F. Levy, A. Lyalenko, P. Wanda, L. O’Sullivan, K. B. Hurley, S. Busygin, I. Pedisich, M. R. Sperling, G. A. Worrell, M. T. Kucewicz, K. A. Davis, T. H. Lucas, C. S. Inman, B. C. Lega, B. C. Jobst, S. A. Sheth, K. Zaghloul, M. J. Jutras, J. M. Stein, S. R. Das, R. Gorniak, D. S. Rizzuto, and M. J. Kahana, “Direct Brain Stimulation Modulates Encoding States and Memory Performance in Humans,” *Curr.*

*Biol.*, vol. 27, no. 9, pp. 1251–1258, 2017.

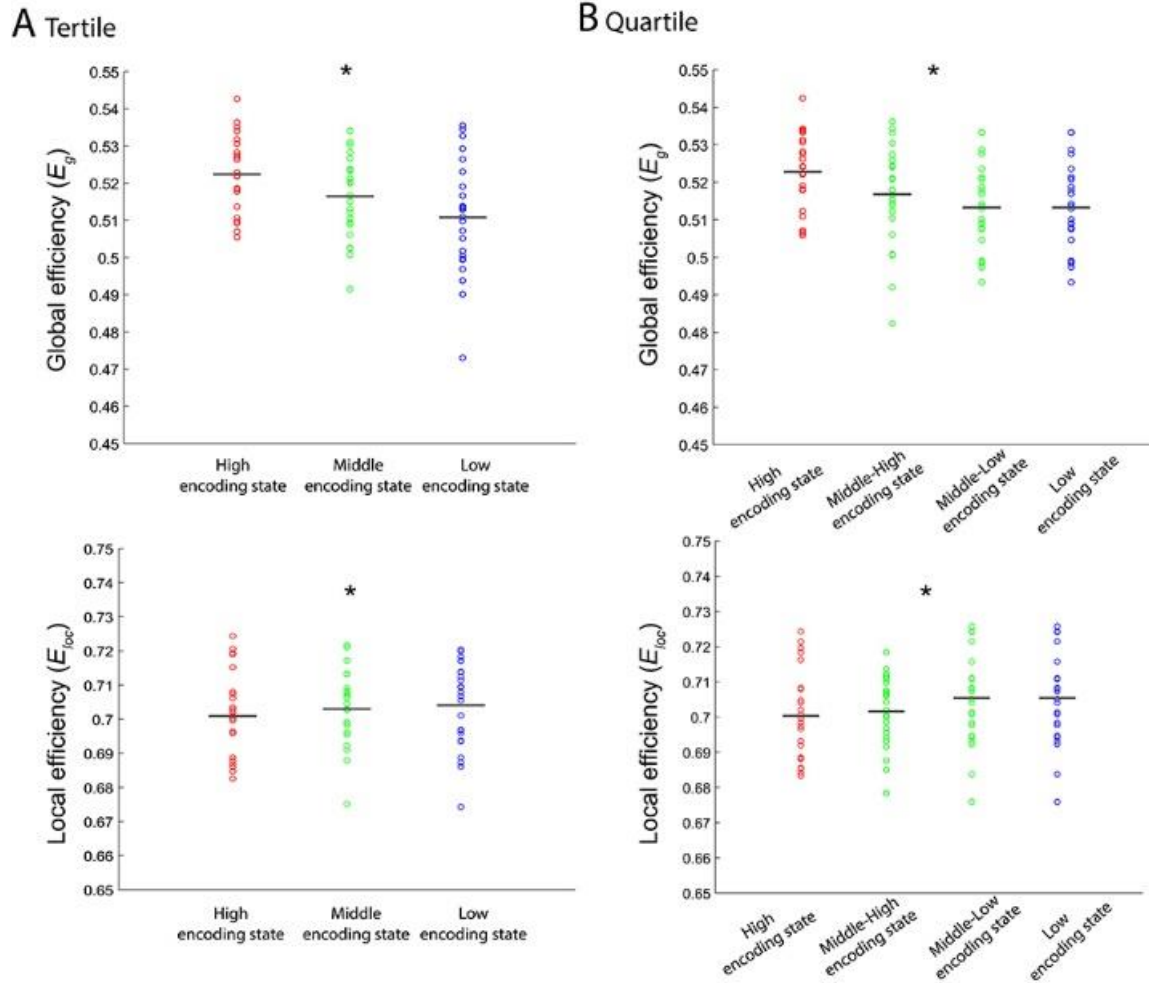
- [68] S. F. Muldoon, F. Pasqualetti, S. Gu, M. Cieslak, S. T. Grafton, J. M. Vettel, and D. S. Bassett, “Stimulation-Based Control of Dynamic Brain Networks,” *PLoS Comput. Biol.*, vol. 12, no. 9, 2016.

### 3.6 Supplementary information for chapter 3

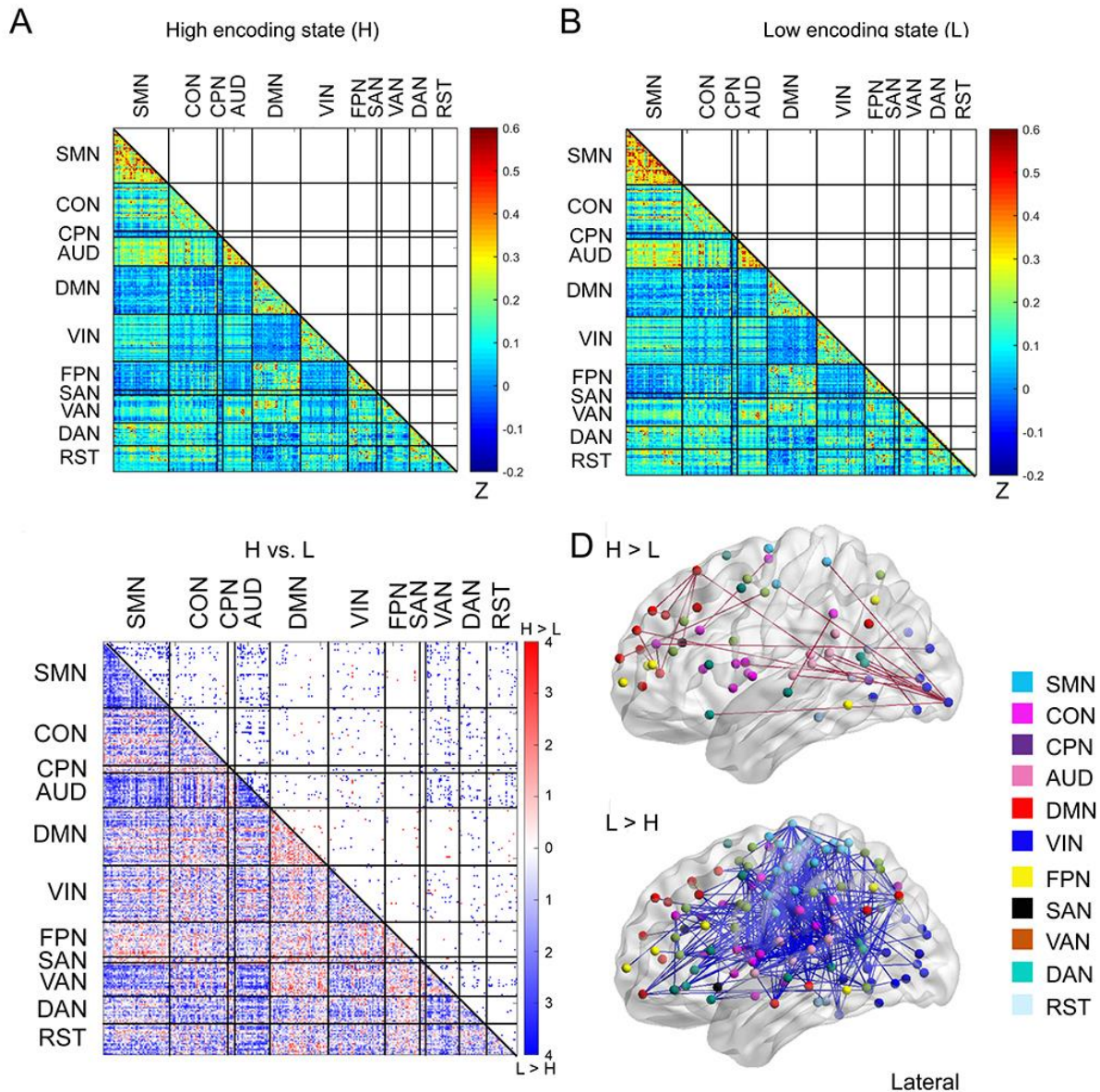
#### 3.6.1 Supplementary figures



**Supplementary figure S1. Difference in functional connectivity patterns between the high and low encoding states in a 226-node network combining the bilateral hippocampus and the Power atlas.** Color bar indicates z values derived from Wilcoxon signed-rank test across participants. L HCP, left hippocampus, R HCP, right hippocampus.



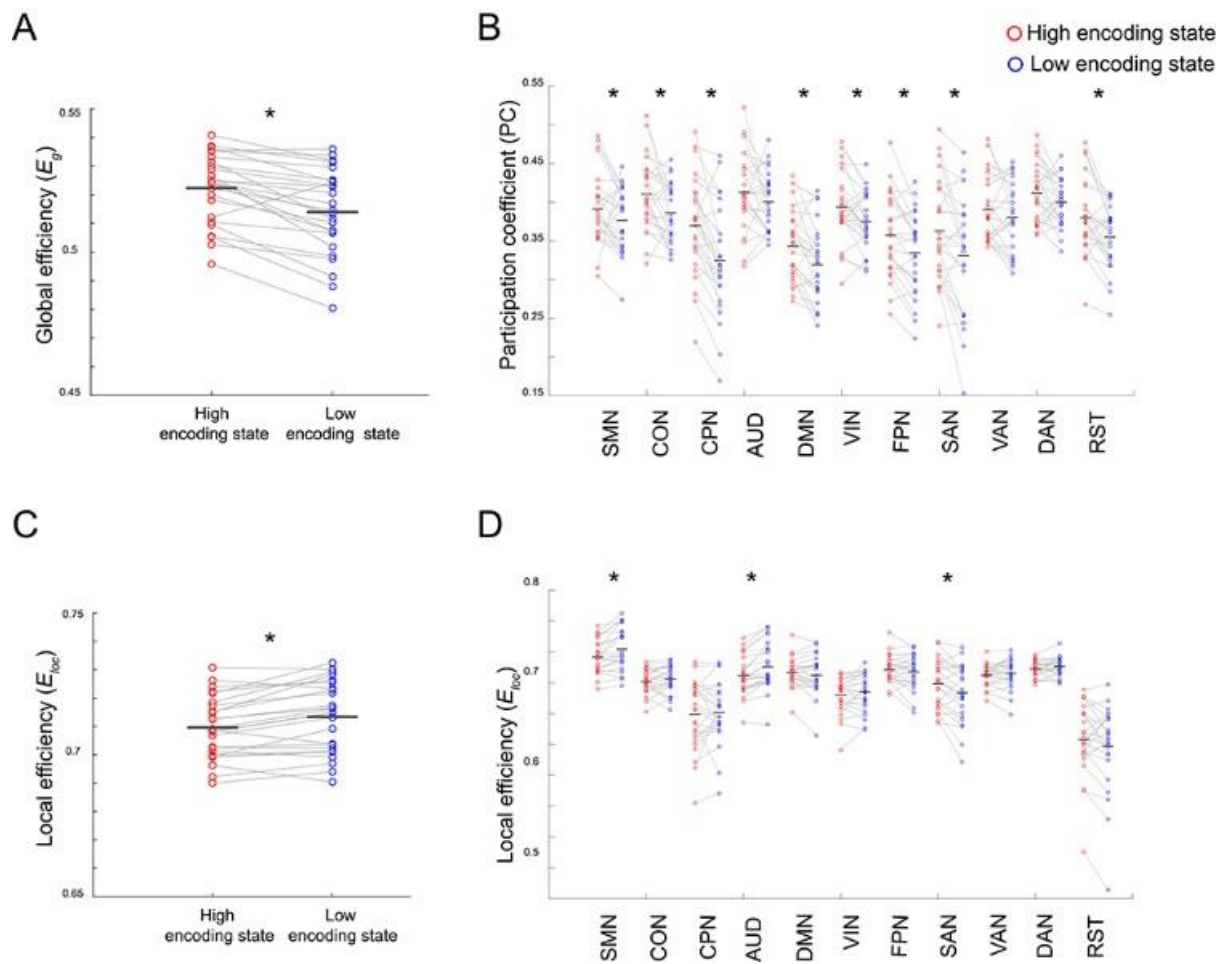
**Supplementary figure S2. Levels of integration/segregation of a 224-node network associated with encoding performance.** (A) Global efficiency and local efficiency during high, middle, and low encoding states. States were defined based on participant-specific tertiles of window-wise encoding performance. (B) Global efficiency and local efficiency during high, middle-high, middle-low, and low encoding states. States were defined based on participant-specific quartiles of window-wise encoding performance. Graph metrics were computed for each time window, then averaged across windows separately for each state. In the analysis shown in this figure, unlike any other analyses, we included 24 participants because we could not define mid tertile or mid quartiles for the remaining one participant. Dots represent individual-participant data. Black horizontal lines indicate across-participant means. Asterisks indicate a significant linear effect of encoding states ( $P < 0.05$ , one-way ANOVA with trend analysis).



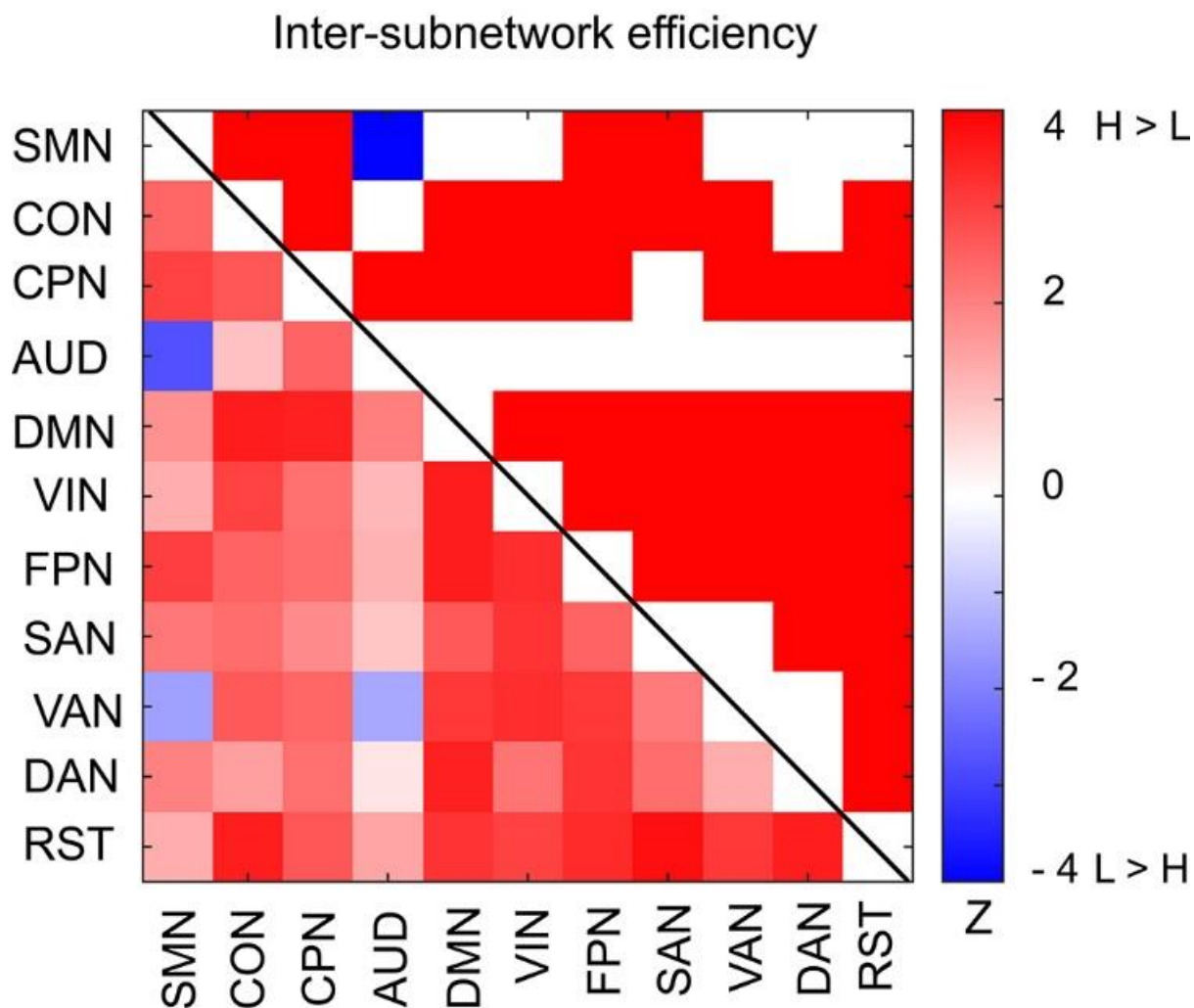
**Supplementary figure S3. Functional connectivity patterns across a 285-node network derived from the Gordon atlas.** (A) Connectivity matrix of the high encoding state, averaged across participants. (B) Connectivity matrix of the low encoding state, averaged across participants. Color bars indicate Fisher's Z-transform of Pearson's correlation coefficients. (C) A matrix illustrating statistical differences in functional connectivity patterns between the high and low encoding states. ROIs belonging to the same subnetwork were grouped together, resulting in 11 subnetworks. Color bar indicates z values derived from Wilcoxon signed-rank test across participants. Connections showing significant differences ( $P < 0.05$ , FDR corrected) are marked in color (red, high > low; blue, low > high) in the upper triangle of the matrix. (D) Three-dimensional (3D) visualizations of significantly greater functional connectivity during the high encoding state. (E) 3D visualizations of significantly greater functional connectivity during the low encoding state. SMN, sensorimotor networks; CON, cingulo-opercular network; CPN,

cingulo-parietal network; AUD, auditory network; DMN, default mode network; VIN, visual network; FPN, fronto-parietal network; SAN, salience network; VAN, ventral attention network; DAN, dorsal attention network; RST, retrosplenial-temporal network.



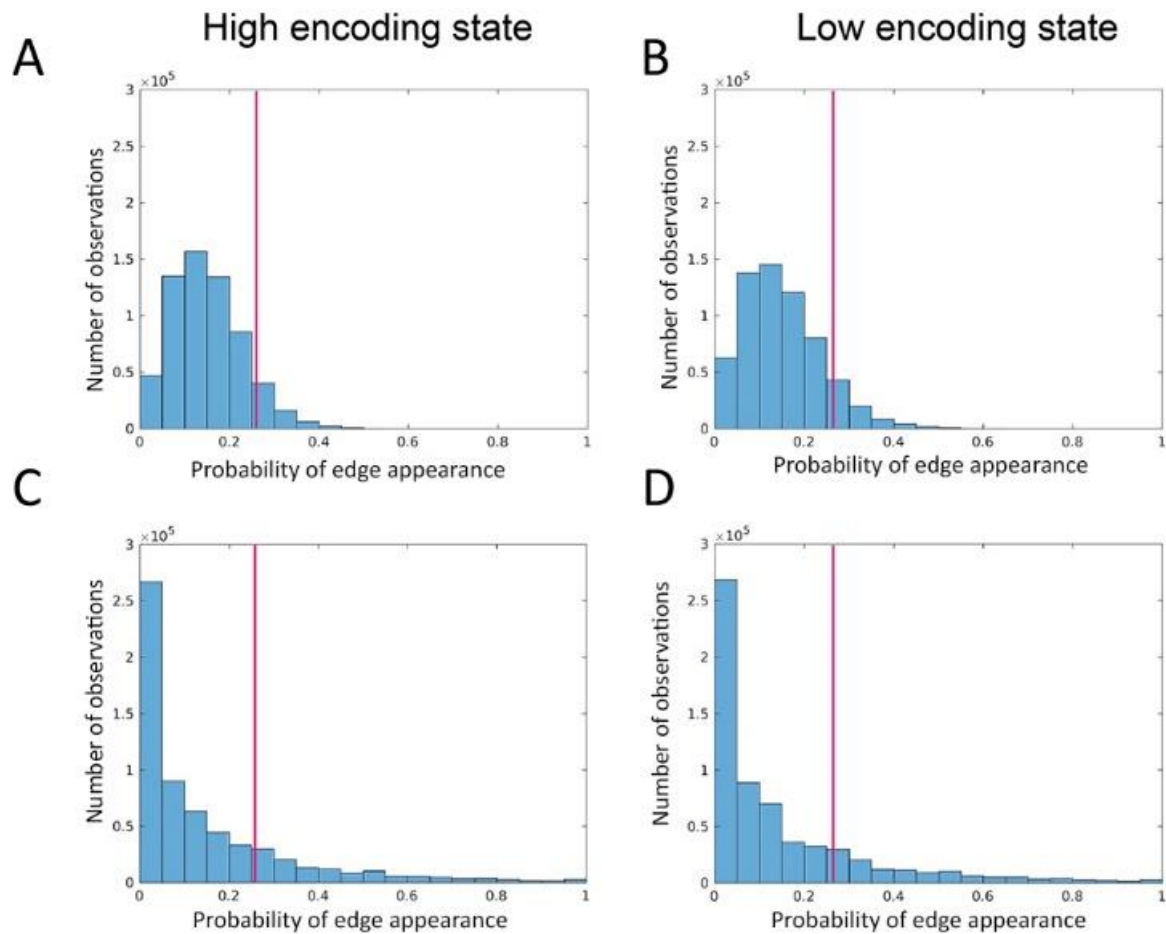


**Supplementary figure S4. Differences in integration/segregation between high and low encoding states for a 285-node network derived from the Gordon atlas.** (A) Global efficiency, a measure of network integration. (B) Participation coefficient (averaged across nodes within each subnetwork), a measure of integration defined at subnetwork level. (C) Local efficiency (averaged across all nodes), a measure of segregation. (D) Local efficiency (averaged across nodes within each subnetwork), a measure of segregation defined at the subnetwork level. Graph metrics were computed for each time window, then averaged across windows separately for each state. Dots represent individual-participant data. Black horizontal lines indicate across-participant means. Asterisks indicate a significant difference between the states ( $P < 0.05$ , FDR corrected for subnetwork-wise metrics).

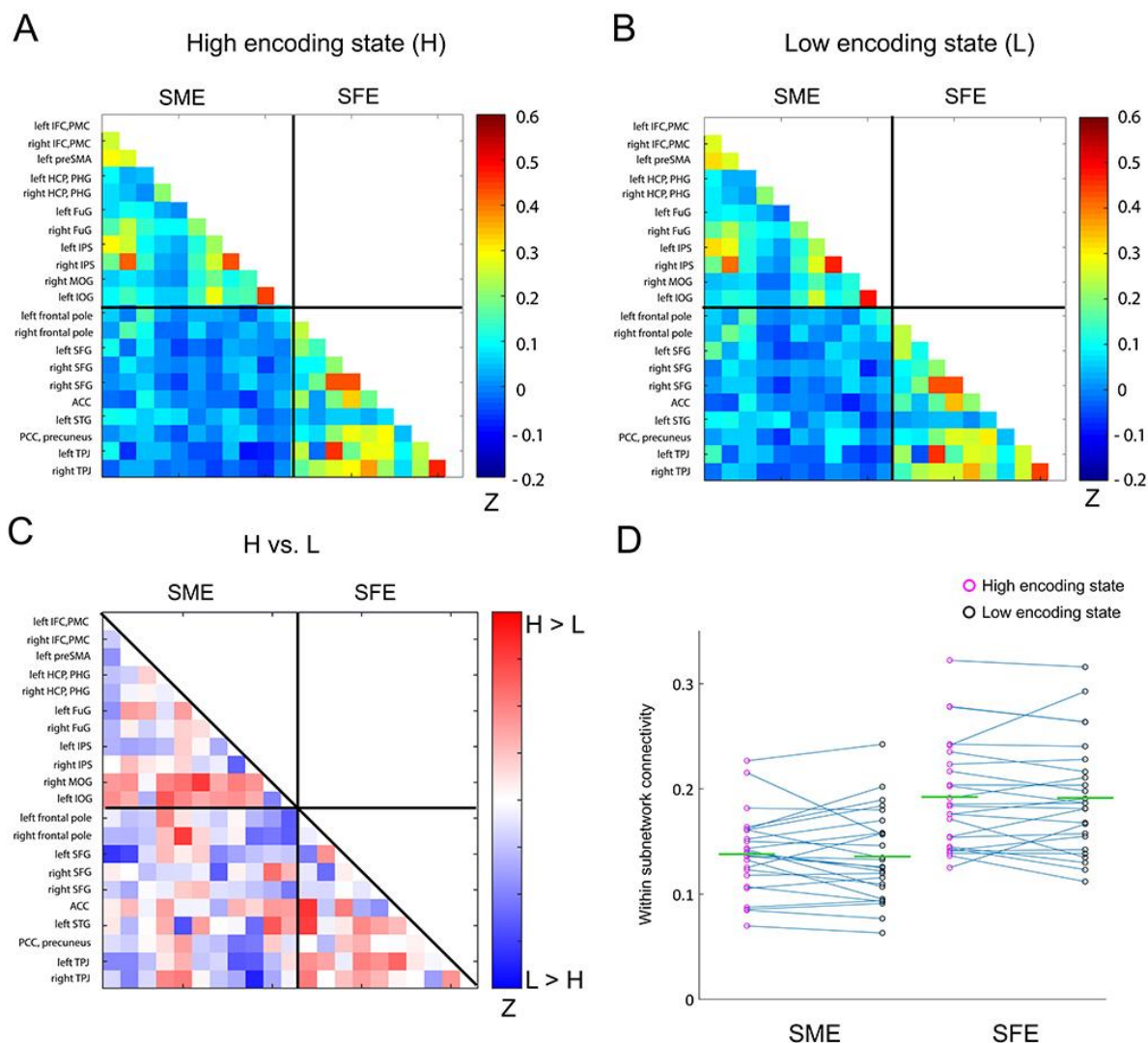


**Supplementary figure S5. Differences in inter-subnetwork efficiency between high and low encoding states for a 285-node network derived from the Gordon atlas.** Inter-subnetwork efficiency ( $E_{is}$ ) was computed for each pair of subnetworks. Color bar indicates z values derived from Wilcoxon signed-rank test across participants. Subnetwork pairs showing significant differences ( $P < 0.05$ , FDR corrected) are marked in color (red, high > low; blue, low > high) in the upper triangle of the matrix.

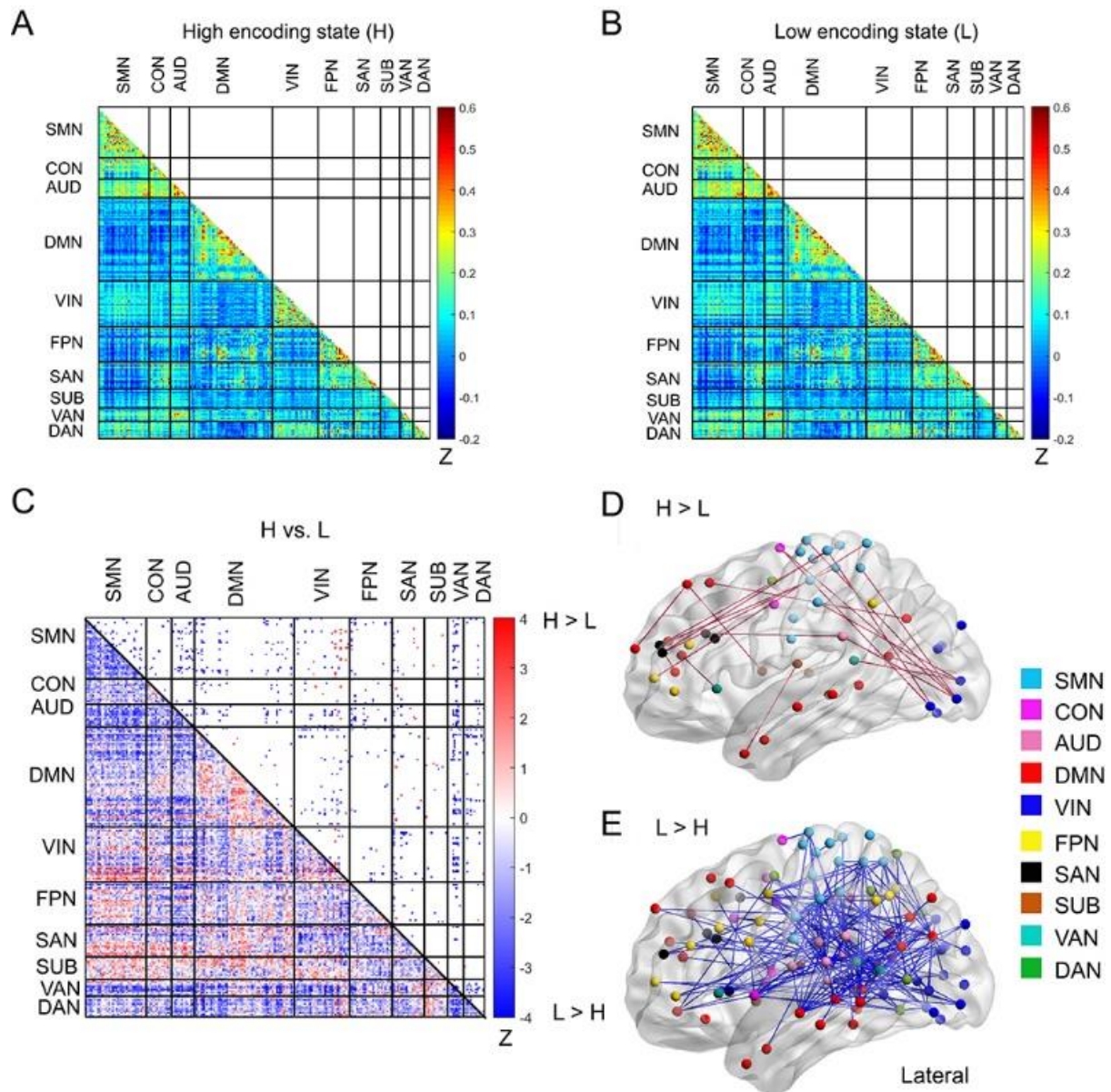




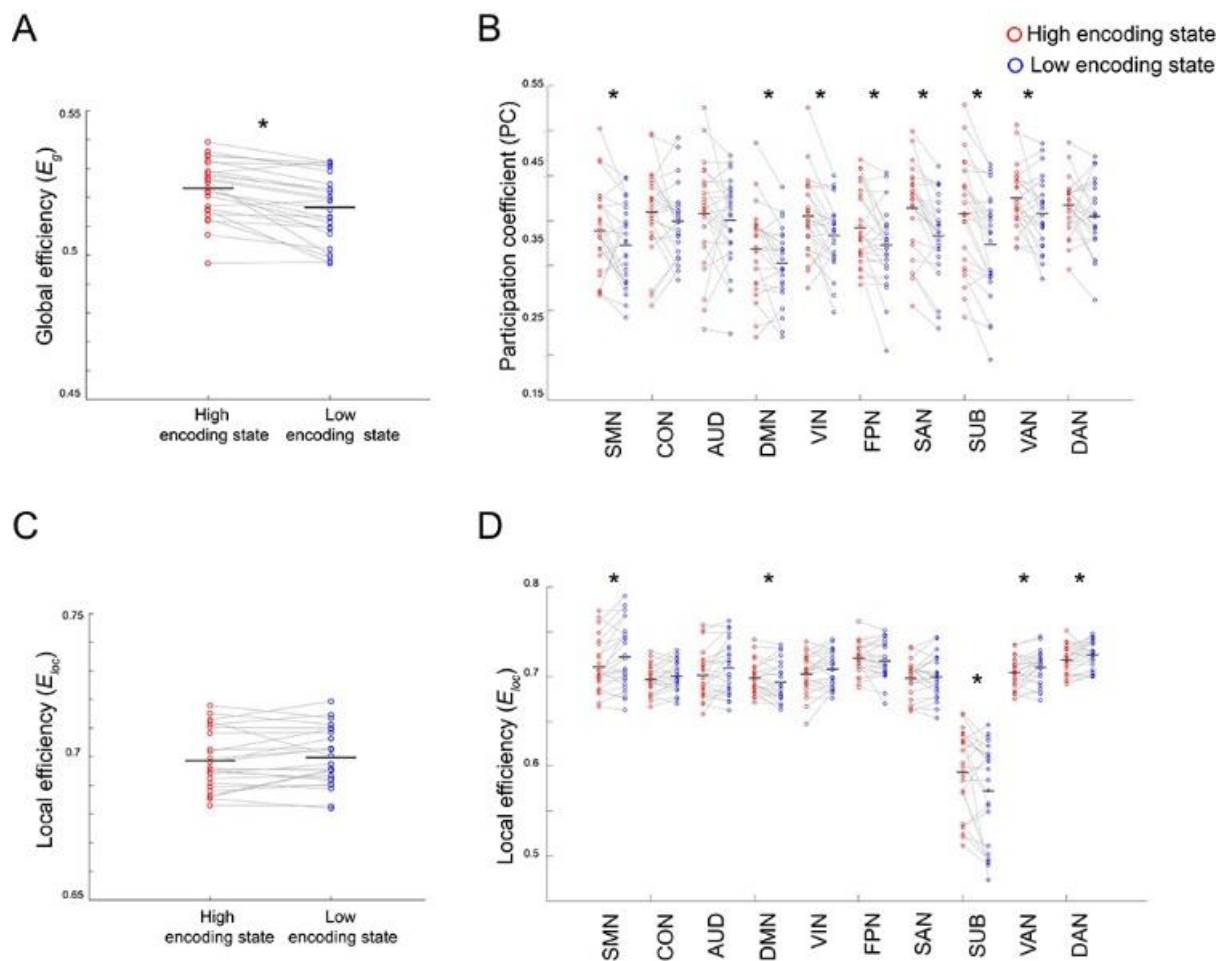
**Supplementary figure S6. Edge reliability analysis.** (A, B) Histograms showing the distributions of the probability of edge appearance in randomized networks. (C, D) Histograms showing the distributions of the probability of edge appearance in real networks. Distributions were first computed for each participant and state, then pooled across participants for illustration. Here, the probability of edge appearance indicates how consistently an edge appears between a given node pair across time windows. An edge is defined as “reliable” if the probability of appearance is higher than the 95th percentile threshold determined by the null distributions derived from randomized networks. The magenta vertical lines indicate the 95th percentile threshold (averaged across participants for illustration).



**Supplementary figure S7. Functional connectivity patterns among memory-related brain regions, derived from 32P+scrubbing denoising.** (A) Connectivity matrix of the high encoding state, averaged across participants. (B) Connectivity matrix of the low encoding state, averaged across participants. Color bars indicate Fisher's Z-transform of Pearson's correlation coefficients. (C) A matrix illustrating statistical differences in functional connectivity patterns between the high and low encoding states. Color bar indicates z values derived from Wilcoxon signed-rank test across participants. (D) Within-subnetwork connectivity for the SME and SFE regions (mean Fisher's Z values of connections within the SME and SFE regions, respectively). Magenta and black circles represent individual-participant data for the high and low encoding states, respectively. Green horizontal lines indicate cross-participant means.

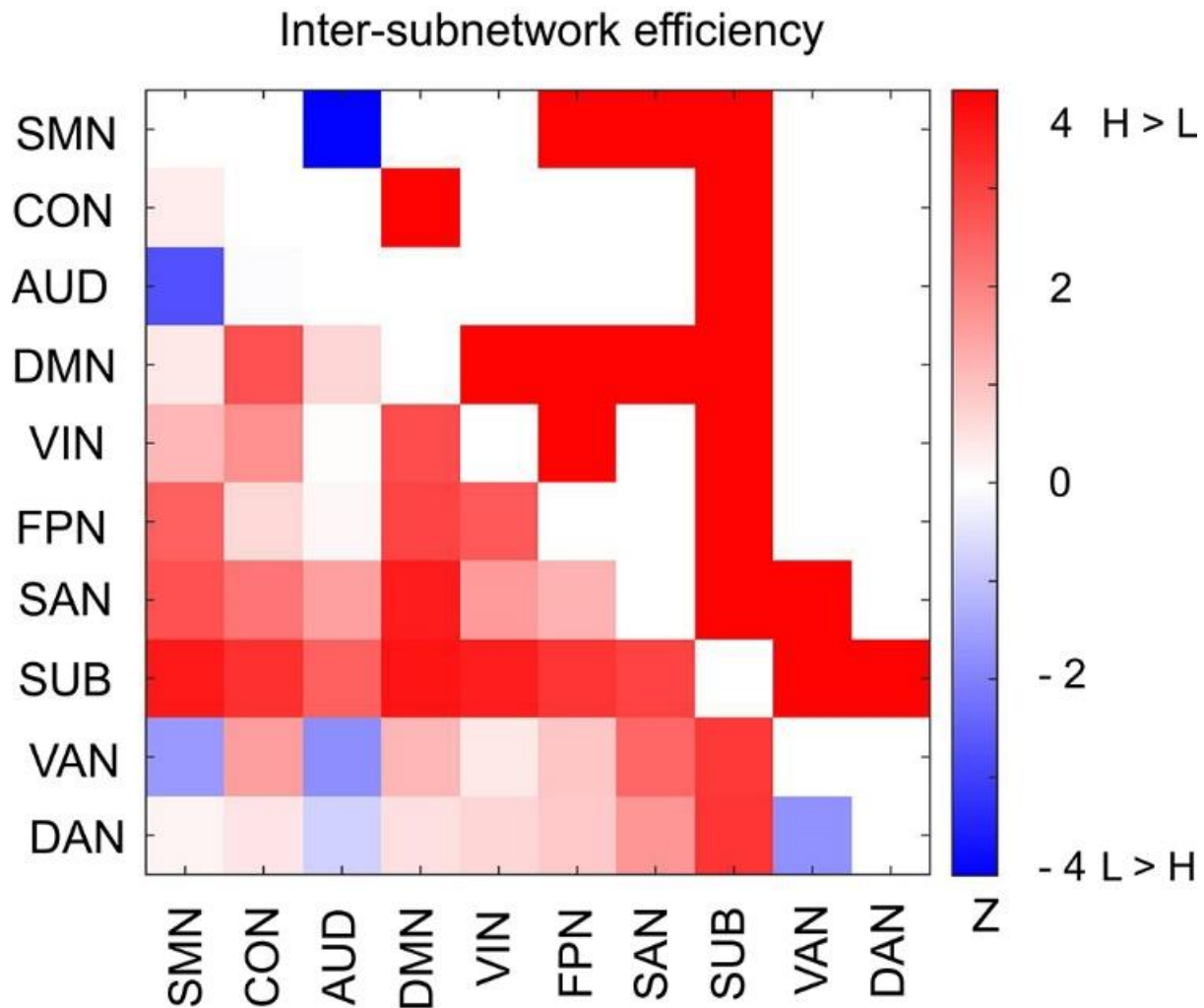


**Supplementary figure S8. Functional connectivity patterns across a 224-node network, derived from 32P+scrubbing denoising.** (A) Connectivity matrix of the high encoding state, averaged across participants. (B) Connectivity matrix of the low encoding state, averaged across participants. Color bars indicate Fisher's Z-transform of Pearson's correlation coefficients. (C) A matrix showing the statistical differences in functional connectivity patterns between the high and low encoding states. ROIs belonging to the same subnetwork were grouped together resulting in 10 subnetworks. Color bar indicates z values derived from Wilcoxon signed-rank test across participants. Connections showing significant differences ( $P < 0.05$ , FDR corrected) are marked in color (red, high > low; blue, low > high) in the upper triangle of the matrix. (D) Three-dimensional (3D) visualizations of significantly greater functional connectivity during the high encoding state. (E) 3D visualizations of significantly greater functional connectivity during the low encoding state.



**Supplementary figure S9. Differences in integration/segregation of a 224-node network between high and low encoding states, derived from 32P+scrubbing denoising.** (A) Global efficiency, a measure of network integration. (B) Participation coefficient (averaged across nodes within each subnetwork), a measure of integration defined at the subnetwork level. (C) Local efficiency (averaged across all nodes), a measure of segregation. (D) Local efficiency (averaged across nodes within each subnetwork), a measure of segregation defined at the subnetwork level. Graph metrics were computed for each time window, then averaged across windows separately for each state. Dots represent individual-participant data. Black horizontal lines indicate across-participant means. Asterisks indicate a significant difference between the states ( $P < 0.05$ , FDR corrected for subnetwork-wise metrics).





**Supplementary figure S10. Differences in inter-subnetwork efficiency between high and low encoding states for a 224-node network, derived from 32P-scrubbing denoising.** Inter-subnetwork efficiency ( $E_{is}$ ) was computed for each pair of subnetworks. Color bar indicates z values derived from Wilcoxon signed-rank test across participants. Subnetwork pairs showing significant differences ( $P < 0.05$ , FDR corrected) are marked in color (red, high > low; blue, low > high) in the upper triangle of the matrix.

### 3.6.2 Supplementary files

#### Supplementary file 1A. Details of 21 ROIs related with memory encoding.

ROI ID	Name of ROI	Hemisphere	MNI coordinates		
			x	y	z
Subsequent memory effect (SME) related areas					
1	Inferior frontal cortex, premotor cortex, precentral gyrus	L	-46	26	19
2	Inferior frontal cortex, premotor cortex	R	48	7	33
3	Pre-supplementary motor cortex	L	-6	14	53
4	Hippocampus, parahippocampal gyrus, amygdala	L	-22	-9	-20
5	Hippocampus, parahippocampal gyrus, amygdala	R	18	-7	-19
6	Fusiform gyrus	L	-42	-46	-29
7	Fusiform gyrus	R	44	-53	-20
8	Intraparietal sulcus	L	-28	-80	35
9	Intraparietal sulcus	R	26	-66	47
10	Middle occipital gyrus	R	28	-89	2
11	Inferior occipital gyrus	L	-32	-92	-12
Subsequent forgotten effect (SFE) related areas					

---

12	Frontal pole	L	-26	54	27
13	Frontal pole	R	38	46	22
14	Superior frontal cortex	L	-36	29	43
15	Superior frontal cortex	R	24	35	41
16	Superior frontal cortex	R	34	31	47
17	Anterior cingulate cortex, ventromedial prefrontal cortex	-	0	45	5
18	Superior temporal gyrus	L	-48	-14	-10
19	Posterior cingulate cortex, precuneus	-	0	-29	40
20	Temporoparietal junction	L	-53	-59	32
21	Temporoparietal junction	R	55	-49	30

*Notes.* ROIs are derived from [1].Table 2 and 6. Coordinates are converted from Talairach to MNI space.

**Supplementary file 1B. Differences in trial-related activation between HH and Miss trials in 21 ROIs related with memory encoding.**

SME				SFE			
Name of ROI	H	<i>z</i>	<i>P</i>	Name of ROI	H	<i>z</i>	<i>P</i>
Inferior frontal cortex (IFC), Premotor cortex (PMC), precentral gyrus	L	4.2647	0.00002	Frontal pole (FP)	L	-1.5471	0.12183
Inferior frontal cortex, Premotor cortex	R	3.6190	0.00030	FP	R	-3.0539	0.00226
Pre-supplementary motor cortex	L	3.0808	0.00206	Superior frontal cortex	L	-2.1929	0.02831
Hippocampus (HCP), Parahippocampal gyrus (PHG), amygdala	L	3.9688	0.00007	Superior frontal cortex	R	-3.7804	0.00016
HCP, PHG, Amygdala	R	4.2647	0.00002	Superior frontal cortex	R	-3.4037	0.00066
Fusiform gyrus	L	3.9419	0.00008	Anterior cingulate cortex (ACC), ventromedial prefrontal cortex (vmPFC)	-	-4.2917	0.00002
Fusiform gyrus	R	4.3724	0.00001	Superior temporal gyrus	L	-1.9508	0.05109
Intraparietal sulcus (IPS)	L	3.6190	0.00030	Posterior cingulate cortex (PCC), precuneus	-	-3.9957	0.00006



Chapter 3

---

IPS	R	3.9150	0.00009	Temporoparietal junction (TPJ)	L	-3.2692	0.00108
Middle occipital gyrus (MOG)	R	4.2917	0.00002	TPJ	R	-4.3724	0.00001
Inferior occipital gyrus	L	3.9150	0.00009				

**Supplementary file 1C. 224 ROIs included in 10 subnetworks of the Power atlas.**

ROI ID	Name of ROI (Automated Anatomical Label)	Hemisphere	MNI coordinates			Assigned network
			x	y	z	
1	Precuneus_L	L	-7	-52	61	SMN
2	undefined	L	- 14	-18	40	SMN
3	Supp_Motor_Area_L	R	0	-15	47	SMN
4	Supp_Motor_Area_R	R	10	-2	45	SMN
5	Paracentral_Lobule_L	L	-7	-21	65	SMN
6	Paracentral_Lobule_L	L	-7	-33	72	SMN
7	Postcentral_R	R	13	-33	75	SMN
8	Parietal_Inf_L	L	- 54	-23	43	SMN
9	Precentral_R	R	29	-17	71	SMN
10	Precuneus_R	R	10	-46	73	SMN
11	Postcentral_L	L	- 23	-30	72	SMN
12	Precentral_L	L	- 40	-19	54	SMN
13	Postcentral_R	R	29	-39	59	SMN
14	Postcentral_R	R	50	-20	42	SMN
15	Postcentral_L	L	- 38	-27	69	SMN

Chapter 3

16	undefined	R	20	-29	60	SMN
17	Precentral_R	R	44	-8	57	SMN
18	Postcentral_L	L	- 29	-43	61	SMN
19	Supp_Motor_Area_R	R	10	-17	74	SMN
20	Postcentral_R	R	22	-42	69	SMN
21	Postcentral_L	L	- 45	-32	47	SMN
22	Postcentral_L	L	- 21	-31	61	SMN
23	Paracentral_Lobule_L	L	- 13	-17	75	SMN
24	Precentral_R	R	42	-20	55	SMN
25	undefined	L	- 38	-15	69	SMN
26	Parietal_Sup_L	L	- 16	-46	73	SMN
27	Paracentral_Lobule_R	R	2	-28	60	SMN
28	Supp_Motor_Area_R	R	3	-17	58	SMN
29	Precentral_R	R	38	-17	45	SMN
30	Postcentral_R	R	47	-30	49	SMN
31	Postcentral_L	L	- 49	-11	35	SMN
32	Insula_R	R	36	-9	14	SMN
33	Postcentral_R	R	51	-6	32	SMN

TOPIC 2: Large-scale Network Integration in the Human Brain  
Tracks Temporal Fluctuations in Memory Encoding Performance

---

34	Postcentral_L	L	- 53	-10	24	SMN
35	Postcentral_R	R	66	-8	25	SMN
36	Supp_Motor_Area_L	L	-3	2	53	CON
37	SupraMarginal_R	R	54	-28	34	CON
38	Frontal_Sup_R	R	19	-8	64	CON
39	Frontal_Sup_L	L	- 16	-5	71	CON
40	Cingulum_Mid_L	L	- 10	-2	42	CON
41	undefined	R	37	1	-4	CON
42	Supp_Motor_Area_R	R	13	-1	70	CON
43	Supp_Motor_Area_R	R	7	8	51	CON
44	Rolandic_Oper_L	L	- 45	0	9	CON
45	Insula_R	R	49	8	-1	CON
46	undefined	L	- 34	3	4	CON
47	Temporal_Pole_Sup_L	L	- 51	8	-2	CON
48	Cingulum_Mid_L	L	-5	18	34	CON
49	undefined	R	36	10	1	CON
50	undefined	R	32	-26	13	AUD
51	Temporal_Sup_R	R	65	-33	20	AUD
52	Temporal_Sup_R	R	58	-16	7	AUD

Chapter 3

53	Rolandic_Oper_L	L	38	-33	17	AUD
54	Temporal_Sup_L	L	60	-25	14	AUD
55	Temporal_Sup_L	L	49	-26	5	AUD
56	Rolandic_Oper_R	R	43	-23	20	AUD
57	SupraMarginal_L	L	50	-34	26	AUD
58	SupraMarginal_L	L	53	-22	23	AUD
59	Rolandic_Oper_L	L	55	-9	12	AUD
60	Rolandic_Oper_R	R	56	-5	13	AUD
61	Postcentral_R	R	59	-17	29	AUD
62	undefined	L	30	-27	12	AUD
63	Occipital_Mid_L	L	41	-75	26	DMN
64	Rectus_R	R	8	48	-15	DMN
65	Precuneus_L	L	13	-40	1	DMN
66	Temporal_Mid_L	L	46	-61	21	DMN
67	Occipital_Mid_R	R	43	-72	28	DMN
68	Temporal_Pole_Mid_L	L	44	12	-34	DMN
69	Temporal_Pole_Mid_R	R	46	16	-30	DMN

TOPIC 2: Large-scale Network Integration in the Human Brain  
Tracks Temporal Fluctuations in Memory Encoding Performance

---

70	Temporal_Mid_L	L	-68	-23	-16	DMN
71	Angular_L	L	-44	-65	35	DMN
72	Angular_L	L	-39	-75	44	DMN
73	Precuneus_L	L	-7	-55	27	DMN
74	Precuneus_R	R	6	-59	35	DMN
75	Precuneus_L	L	-11	-56	16	DMN
76	Precuneus_L	L	-3	-49	13	DMN
77	Cingulum_Mid_R	R	8	-48	31	DMN
78	Precuneus_R	R	15	-63	26	DMN
79	Cingulum_Mid_L	L	-2	-37	44	DMN
80	Precuneus_R	R	11	-54	17	DMN
81	Angular_R	R	52	-59	36	DMN
82	Frontal_Sup_R	R	23	33	48	DMN
83	Frontal_Sup_Medial_L	L	-10	39	52	DMN
84	Frontal_Sup_L	L	-16	29	53	DMN
85	Frontal_Mid_L	L	-35	20	51	DMN
86	Frontal_Sup_R	R	22	39	39	DMN
87	Frontal_Sup_R	R	13	55	38	DMN

88	Frontal_Sup_L	L	-10	55	39	DMN
89	Frontal_Sup_L	L	-20	45	39	DMN
90	Frontal_Sup_Medial_R	R	6	54	16	DMN
91	Frontal_Sup_Medial_R	R	6	64	22	DMN
92	Cingulum_Ant_L	L	-7	51	-1	DMN
93	Frontal_Sup_Medial_R	R	9	54	3	DMN
94	Frontal_Med_Orb_L	L	-3	44	-9	DMN
95	Frontal_Med_Orb_R	R	8	42	-5	DMN
96	Cingulum_Ant_L	L	-11	45	8	DMN
97	Frontal_Sup_Medial_L	L	-2	38	36	DMN
98	Cingulum_Ant_L	L	-3	42	16	DMN
99	Frontal_Sup_L	L	-20	64	19	DMN
100	Frontal_Sup_Medial_L	L	-8	48	23	DMN
101	Temporal_Mid_R	R	65	-12	-19	DMN
102	Temporal_Mid_L	L	-56	-13	-10	DMN
103	Temporal_Mid_L	L	-58	-30	-4	DMN
104	Temporal_Mid_R	R	65	-31	-9	DMN
105	Temporal_Mid_L	L	-68	-41	-5	DMN
106	Frontal_Sup_Medial_R	R	13	30	59	DMN

TOPIC 2: Large-scale Network Integration in the Human Brain  
Tracks Temporal Fluctuations in Memory Encoding Performance

---

107	Cingulum_Ant_R	R	12	36	20	DMN
108	Temporal_Mid_R	R	52	-2	-16	DMN
109	ParaHippocampal_L	L	- 26	-40	-8	DMN
110	Fusiform_R	R	27	-37	-13	DMN
111	Fusiform_L	L	- 34	-38	-16	DMN
112	Cerebelum_Crus1_R	R	28	-77	-32	DMN
113	Temporal_Pole_Mid_R	R	52	7	-30	DMN
114	Temporal_Mid_L	L	- 53	3	-27	DMN
115	Angular_R	R	47	-50	29	DMN
116	Temporal_Mid_L	L	- 49	-42	1	DMN
117	Frontal_Inf_Orb_L	L	- 46	31	-13	DMN
118	Frontal_Inf_Orb_R	R	49	35	-12	DMN
119	Lingual_R	R	18	-47	-10	VIN
120	Occipital_Mid_R	R	40	-72	14	VIN
121	Calcarine_R	R	8	-72	11	VIN
122	Calcarine_L	L	-8	-81	7	VIN
123	Occipital_Mid_L	L	- 28	-79	19	VIN
124	Lingual_R	R	20	-66	2	VIN



Chapter 3

125	Occipital_Mid_L	L	- 24	-91	19	VIN
126	Fusiform_R	R	27	-59	-9	VIN
127	Lingual_L	L	- 15	-72	-8	VIN
128	Calcarine_L	L	- 18	-68	5	VIN
129	Occipital_Inf_R	R	43	-78	-12	VIN
130	Occipital_Inf_L	L	- 47	-76	-10	VIN
131	Occipital_Sup_L	L	- 14	-91	31	VIN
132	Cuneus_R	R	15	-87	37	VIN
133	Occipital_Mid_R	R	29	-77	25	VIN
134	Lingual_R	R	20	-86	-2	VIN
135	Cuneus_R	R	15	-77	31	VIN
136	Lingual_L	L	- 16	-52	-1	VIN
137	Temporal_Inf_R	R	42	-66	-8	VIN
138	Occipital_Sup_R	R	24	-87	24	VIN
139	Cuneus_R	R	6	-72	24	VIN
140	Occipital_Mid_L	L	- 42	-74	0	VIN
141	Fusiform_R	R	26	-79	-16	VIN
142	Cuneus_L	L	- 16	-77	34	VIN

TOPIC 2: Large-scale Network Integration in the Human Brain  
Tracks Temporal Fluctuations in Memory Encoding Performance

---

143	Cuneus_L	L	-3	-81	21	VIN
144	Occipital_Mid_L	L	- 40	-88	-6	VIN
145	Occipital_Mid_R	R	37	-84	13	VIN
146	Calcarine_R	R	6	-81	6	VIN
147	Occipital_Mid_L	L	- 26	-90	3	VIN
148	Fusiform_L	L	- 33	-79	-13	VIN
149	Occipital_Mid_R	R	37	-81	1	VIN
150	Precentral_L	L	- 44	2	46	FPN
151	Frontal_Inf_Tri_R	R	48	25	27	FPN
152	Frontal_Inf_Tri_L	L	- 47	11	23	FPN
153	Parietal_Inf_L	L	- 53	-49	43	FPN
154	Frontal_Mid_L	L	- 23	11	64	FPN
155	Temporal_Inf_R	R	58	-53	-14	FPN
156	Frontal_Sup_Orb_R	R	24	45	-15	FPN
157	Frontal_Mid_Orb_R	R	34	54	-13	FPN
158	Precentral_R	R	47	10	33	FPN
159	Precentral_L	L	- 41	6	33	FPN
160	Frontal_Mid_R	R	38	43	15	FPN

Chapter 3

161	Parietal_Inf_R	R	49	-42	45	FPN
162	Parietal_Inf_L	L	-28	-58	48	FPN
163	Parietal_Inf_R	R	44	-53	47	FPN
164	Frontal_Mid_R	R	32	14	56	FPN
165	Angular_R	R	37	-65	40	FPN
166	Parietal_Inf_L	L	-42	-55	45	FPN
167	Frontal_Mid_R	R	40	18	40	FPN
168	Frontal_Mid_L	L	-34	55	4	FPN
169	Frontal_Mid_Orb_L	L	-42	45	-2	FPN
170	Angular_R	R	33	-53	44	FPN
171	Frontal_Mid_Orb_R	R	43	49	-2	FPN
172	Frontal_Inf_Tri_L	L	-42	25	30	FPN
173	Frontal_Sup_Medial_L	L	-3	26	44	FPN
174	Cingulum_Mid_R	R	11	-39	50	SAN
175	Parietal_Inf_R	R	55	-45	37	SAN
176	Precentral_R	R	42	0	47	SAN
177	Frontal_Mid_R	R	31	33	26	SAN
178	Frontal_Inf_Tri_R	R	48	22	10	SAN
179	Insula_L	L	-35	20	0	SAN

TOPIC 2: Large-scale Network Integration in the Human Brain  
Tracks Temporal Fluctuations in Memory Encoding Performance

---

180	Insula_R	R	36	22	3	SAN
181	Frontal_Inf_Orb_R	R	37	32	-2	SAN
182	Insula_R	R	34	16	-8	SAN
183	undefined	L	- 11	26	25	SAN
184	Supp_Motor_Area_L	L	-1	15	44	SAN
185	Frontal_Mid_L	L	- 28	52	21	SAN
186	Cingulum_Ant_L	L	0	30	27	SAN
187	Cingulum_Mid_R	R	5	23	37	SAN
188	Cingulum_Ant_R	R	10	22	27	SAN
189	Frontal_Mid_R	R	31	56	14	SAN
190	Frontal_Mid_R	R	26	50	27	SAN
191	Frontal_Mid_L	L	- 39	51	17	SAN
192	Thalamus_R	R	6	-24	0	SUB
193	Thalamus_L	L	-2	-13	12	SUB
194	Thalamus_L	L	- 10	-18	7	SUB
195	Thalamus_R	R	12	-17	8	SUB
196	undefined	L	-5	-28	-4	SUB
197	Putamen_L	L	- 22	7	-5	SUB
198	undefined	L	- 15	4	8	SUB

Chapter 3

199	Putamen_R	R	31	-14	2	SUB
200	Putamen_R	R	23	10	1	SUB
201	Putamen_R	R	29	1	4	SUB
202	undefined	L	31	-11	0	SUB
203	undefined	R	15	5	7	SUB
204	undefined	R	9	-4	6	SUB
205	Supp_Motor_Area_L	L	10	11	67	VAN
206	Temporal_Sup_R	R	54	-43	22	VAN
207	Temporal_Mid_L	L	56	-50	10	VAN
208	Temporal_Sup_L	L	55	-40	14	VAN
209	Temporal_Sup_R	R	52	-33	8	VAN
210	Temporal_Mid_R	R	51	-29	-4	VAN
211	Temporal_Sup_R	R	56	-46	11	VAN
212	Frontal_Inf_Tri_R	R	53	33	1	VAN
213	Frontal_Inf_Tri_L	L	49	25	-1	VAN
214	Precuneus_R	R	10	-62	61	DAN
215	Temporal_Mid_L	L	52	-63	5	DAN
216	Parietal_Sup_R	R	22	-65	48	DAN
217	Temporal_Mid_R	R	46	-59	4	DAN

TOPIC 2: Large-scale Network Integration in the Human Brain  
Tracks Temporal Fluctuations in Memory Encoding Performance

---

218	Parietal_Sup_R	R	25	-58	60	DAN
219	Parietal_Inf_L	L	33	-46	47	DAN
220	Occipital_Mid_L	L	27	-71	37	DAN
221	Precentral_L	L	32	-1	54	DAN
222	Temporal_Inf_L	L	42	-60	-9	DAN
223	Parietal_Sup_L	L	17	-59	64	DAN
224	Precentral_R	R	29	-5	54	DAN

*Note.* SMN, sensorimotor networks; CON, cingulo-opercular network; AUD, auditory network; DMN, default mode network; VIN, visual network; FPN, fronto-parietal network; SAN, salience network; SUB, subcortical nodes; VAN, ventral attention network; DAN, dorsal attention network.

---

**Supplementary file 1D. 72 connections showing significant increase in FC during the high encoding state.**

Subnetwork pairs		ROI pairs		<i>z</i>	<i>P</i>
CON	CON	Frontal_Sup_R	Supp_Motor_Area_L	3.7266	0.0002
		Supp_Motor_Area_R	Frontal_Sup_R	3.8880	0.0001
DMN	SMN	Frontal_Sup_L	Precentral_L	3.3499	0.0008
		Frontal_Sup_L	Paracentral_Lobule_R	3.4575	0.0005
		Frontal_Sup_L	Supp_Motor_Area_R	3.5383	0.0004
		Frontal_Sup_Medial_R	Postcentral_L	3.3499	0.0008
		Cingulum_Ant_R	Precentral_R	3.5652	0.0004
	CON	Frontal_Sup_Medial_R	Rolandic_Oper_L	3.4306	0.0006
		Frontal_Sup_Medial_R	Temporal_Pole_Sup_L	3.5921	0.0003
	DMN	Frontal_Sup_L	Precuneus_L	3.6190	0.0003
		Frontal_Sup_L	Angular_L	4.1033	0.0000
		Frontal_Sup_Medial_R	Precuneus_L	3.3768	0.0007
		Frontal_Sup_L	Precuneus_L	3.6190	0.0003
		Temporal_Mid_L	Frontal_Sup_Medial_L	3.5114	0.0004
		Temporal_Mid_R	Frontal_Sup_Medial_L	3.6459	0.0003
		Temporal_Pole_Mid_R	Frontal_Sup_Medial_R	3.4575	0.0005
Angular_R	Frontal_Sup_Medial_L	3.5114	0.0004		

TOPIC 2: Large-scale Network Integration in the Human Brain  
Tracks Temporal Fluctuations in Memory Encoding Performance

		Frontal_Inf_Orb_R	Frontal_Sup_Medial_L	3.4037	0.0007
VIN	SMN	Occipital_Mid_L	Precentral_R	3.3499	0.0008
		Occipital_Inf_R	Insula_R	3.5114	0.0004
		Occipital_Inf_L	Precentral_R	3.8073	0.0001
		Fusiform_R	Postcentral_L	4.3724	0.0000
		Fusiform_R	Postcentral_L	3.5383	0.0004
		Fusiform_R	Insula_R	4.0495	0.0001
		Fusiform_R	Postcentral_L	3.6190	0.0003
		Occipital_Mid_L	Postcentral_R	4.0226	0.0001
		Occipital_Mid_L	Postcentral_L	3.4306	0.0006
		Occipital_Mid_L	Postcentral_R	3.4575	0.0005
		Occipital_Mid_L	Postcentral_L	3.5921	0.0003
		Occipital_Mid_L	Precentral_R	3.6190	0.0003
		Occipital_Mid_L	Precentral_R	3.5383	0.0004
		Fusiform_L	Postcentral_L	3.5921	0.0003
	CON	Fusiform_R	Frontal_Sup_R	3.4844	0.0005
		Fusiform_R	Rolandic_Oper_L	3.8880	0.0001
	AUD	Occipital_Mid_L	undefined	3.4037	0.0007
	DMN	Calcarine_R	Frontal_Sup_L	3.4306	0.0006



		Lingual_R	Precuneus_L	3.3768	0.0007
		Fusiform_R	Temporal_Mid_L	3.5383	0.0004
		Occipital_Mid_L	Temporal_Pole_Mid_R	3.6459	0.0003
		Occipital_Mid_L	Temporal_Mid_L	3.5652	0.0004
	VIN	Fusiform_R	Lingual_R	3.7266	0.0002
	VIN	Fusiform_R	Cuneus_R	3.6190	0.0003
	VIN	Cuneus_L	Fusiform_R	4.0226	0.0001
	VIN	Occipital_Mid_R	Occipital_Mid_L	3.4844	0.0005
FPN	CON	Frontal_Mid_L	Cingulum_Mid_L	3.3768	0.0007
	AUD	Precentral_L	Rolandic_Oper_R	3.4306	0.0006
	DMN	Precentral_L	Temporal_Pole_Mid_L	3.4844	0.0005
		Frontal_Mid_R	Temporal_Pole_Mid_L	3.6459	0.0003
		Frontal_Sup_Orb_R	Temporal_Pole_Mid_R	3.5383	0.0004
SAN	SMN	Cingulum_Mid_R	Precentral_R	3.3499	0.0008
	CON	Frontal_Mid_L	Rolandic_Oper_L	3.3499	0.0008
	DMN	Parietal_Inf_R	Temporal_Pole_Mid_L	3.4844	0.0005
		Frontal_Inf_Tri_R	Frontal_Sup_L	3.5114	0.0004
		Frontal_Inf_Tri_R	Frontal_Sup_Medial_L	3.5383	0.0004
		Frontal_Mid_L	Precuneus_L	3.5652	0.0004

TOPIC 2: Large-scale Network Integration in the Human Brain  
Tracks Temporal Fluctuations in Memory Encoding Performance

		Frontal_Mid_R	Frontal_Sup_Medial_R	3.3768	0.0007
SUB	SMN	Putamen_R	Supp_Motor_Area_R	3.5921	0.0003
		undefined	Paracentral_Lobule_L	4.1033	0.0000
	DMN	Thalamus_R	Temporal_Mid_L	3.5921	0.0003
		Thalamus_R	Cerebelum_Crus1_R	3.8073	0.0001
		undefined	Cerebelum_Crus1_R	3.4037	0.0007
		undefined	Temporal_Mid_L	3.3499	0.0008
		undefined	Temporal_Mid_L	3.5652	0.0004
		undefined	Temporal_Mid_L	4.0764	0.0000
	VIN	Thalamus_R	Occipital_Mid_L	4.1033	0.0000
		Thalamus_R	Occipital_Mid_R	3.4037	0.0007
		Putamen_R	Cuneus_R	3.4575	0.0005
VAN	DMN	Temporal_Mid_R	Frontal_Sup_L	3.5383	0.0004
	SAN	Temporal_Sup_R	Frontal_Mid_L	3.3499	0.0008
	SUB	Temporal_Sup_L	undefined	3.7535	0.0002
DAN	FPN	Parietal_Sup_R	Frontal_Inf_Tri_L	3.5383	0.0004
	SUB	Parietal_Sup_R	Thalamus_R	3.3499	0.0008

---

**Supplementary file 1E. 335 connections showing significant decrease in FC during the high encoding state.**

Subnetwork pairs		ROI pairs		<i>z</i>	<i>P</i>
SMN	SMN	Paracentral_Lobule_L	Supp_Motor_Area_R	-3.6728	0.0002
		Parietal_Inf_L	Supp_Motor_Area_L	-3.8611	0.0001
		Parietal_Inf_L	Paracentral_Lobule_L	-3.5114	0.0004
		Precentral_L	Supp_Motor_Area_L	-3.8611	0.0001
		Precentral_L	Paracentral_Lobule_L	-3.3499	0.0008
		Postcentral_R	Supp_Motor_Area_L	-3.5383	0.0004
		Postcentral_L	Paracentral_Lobule_L	-3.6190	0.0003
		Postcentral_L	Precentral_R	-3.5383	0.0004
		undefined	Postcentral_R	-3.6459	0.0003
		Precentral_R	Precuneus_L	-3.4306	0.0006
		Postcentral_L	Supp_Motor_Area_L	-3.3499	0.0008
		Postcentral_L	Precuneus_L	-3.3499	0.0008
		Postcentral_L	Postcentral_R	-3.4575	0.0005
		Paracentral_Lobule_L	Postcentral_R	-3.7535	0.0002
		Paracentral_Lobule_L	Postcentral_R	-3.7266	0.0002
		undefined	Paracentral_Lobule_L	-4.0226	0.0001
		Parietal_Sup_L	Postcentral_L	-3.7266	0.0002

TOPIC 2: Large-scale Network Integration in the Human Brain  
Tracks Temporal Fluctuations in Memory Encoding Performance

---

		Supp_Motor_Area_R	Supp_Motor_Area_R	-4.0495	0.0001
		Supp_Motor_Area_R	Precentral_L	-3.9957	0.0001
		Supp_Motor_Area_R	Postcentral_L	-3.9150	0.0001
		Supp_Motor_Area_R	Precentral_R	-3.8073	0.0001
		Supp_Motor_Area_R	Postcentral_L	-3.5383	0.0004
		Supp_Motor_Area_R	Postcentral_L	-3.8342	0.0001
		Supp_Motor_Area_R	Precentral_R	-3.6728	0.0002
		Supp_Motor_Area_R	undefined	-3.4306	0.0006
		Postcentral_L	Paracentral_Lobule_L	-3.5921	0.0003
		Postcentral_L	Postcentral_L	-3.5652	0.0004
		Postcentral_L	Postcentral_L	-3.6997	0.0002
		Postcentral_L	Paracentral_Lobule_L	-4.1033	0.0000
		Insula_R	undefined	-3.3768	0.0007
		Insula_R	Supp_Motor_Area_R	-4.1302	0.0000
		Insula_R	Postcentral_L	-3.5921	0.0003
		Insula_R	Precentral_R	-3.4037	0.0007
		Insula_R	Postcentral_L	-3.6997	0.0002
		Insula_R	Precentral_R	-3.3499	0.0008
		Insula_R	Supp_Motor_Area_R	-3.5114	0.0004

		Postcentral_R	Paracentral_Lobule_L	-4.0764	0.0000
		Postcentral_R	Supp_Motor_Area_R	-3.4306	0.0006
		Postcentral_L	Paracentral_Lobule_L	-3.4575	0.0005
		Postcentral_L	Supp_Motor_Area_R	-3.4037	0.0007
		Postcentral_L	Paracentral_Lobule_L	-4.0764	0.0000
		Postcentral_R	Paracentral_Lobule_L	-3.3499	0.0008
		Postcentral_R	Paracentral_Lobule_L	-3.8342	0.0001
		Postcentral_R	Postcentral_R	-3.7266	0.0002
		Postcentral_R	Paracentral_Lobule_L	-3.9688	0.0001
CON	SMN	Frontal_Sup_L	Paracentral_Lobule_L	-4.1840	0.0000
		Cingulum_Mid_L	Insula_R	-3.9688	0.0001
		Rolandic_Oper_L	Supp_Motor_Area_R	-3.4844	0.0005
	CON	Temporal_Pole_Sup_L	Rolandic_Oper_L	-3.5114	0.0004
AUD	SMN	undefined	Supp_Motor_Area_R	-3.5114	0.0004
		Temporal_Sup_R	Paracentral_Lobule_L	-3.6459	0.0003
		Rolandic_Oper_L	Paracentral_Lobule_L	-3.5652	0.0004
		Rolandic_Oper_L	Precentral_L	-3.5114	0.0004
		Rolandic_Oper_L	Postcentral_L	-3.3499	0.0008
		Rolandic_Oper_L	Supp_Motor_Area_R	-3.7266	0.0002

TOPIC 2: Large-scale Network Integration in the Human Brain  
Tracks Temporal Fluctuations in Memory Encoding Performance

		Temporal_Sup_L	Supp_Motor_Area_R	-3.3499	0.0008
		Temporal_Sup_L	undefined	-3.4844	0.0005
		Temporal_Sup_L	Postcentral_L	-4.1840	0.0000
		Temporal_Sup_L	Supp_Motor_Area_R	-3.6728	0.0002
		Temporal_Sup_L	Supp_Motor_Area_L	-3.3499	0.0008
		Temporal_Sup_L	Paracentral_Lobule_L	-4.1840	0.0000
		Temporal_Sup_L	Parietal_Inf_L	-3.5652	0.0004
		Temporal_Sup_L	Postcentral_L	-3.6728	0.0002
		Temporal_Sup_L	undefined	-3.5652	0.0004
		Temporal_Sup_L	Postcentral_L	-3.9688	0.0001
		Temporal_Sup_L	Paracentral_Lobule_L	-4.0764	0.0000
		Rolandic_Oper_R	Postcentral_L	-3.4575	0.0005
		Rolandic_Oper_R	Precentral_R	-4.2109	0.0000
		Rolandic_Oper_R	Precentral_R	-3.5114	0.0004
		Rolandic_Oper_R	Insula_R	-3.3499	0.0008
		SupraMarginal_L	Paracentral_Lobule_L	-3.8342	0.0001
		SupraMarginal_L	Postcentral_R	-3.5383	0.0004
		SupraMarginal_L	Precentral_R	-3.9419	0.0001
		SupraMarginal_L	Postcentral_L	-3.6459	0.0003

		SupraMarginal_L	Paracentral_Lobule_L	-3.7804	0.0002
		SupraMarginal_L	Precentral_R	-3.5383	0.0004
		SupraMarginal_L	undefined	-3.7535	0.0002
		SupraMarginal_L	Supp_Motor_Area_R	-3.3499	0.0008
		SupraMarginal_L	Paracentral_Lobule_L	-3.3499	0.0008
		Rolandic_Oper_L	Supp_Motor_Area_L	-3.4575	0.0005
		Rolandic_Oper_L	Supp_Motor_Area_R	-3.3768	0.0007
		Rolandic_Oper_L	Paracentral_Lobule_L	-3.3499	0.0008
		Rolandic_Oper_L	Postcentral_L	-3.5921	0.0003
		Rolandic_Oper_L	Supp_Motor_Area_R	-3.9419	0.0001
		Rolandic_Oper_L	Insula_R	-3.6997	0.0002
		Rolandic_Oper_R	Paracentral_Lobule_L	-3.4575	0.0005
		Rolandic_Oper_R	Paracentral_Lobule_L	-3.7804	0.0002
		undefined	Paracentral_Lobule_L	-3.5652	0.0004
	CON	Rolandic_Oper_R	Rolandic_Oper_L	-3.5114	0.0004
	CON	Rolandic_Oper_L	Rolandic_Oper_L	-3.8342	0.0001
	CON	Rolandic_Oper_L	Temporal_Pole_Sup_L	-3.4037	0.0007
	AUD	Temporal_Sup_L	Temporal_Sup_R	-3.6728	0.0002
	AUD	SupraMarginal_L	Temporal_Sup_L	-3.5921	0.0003

TOPIC 2: Large-scale Network Integration in the Human Brain  
Tracks Temporal Fluctuations in Memory Encoding Performance

		SupraMarginal_L	Temporal_Sup_L	-3.4037	0.0007
		Rolandic_Oper_R	Temporal_Sup_L	-3.9419	0.0001
DMN	SMN	Occipital_Mid_L	Precuneus_L	-3.5114	0.0004
		Rectus_R	Postcentral_L	-3.7804	0.0002
		Rectus_R	Postcentral_R	-4.3724	0.0000
		Temporal_Mid_L	Precuneus_L	-3.5114	0.0004
		Temporal_Mid_L	Postcentral_L	-3.7535	0.0002
		Temporal_Mid_L	Postcentral_R	-3.5652	0.0004
		Temporal_Mid_L	Postcentral_L	-3.4037	0.0007
		Temporal_Mid_L	Paracentral_Lobule_L	-3.6190	0.0003
		Temporal_Mid_L	Precentral_R	-3.3768	0.0007
		Occipital_Mid_R	Precuneus_L	-3.3768	0.0007
		Temporal_Pole_Mid_R	Postcentral_L	-3.5114	0.0004
		Temporal_Pole_Mid_R	Supp_Motor_Area_R	-3.4037	0.0007
		Temporal_Pole_Mid_R	Insula_R	-3.4037	0.0007
		Angular_L	Precuneus_L	-3.6997	0.0002
		Precuneus_L	Postcentral_L	-3.4037	0.0007
		Precuneus_L	Postcentral_R	-3.9688	0.0001
		Precuneus_L	Precuneus_L	-3.4575	0.0005



		Precuneus_L	Postcentral_L	-3.3499	0.0008
		Precuneus_L	Postcentral_L	-3.4306	0.0006
		Precuneus_L	Precentral_R	-3.8073	0.0001
		Precuneus_L	Postcentral_R	-3.6190	0.0003
		Precuneus_L	Postcentral_L	-3.4575	0.0005
		Precuneus_R	Postcentral_R	-3.4037	0.0007
		Precuneus_R	Insula_R	-3.5114	0.0004
		Frontal_Sup_R	Paracentral_Lobule_L	-3.5114	0.0004
		Frontal_Sup_R	Paracentral_Lobule_L	-3.7266	0.0002
		Frontal_Sup_R	Precuneus_L	-3.4306	0.0006
		Frontal_Sup_Medial_R	Paracentral_Lobule_L	-3.4306	0.0006
		Frontal_Med_Orb_L	Postcentral_L	-3.7804	0.0002
		Frontal_Med_Orb_L	Postcentral_R	-3.6997	0.0002
		Frontal_Med_Orb_L	Postcentral_L	-3.7266	0.0002
		Frontal_Sup_Medial_L	Postcentral_R	-3.9150	0.0001
		Frontal_Sup_Medial_L	Paracentral_Lobule_L	-3.3768	0.0007
		Frontal_Sup_Medial_L	Parietal_Sup_L	-3.4575	0.0005
		Temporal_Mid_L	undefined	-3.4844	0.0005
		Temporal_Mid_L	Paracentral_Lobule_L	-3.6459	0.0003

TOPIC 2: Large-scale Network Integration in the Human Brain  
Tracks Temporal Fluctuations in Memory Encoding Performance

		Temporal_Mid_L	Supp_Motor_Area_R	-3.8342	0.0001
		Temporal_Mid_L	Paracentral_Lobule_L	-3.5383	0.0004
		Temporal_Mid_L	Parietal_Inf_L	-3.6997	0.0002
		Temporal_Mid_L	Postcentral_R	-3.4844	0.0005
		Temporal_Mid_L	Postcentral_L	-3.8073	0.0001
		Temporal_Mid_L	Paracentral_Lobule_L	-3.6459	0.0003
		Temporal_Mid_L	Parietal_Sup_L	-3.3499	0.0008
		Temporal_Mid_R	Supp_Motor_Area_R	-3.4306	0.0006
		Temporal_Mid_R	Postcentral_R	-3.7535	0.0002
		ParaHippocampal_L	Postcentral_L	-3.5114	0.0004
		ParaHippocampal_L	Postcentral_R	-3.3499	0.0008
		Fusiform_R	Paracentral_Lobule_L	-3.5114	0.0004
		Fusiform_L	Postcentral_R	-3.6997	0.0002
		Temporal_Mid_L	Supp_Motor_Area_R	-3.5921	0.0003
		Temporal_Mid_L	Supp_Motor_Area_R	-3.5383	0.0004
	CON	Occipital_Mid_L	SupraMarginal_R	-3.3499	0.0008
	CON	Rectus_R	Frontal_Sup_R	-3.3768	0.0007
	CON	Angular_L	Frontal_Sup_R	-3.7266	0.0002
	CON	Temporal_Mid_L	undefined	-3.4844	0.0005

		Temporal_Mid_L	SupraMarginal_R	-3.4037	0.0007
		Temporal_Mid_L	Frontal_Sup_R	-3.4037	0.0007
		Fusiform_L	Frontal_Sup_R	-3.8073	0.0001
		Temporal_Pole_Mid_R	Frontal_Sup_L	-3.4306	0.0006
	AUD	Occipital_Mid_L	Temporal_Sup_R	-3.5383	0.0004
		Occipital_Mid_L	Temporal_Sup_L	-3.4037	0.0007
		Occipital_Mid_R	Rolandic_Oper_L	-3.4844	0.0005
		Precuneus_L	undefined	-3.9419	0.0001
		Precuneus_L	Rolandic_Oper_L	-3.5921	0.0003
		Precuneus_L	Rolandic_Oper_R	-3.8342	0.0001
		Precuneus_L	undefined	-3.3768	0.0007
		Precuneus_L	Rolandic_Oper_L	-4.2378	0.0000
		Precuneus_L	SupraMarginal_L	-3.7535	0.0002
		Precuneus_L	undefined	-3.6728	0.0002
		Precuneus_R	undefined	-3.4575	0.0005
		Temporal_Mid_L	Temporal_Sup_L	-3.3768	0.0007
		Temporal_Mid_L	SupraMarginal_L	-3.5114	0.0004
		Fusiform_R	Postcentral_R	-3.5921	0.0003
		DMN	ParaHippocampal_L	Rectus_R	-4.1302

TOPIC 2: Large-scale Network Integration in the Human Brain  
Tracks Temporal Fluctuations in Memory Encoding Performance

		ParaHippocampal_L	Temporal_Mid_R	-3.3768	0.0007
		ParaHippocampal_L	Temporal_Mid_L	-3.3768	0.0007
VIN	SMN	Occipital_Mid_R	Precuneus_L	-3.5383	0.0004
		Occipital_Mid_R	Postcentral_R	-3.4306	0.0006
		Calcarine_R	Precuneus_L	-3.6190	0.0003
		Calcarine_L	Precuneus_L	-3.3499	0.0008
		Lingual_R	Parietal_Inf_L	-3.7266	0.0002
		Occipital_Mid_R	Precuneus_L	-3.5652	0.0004
		Cuneus_R	Paracentral_Lobule_L	-3.3768	0.0007
		Cuneus_R	Postcentral_R	-3.6459	0.0003
		Cuneus_R	Supp_Motor_Area_R	-3.5114	0.0004
		Cuneus_L	Precuneus_L	-3.3499	0.0008
		Cuneus_L	Precuneus_L	-3.8611	0.0001
		Cuneus_L	Supp_Motor_Area_R	-3.6997	0.0002
		Cuneus_L	Paracentral_Lobule_R	-3.3499	0.0008
		Cuneus_L	Supp_Motor_Area_R	-3.6459	0.0003
		Occipital_Mid_R	Precuneus_L	-3.3499	0.0008
	AUD	Lingual_L	SupraMarginal_L	-3.7535	0.0002
		Calcarine_L	Temporal_Sup_L	-3.4575	0.0005

		Calcarine_L	SupraMarginal_L	-3.4037	0.0007
		Cuneus_R	Postcentral_R	-3.4037	0.0007
		Cuneus_R	Postcentral_R	-3.3768	0.0007
		Cuneus_L	Rolandic_Oper_L	-3.6997	0.0002
	DMN	Occipital_Mid_R	Occipital_Mid_L	-3.5652	0.0004
		Calcarine_R	Occipital_Mid_L	-3.3768	0.0007
		Calcarine_L	Occipital_Mid_R	-3.5383	0.0004
		Lingual_R	Occipital_Mid_L	-3.5652	0.0004
		Occipital_Mid_L	Cingulum_Mid_L	-3.4844	0.0005
		Calcarine_L	Angular_R	-3.5383	0.0004
		Calcarine_L	Temporal_Mid_R	-3.6997	0.0002
		Cuneus_R	Occipital_Mid_L	-3.7535	0.0002
		Cuneus_R	Temporal_Mid_L	-3.4306	0.0006
		Cuneus_R	Fusiform_L	-3.6997	0.0002
		Temporal_Inf_R	Fusiform_L	-3.4844	0.0005
		Occipital_Sup_R	Temporal_Mid_L	-3.5383	0.0004
		Occipital_Mid_L	Occipital_Mid_L	-3.4844	0.0005
		Occipital_Mid_L	Angular_L	-3.5114	0.0004
		Occipital_Mid_L	Cingulum_Mid_L	-3.7535	0.0002

TOPIC 2: Large-scale Network Integration in the Human Brain  
Tracks Temporal Fluctuations in Memory Encoding Performance

		Occipital_Mid_L	Frontal_Sup_R	-3.3499	0.0008	
		Occipital_Mid_L	Cingulum_Ant_L	-3.4306	0.0006	
		Cuneus_L	Occipital_Mid_L	-4.1302	0.0000	
		Cuneus_L	Fusiform_R	-3.3499	0.0008	
		Cuneus_L	Precuneus_R	-3.5383	0.0004	
		Occipital_Mid_L	Angular_R	-3.4037	0.0007	
		Calcarine_R	Occipital_Mid_R	-3.4037	0.0007	
		Occipital_Mid_R	Temporal_Mid_L	-3.3499	0.0008	
	VIN	Cuneus_L	Lingual_R	-3.6459	0.0003	
		Cuneus_L	Occipital_Mid_R	-3.5114	0.0004	
		Cuneus_L	Cuneus_L	-3.3499	0.0008	
	FPN	SMN	Precentral_L	Precuneus_L	-3.7266	0.0002
			Precentral_L	Supp_Motor_Area_L	-3.9688	0.0001
Precentral_L			Paracentral_Lobule_L	-4.1033	0.0000	
Precentral_L			Paracentral_Lobule_L	-3.6459	0.0003	
CON		Frontal_Sup_Orb_R	SupraMarginal_R	-3.7266	0.0002	
		Angular_R	SupraMarginal_R	-3.6190	0.0003	
		Parietal_Inf_L	undefined	-3.4844	0.0005	
		Frontal_Sup_Medial_L	Supp_Motor_Area_L	-3.5383	0.0004	

	AUD	Precentral_L	Temporal_Sup_R	-3.4844	0.0005
		Precentral_L	Temporal_Sup_L	-3.7266	0.0002
		Precentral_L	SupraMarginal_L	-4.1840	0.0000
		Frontal_Inf_Tri_R	SupraMarginal_L	-4.1571	0.0000
		Frontal_Inf_Tri_L	SupraMarginal_L	-3.8342	0.0001
		Frontal_Inf_Tri_L	SupraMarginal_L	-3.7535	0.0002
	DMN	Frontal_Inf_Tri_L	ParaHippocampal_L	-3.4306	0.0006
	VIN	Frontal_Mid_L	Occipital_Mid_R	-3.6190	0.0003
		Frontal_Sup_Orb_R	Occipital_Mid_L	-3.4037	0.0007
SAN	SMN	Cingulum_Mid_R	Precuneus_L	-3.3768	0.0007
		Cingulum_Mid_R	Supp_Motor_Area_L	-3.5921	0.0003
		Cingulum_Mid_R	Precentral_R	-3.5383	0.0004
		Cingulum_Mid_R	Postcentral_R	-4.1571	0.0000
		Insula_L	Insula_R	-3.3768	0.0007
	AUD	Cingulum_Mid_R	Rolandic_Oper_L	-3.4844	0.0005
		Precentral_R	Temporal_Sup_R	-3.9688	0.0001
		Precentral_R	Temporal_Sup_R	-3.4575	0.0005
		Frontal_Inf_Tri_R	undefined	-3.5114	0.0004
		Frontal_Inf_Tri_R	Temporal_Sup_R	-3.5114	0.0004

TOPIC 2: Large-scale Network Integration in the Human Brain  
Tracks Temporal Fluctuations in Memory Encoding Performance

	DMN	Cingulum_Mid_R	Occipital_Mid_R	-3.4844	0.0005	
		Cingulum_Ant_R	Cingulum_Ant_R	-3.3768	0.0007	
	VIN	Cingulum_Mid_R	Occipital_Mid_R	-3.3499	0.0008	
		Cingulum_Mid_R	Calcarine_R	-3.6190	0.0003	
		Cingulum_Mid_R	Calcarine_L	-3.4844	0.0005	
		Cingulum_Mid_R	Lingual_R	-3.3499	0.0008	
		Cingulum_Mid_R	Cuneus_R	-3.4844	0.0005	
		Parietal_Inf_R	Occipital_Mid_L	-3.4844	0.0005	
		Parietal_Inf_R	Occipital_Mid_L	-3.8880	0.0001	
		Frontal_Mid_R	Occipital_Mid_L	-3.7535	0.0002	
		Frontal_Mid_R	Occipital_Inf_R	-3.4037	0.0007	
	FPN	Cingulum_Mid_R	Angular_R	-3.4575	0.0005	
		Supp_Motor_Area_L	Frontal_Sup_Medial_L	-3.4575	0.0005	
		Frontal_Mid_L	Frontal_Inf_Tri_R	-3.3768	0.0007	
		Frontal_Mid_L	Frontal_Mid_Orb_R	-3.4575	0.0005	
	SAN	Cingulum_Ant_R	Frontal_Mid_R	-3.6190	0.0003	
	SUB	SAN	Putamen_L	Frontal_Mid_L	-3.4844	0.0005
	VAN	SMN	Temporal_Mid_L	Precuneus_L	-3.3499	0.0008
			Temporal_Mid_L	Supp_Motor_Area_R	-3.8342	0.0001



		Temporal_Mid_L	Paracentral_Lobule_L	-3.7266	0.0002
		Temporal_Mid_L	Paracentral_Lobule_R	-3.8342	0.0001
		Temporal_Sup_L	Paracentral_Lobule_L	-3.5114	0.0004
		Temporal_Sup_L	Precentral_R	-3.5383	0.0004
		Temporal_Sup_L	Postcentral_L	-3.4306	0.0006
		Temporal_Sup_L	Precentral_R	-3.5383	0.0004
		Temporal_Sup_L	Paracentral_Lobule_R	-3.4306	0.0006
		Temporal_Sup_L	Supp_Motor_Area_R	-4.2109	0.0000
		Temporal_Mid_R	Precuneus_L	-3.5652	0.0004
		Temporal_Mid_R	Postcentral_R	-3.5652	0.0004
		Temporal_Mid_R	undefined	-3.6728	0.0002
		Frontal_Inf_Tri_L	Precuneus_L	-3.3768	0.0007
		Frontal_Inf_Tri_L	Supp_Motor_Area_R	-3.5114	0.0004
	CON	Temporal_Mid_R	Frontal_Sup_R	-3.3499	0.0008
	AUD	Temporal_Mid_L	Temporal_Sup_R	-3.7804	0.0002
		Temporal_Mid_L	Rolandic_Oper_L	-3.3768	0.0007
		Temporal_Mid_L	Temporal_Sup_L	-3.7804	0.0002
		Temporal_Mid_R	Rolandic_Oper_L	-3.7266	0.0002
	DMN	Temporal_Sup_R	Precuneus_L	-3.4575	0.0005

TOPIC 2: Large-scale Network Integration in the Human Brain  
Tracks Temporal Fluctuations in Memory Encoding Performance

		Temporal_Sup_R	Precuneus_R	-3.6190	0.0003
		Temporal_Mid_L	Precuneus_L	-3.5921	0.0003
		Temporal_Mid_L	Precuneus_R	-3.7535	0.0002
		Temporal_Sup_L	Temporal_Mid_L	-3.3768	0.0007
		Temporal_Sup_L	Temporal_Pole_Mid_R	-3.8611	0.0001
		Temporal_Sup_L	Precuneus_L	-3.8073	0.0001
		Temporal_Sup_L	Precuneus_L	-3.4037	0.0007
		Temporal_Sup_L	Temporal_Mid_L	-4.0226	0.0001
		Temporal_Sup_L	Temporal_Mid_L	-3.6728	0.0002
		Temporal_Sup_L	Temporal_Mid_L	-3.4575	0.0005
		Temporal_Sup_R	Temporal_Mid_R	-3.6459	0.0003
		Temporal_Mid_R	Temporal_Mid_L	-3.4575	0.0005
		Temporal_Sup_R	Temporal_Mid_L	-3.9150	0.0001
		Temporal_Sup_R	Precuneus_L	-3.5114	0.0004
	VIN	Temporal_Mid_L	Lingual_R	-3.5114	0.0004
	VIN	Temporal_Mid_L	Occipital_Mid_R	-3.4844	0.0005
	VIN	Temporal_Mid_L	Occipital_Sup_R	-3.5383	0.0004
	VIN	Temporal_Sup_L	Cuneus_R	-3.5652	0.0004
	VIN	Temporal_Sup_L	Cuneus_L	-3.4575	0.0005

		Temporal_Sup_R	Occipital_Sup_R	-3.4844	0.0005
	FPN	Temporal_Sup_L	Precentral_L	-3.7804	0.0002
		Temporal_Sup_R	Precentral_L	-3.4844	0.0005
	VAN	Temporal_Sup_R	Temporal_Mid_L	-3.9419	0.0001
		Temporal_Sup_R	Temporal_Sup_L	-3.3499	0.0008
DAN	SMN	Temporal_Mid_R	Supp_Motor_Area_L	-3.4037	0.0007
		Temporal_Mid_R	Insula_R	-3.3499	0.0008
		Temporal_Mid_R	Postcentral_R	-3.4306	0.0006
		Precentral_R	Supp_Motor_Area_L	-3.9150	0.0001
	AUD	Temporal_Mid_R	Temporal_Sup_R	-3.4306	0.0006
		Temporal_Mid_R	Postcentral_R	-3.6190	0.0003
		Occipital_Mid_L	SupraMarginal_L	-3.4306	0.0006
		Precentral_L	Temporal_Sup_R	-3.7266	0.0002
		Precentral_R	Temporal_Sup_R	-3.5383	0.0004
		Precentral_R	Temporal_Sup_L	-3.3768	0.0007
	DMN	Temporal_Mid_L	Temporal_Mid_L	-3.9957	0.0001
		Temporal_Mid_L	Precuneus_L	-3.5921	0.0003
		Temporal_Mid_R	Occipital_Mid_L	-3.6190	0.0003
		Temporal_Mid_R	Temporal_Mid_L	-3.6728	0.0002

TOPIC 2: Large-scale Network Integration in the Human Brain  
Tracks Temporal Fluctuations in Memory Encoding Performance

---

		Temporal_Mid_R	Temporal_Mid_L	-3.3499	0.0008
		Temporal_Mid_R	Temporal_Mid_L	-3.4037	0.0007
		Temporal_Mid_R	Fusiform_R	-3.4037	0.0007
		Temporal_Mid_R	Fusiform_L	-3.8880	0.0001
		Parietal_Inf_L	Precuneus_L	-3.5652	0.0004
		Precentral_L	Precuneus_L	-3.4306	0.0006
		Precentral_R	Temporal_Pole_Mid_R	-3.5114	0.0004
		Precentral_R	Precuneus_L	-3.6190	0.0003
	VIN	Temporal_Mid_L	Cuneus_L	-3.4306	0.0006
	FPN	Parietal_Sup_R	Frontal_Sup_Orb_R	-3.4037	0.0007
	VAN	Occipital_Mid_L	Temporal_Sup_R	-3.3768	0.0007
		Precentral_L	Temporal_Sup_L	-3.4575	0.0005
		Precentral_L	Temporal_Sup_R	-3.5114	0.0004
		Precentral_R	Temporal_Sup_R	-3.6997	0.0002

**Supplementary file 1F. Robustness of graph-analysis results in different window sizes and proportional thresholds.** We confirmed that the results of graph analysis comparing the high and low encoding states were robust across a range of window sizes (i.e., duration of time window; 7.2 s, 14.4 s, 21.6 s, 30 s, 36 s, 45 s, and 60 s) and proportional thresholds (0.1, 0.15, 0.2, and 0.25).

Duration of time window	Threshold	$E_g$		$E_{loc}$		PC		Modularity	
		$z$	$P$	$z$	$P$	$z$	$P$	$z$	$P$
10TR (7.2 s)	0.10	3.1347	0.0017	1.9238	0.0544	2.1122	0.0347	1.9238	0.0544
	0.15	3.2154	0.0013	0.4440	0.6571	1.3857	0.1658	1.3588	0.1742
	0.20	3.0808	0.0021	-1.3857	0.1658	1.9238	0.0544	1.0090	0.3130
	0.25	3.0270	0.0025	-2.1122	0.0347	2.0315	0.0422	0.9552	0.3395
20TR (14.4 s)	0.10	3.6459	0.0003	1.3050	0.1919	2.7580	0.0058	2.4351	0.0149
	0.15	3.6459	0.0003	0.1480	0.8824	1.2781	0.2012	1.9238	0.0544
	0.20	3.7535	0.0002	-2.7580	0.0058	1.7893	0.0736	1.6010	0.1094
	0.25	3.7535	0.0002	-3.4306	0.0006	1.5471	0.1218	1.3319	0.1829
30TR (21.6 s)	0.10	3.5652	0.0004	0.0673	0.9464	3.2154	0.0013	1.6548	0.0980
	0.15	3.5652	0.0004	-1.7355	0.0827	3.3768	0.0007	0.9552	0.3395
	0.20	3.5114	0.0004	-3.0001	0.0027	3.1077	0.0019	0.0404	0.9678
	0.25	3.4844	0.0005	-3.3768	0.0007	3.0539	0.0023	-0.7938	0.4273
41TR (30 s)	0.10	3.4306	0.0006	-0.7399	0.4593	2.8387	0.0045	1.2781	0.2012
	0.15	3.4037	0.0007	-2.5427	0.0110	1.8162	0.0693	0.4978	0.6186
	0.20	3.5921	0.0003	-3.5921	0.0003	1.0897	0.2758	0.1480	0.8824

TOPIC 2: Large-scale Network Integration in the Human Brain  
Tracks Temporal Fluctuations in Memory Encoding Performance

---

	0.25	3.6728	0.0002	-3.8611	0.0001	1.0897	0.2758	-0.3363	0.7366
50TR (36 s)	0.10	3.9150	0.0001	-1.1705	0.2418	3.4575	0.0005	1.3319	0.1829
	0.15	3.8611	0.0001	-3.0808	0.0021	3.5114	0.0004	0.1480	0.8824
	0.20	3.8880	0.0001	-3.6190	0.0003	2.8118	0.0049	-0.5516	0.5812
	0.25	3.7535	0.0002	-3.5921	0.0003	3.3230	0.0009	-1.1705	0.2418
62TR (45 s)	0.10	4.0226	0.0001	0.9821	0.3260	3.6190	0.0003	2.2198	0.0264
	0.15	4.0764	0.0000	-2.6503	0.0080	3.8342	0.0001	1.7086	0.0875
	0.20	4.0226	0.0001	-3.4037	0.0007	3.5652	0.0004	1.2243	0.2209
	0.25	4.0226	0.0001	-3.8342	0.0001	3.2423	0.0012	0.2556	0.7982
83TR (60 s)	0.10	3.3230	0.0009	-0.3632	0.7164	2.9194	0.0035	2.7311	0.0063
	0.15	3.3499	0.0008	-2.5427	0.0110	3.5652	0.0004	2.0584	0.0396
	0.20	3.5652	0.0004	-3.1077	0.0019	2.1660	0.0303	1.2512	0.2109
	0.25	3.4037	0.0007	-3.5921	0.0003	2.3274	0.0199	0.4440	0.6571

*Notes.* Statistics are derived from Wilcoxon signed-rank tests. Graph metrics ( $E_g$ : global efficiency;  $E_{loc}$ : local efficiency; PC: participation coefficient; Modularity) were computed at the entire-network level.

**Supplementary file 1G. Results of graph analysis using overlapping sliding windows.** We confirmed that the results of graph analysis comparing the high and low encoding states were unchanged when we used sliding windows (in steps of 1 TR, resulting in 2,100 windows per participant).

Duration of time window	Threshold	$E_g$		$E_{loc}$		PC		Modularity	
		$z$	$P$	$z$	$P$	$z$	$P$	$z$	$P$
36 s	0.10	3.8880	0.0001	0.1480	0.8824	3.1347	0.0017	2.5427	0.0110
	0.15	3.9419	0.0001	-2.3544	0.0186	3.0539	0.0023	1.8969	0.0578
	0.20	3.8342	0.0001	-3.5383	0.0004	3.2423	0.0012	1.1166	0.2644
	0.25	3.8073	0.0001	-3.6997	0.0002	3.1077	0.0019	0.3363	0.7366

*Notes.* Statistics are derived from Wilcoxon signed-rank tests. Graph metrics ( $E_g$ : global efficiency;  $E_{loc}$ : local efficiency; PC: participation coefficient; Modularity) were computed at the entire-network level.

**Supplementary file 1H. Results of graph analysis using time series shifted by 5 s.** We confirmed that the results of graph analysis comparing the high and low encoding states were unchanged when we shifted time series (before dividing it into short time windows) by 5 s to take the hemodynamic delay of BOLD response into account (5s, according to canonical hemodynamic response function provided by SPM12).

Duration of time window	Threshold	$E_g$		$E_{loc}$		PC		Modularity	
		$z$	$P$	$z$	$P$	$z$	$P$	$z$	$P$
36 s	0.10	3.9688	0.0001	-0.4709	0.6377	2.8387	0.0045	1.7086	0.0875
	0.15	3.8342	0.0001	-2.4351	0.0149	3.2961	0.0010	0.7938	0.4273
	0.20	3.8611	0.0001	-3.2423	0.0012	3.0539	0.0023	0.1211	0.9036
	0.25	3.8611	0.0001	-3.6728	0.0002	2.7580	0.0058	-0.7399	0.4593

*Notes.* Statistics are derived from Wilcoxon signed-rank tests. Graph metrics ( $E_g$ : global efficiency;  $E_{loc}$ : local efficiency; PC: participation coefficient; Modularity) were computed at the entire-network level.



**Supplementary file 1I. Results of graph analysis using time series that contain task-related signals.** We confirmed that the results of graph analysis comparing the high and low encoding states were unchanged when we used time series that kept task-related signals instead of residual time series.

Duration of time window	Threshold	$E_g$		$E_{loc}$		PC		Modularity	
		$z$	$P$	$z$	$P$	$z$	$P$	$z$	$P$
36 s	0.10	4.1571	0.00003	0.6323	0.5272	3.3230	0.0009	3.2692	0.0011
	0.15	4.1302	0.0000	-2.0046	0.0450	2.8656	0.0042	2.1660	0.0303
	0.20	4.1033	0.00004	-3.2692	0.0011	3.2423	0.0012	1.0897	0.2758
	0.25	4.1302	0.00004	-3.9688	0.0001	3.0270	0.0025	0.3902	0.6964

*Notes.* Statistics are derived from Wilcoxon signed-rank tests. Graph metrics ( $E_g$ : global efficiency;  $E_{loc}$ : local efficiency; PC: participation coefficient; Modularity) were computed at the entire-network level.

**Supplementary file 1J. Results of graph analysis including low-confidence hit trials.** We confirmed that the results of graph analysis comparing the high and low encoding states were unchanged when we defined the window-wise encoding performance by using both high- and low-confidence hit trials (i.e., the number of HH plus LH trials divided by that of the picture trials, computed within each time window).

Duration of time window	Threshold	$E_g$		$E_{loc}$		PC		Modularity	
		$z$	$P$	$z$	$P$	$z$	$P$	$z$	$P$
36 s	0.10	3.1077	0.0019	0.9283	0.3533	2.6772	0.0074	1.4395	0.1500
	0.15	3.2692	0.0011	-1.3857	0.1658	3.3768	0.0007	0.6861	0.4926
	0.20	3.0808	0.0021	-2.4082	0.0160	3.0808	0.0021	0.1480	0.8824
	0.25	2.7849	0.0054	-2.7849	0.0054	3.1885	0.0014	-0.5785	0.5629

*Notes.* Statistics are derived from Wilcoxon signed-rank tests. Graph metrics ( $E_g$ : global efficiency;  $E_{loc}$ : local efficiency; PC: participation coefficient; Modularity) were computed at the entire-network level.

**Supplementary file 1K. Graph-analysis results using tertiles to classify high and low encoding states.** In this control analysis, we classified the time windows based on participant-specific tertiles of window-wise encoding performance, and compared graph metrics between the top and bottom tertiles. The proportion of HH trials was  $69.7\% \pm 16.3\%$  ( $5.58 \pm 1.33$  trials per window) for the top tertile and  $28.4 \pm 14.4\%$  ( $2.24 \pm 1.13$  trials per window) for the bottom tertile.

Duration of time window	Threshold	$E_g$		$E_{loc}$		PC		Modularity	
		$z$	$P$	$z$	$P$	$z$	$P$	$z$	$P$
41TR (30 s)	0.10	3.7429	0.0002	0.4000	0.6892	3.2000	0.0014	1.7143	0.0865
	0.15	3.7429	0.0002	-1.8571	0.0633	3.8571	0.0001	1.3714	0.1702
	0.20	3.7714	0.0002	-3.3429	0.0008	2.8571	0.0043	0.7429	0.4576
	0.25	3.6000	0.0003	-3.7143	0.0002	2.4000	0.0164	0.2286	0.8192
50TR (36 s)	0.10	3.9419	0.0001	-0.1480	0.8824	3.8611	0.0001	2.3544	0.0186
	0.15	3.9419	0.0001	-2.3813	0.0173	3.4037	0.0007	1.2781	0.2012
	0.20	3.8880	0.0001	-3.4844	0.0005	2.9463	0.0032	0.5785	0.5629
	0.25	3.8342	0.0001	-3.6728	0.0002	3.4844	0.0005	-0.3632	0.7164
62TR (45 s)	0.10	3.7804	0.0002	0.1749	0.8612	3.9688	0.0001	1.3857	0.1658
	0.15	3.9150	0.0001	-2.8387	0.0045	3.9688	0.0001	0.7130	0.4758
	0.20	3.8342	0.0001	-3.5652	0.0004	3.2154	0.0013	0.0404	0.9678
	0.25	3.8073	0.0001	-3.8342	0.0001	2.9732	0.0029	-1.0897	0.2758
83TR (60 s)	0.10	3.3768	0.0007	0.1749	0.8612	2.1929	0.0283	2.1660	0.0303

TOPIC 2: Large-scale Network Integration in the Human Brain  
Tracks Temporal Fluctuations in Memory Encoding Performance

---

0.15	3.2154	0.0013	-2.3544	0.0186	3.4037	0.0007	1.4664	0.1425
0.20	3.1347	0.0017	-3.4575	0.0005	2.6772	0.0074	1.0090	0.3130
0.25	3.0808	0.0021	-3.5921	0.0003	2.7849	0.0054	0.5785	0.5629

*Notes.* Statistics are derived from Wilcoxon signed-rank tests. Graph metrics ( $E_g$ : global efficiency;  $E_{loc}$ : local efficiency; PC: participation coefficient; Modularity) were computed at the entire-network level.

**Supplementary file 1L. Graph-analysis results using quartiles to classify high and low encoding states.** In this control analysis, we classified the time windows based on participant-specific quartiles of window-wise encoding performance, and compared graph metrics between the top and bottom quartiles. The proportion of HH trials was  $73.2\% \pm 16.2\%$  ( $5.91 \pm 1.37$  trials per window) for the top quartile and  $24.7 \pm 14.1\%$  ( $1.94 \pm 1.11$  trials per window) for the bottom quartile.

Duration of time window	Threshold	$E_g$		$E_{loc}$		PC		Modularity	
		$z$	$P$	$z$	$P$	$z$	$P$	$z$	$P$
41TR (30 s)	0.10	4.2378	0.0000	-0.6323	0.5272	3.5383	0.0004	1.8700	0.0615
	0.15	4.2109	0.0000	-2.7041	0.0068	3.7266	0.0002	1.1435	0.2528
	0.20	4.2109	0.0000	-3.5921	0.0003	3.3499	0.0008	0.4978	0.6186
	0.25	4.0226	0.0001	-4.1033	0.0000	2.9732	0.0029	-0.1480	0.8824
50TR (36 s)	0.10	3.5383	0.0004	-0.2287	0.8191	3.3499	0.0008	2.1391	0.0324
	0.15	3.5652	0.0004	-2.0315	0.0422	3.0270	0.0025	0.8745	0.3819
	0.20	3.4844	0.0005	-3.1347	0.0017	2.7041	0.0068	0.2018	0.8401
	0.25	3.4575	0.0005	-3.4575	0.0005	2.6772	0.0074	-0.8476	0.3967
62TR (45 s)	0.10	3.5383	0.0004	0.1480	0.8824	3.5652	0.0004	1.9508	0.0511
	0.15	3.7535	0.0002	-2.3274	0.0199	3.3230	0.0009	1.0628	0.2879
	0.20	3.6728	0.0002	-3.2961	0.0010	2.2736	0.0230	0.7938	0.4273
	0.25	3.5921	0.0003	-3.6190	0.0003	2.0853	0.0370	-0.1211	0.9036
83TR (60 s)	0.10	3.5921	0.0003	0.2825	0.7775	3.2692	0.0011	2.6234	0.0087

TOPIC 2: Large-scale Network Integration in the Human Brain  
Tracks Temporal Fluctuations in Memory Encoding Performance

---

0.15	3.4306	0.0006	-3.0539	0.0023	3.5114	0.0004	1.7893	0.0736
0.20	3.4575	0.0005	-3.5652	0.0004	2.9463	0.0032	0.8207	0.4118
0.25	3.4844	0.0005	-3.5921	0.0003	3.0270	0.0025	-0.1480	0.8824

*Notes.* Statistics are derived from Wilcoxon signed-rank tests. Graph metrics ( $E_g$ : global efficiency;  $E_{loc}$ : local efficiency; PC: participation coefficient; Modularity) were computed at the entire-network level.

**Supplementary file 1M. Results of graph analysis controlling for time passed within a session or across sessions.** We confirmed that the results of graph analysis comparing the high and low encoding states were unchanged when we regressed out the effect of the amount of time passed within sessions (defined by a dummy variable denoting the order of windows [1, 2, 3, ... 15] in each session) or time passed across sessions (defined by a dummy variable denoting session ID [1, 1, ... 2, 2, ... 3, 3, ...]) on a window-by-window basis.

Covariate	$E_g$		$E_{loc}$		PC		Modularity	
	$z$	$P$	$z$	$P$	$z$	$P$	$z$	$P$
Time passed within each session, linear	3.5383	0.0004	-3.1077	0.0019	3.0270	0.0025	0.2018	0.8401
Time passed within each session, quadratic	3.8611	0.0001	-2.9732	0.0029	3.4306	0.0006	0.2287	0.8191
Time passed across sessions, linear	3.8880	0.0001	-3.2423	0.0012	3.5114	0.0004	0.0942	0.925
Time passed across sessions, quadratic	3.7804	0.0002	-3.2961	0.0010	3.3499	0.0008	0.3902	0.6964

*Notes.* Statistics are derived from Wilcoxon signed-rank tests. Graph metrics ( $E_g$ : global efficiency;  $E_{loc}$ : local efficiency; PC: participation coefficient; Modularity) were computed at the entire-network level.

**Supplementary file 1N. Results of control analysis testing effect of proportion of picture trials.** In this control analysis, we classified the time windows based on the proportion of the picture trials and compared the graph metrics between “more pic” and “fewer pic” periods.

Duration of time window	Threshold	$E_g$		$E_{loc}$		PC		Modularity	
		$z$	$P$	$z$	$P$	$z$	$P$	$z$	$P$
36 s	0.10	0.3363	0.7366	-0.9283	0.3533	-0.4978	0.6186	0.5247	0.5998
	0.15	0.5247	0.5998	-0.2287	0.8191	-0.6861	0.4926	0.7399	0.4593
	0.20	0.2556	0.7982	0.4709	0.6377	-0.5247	0.5998	0.9552	0.3395
	0.25	0.4171	0.6766	0.2018	0.8401	-0.6861	0.4926	0.6592	0.5098

*Notes.* Statistics are derived from Wilcoxon signed-rank tests. Graph metrics ( $E_g$ : global efficiency;  $E_{loc}$ : local efficiency; PC: participation coefficient; Modularity) were computed at the entire-network level.



**Supplementary file 1O. Results of control analysis testing effect of reaction time for semantic judgment.** In this control analysis, we classified the time windows based on mean RT (computed within each time window) for semantic judgment and compared the graph metrics between “longer RT” and “shorter RT” periods.

Duration of time window	Threshold	$E_g$		$E_{loc}$		PC		Modularity	
		$z$	$P$	$z$	$P$	$z$	$P$	$z$	$P$
36 s	0.10	-1.3588	0.1742	0.7668	0.4432	-1.2781	0.2012	-0.4709	0.6377
	0.15	-1.9508	0.0511	1.4126	0.1578	-1.7893	0.0736	-0.4440	0.6571
	0.20	-2.0046	0.0450	1.6010	0.1094	-0.9014	0.3674	-0.1211	0.9036
	0.25	-1.8969	0.0578	1.8700	0.0615	-0.9552	0.3395	0.2018	0.8401

*Notes.* Statistics are derived from Wilcoxon signed-rank tests. Graph metrics ( $E_g$ : global efficiency;  $E_{loc}$ : local efficiency; PC: participation coefficient; Modularity) were computed at the entire-network level.

**Supplementary file 1P. 285 ROIs included in 11 subnetworks of the Gordon atlas.**

ROI ID	MNI coordinates			Assigned network
	x	y	z	
1	-18.80	-48.70	65.00	SMN
2	-10.70	-47.50	60.30	SMN
3	-15.60	-33.10	66.10	SMN
4	-10.90	-29.30	69.50	SMN
5	-6.60	-20.40	74.20	SMN
6	-10.80	-41.10	64.90	SMN
7	-5.00	-28.20	60.40	SMN
8	-5.40	-15.90	48.80	SMN
9	-35.80	-29.70	54.50	SMN
10	-36.80	-22.80	61.90	SMN
11	-20.50	-24.90	64.50	SMN
12	-23.40	-13.80	64.20	SMN
13	-17.20	-8.60	67.90	SMN
14	-28.60	-44.70	61.70	SMN
15	-54.10	-21.30	40.80	SMN

Chapter 3

---

16	-35.20	-35.30	42.00	SMN
17	-27.50	-37.20	61.40	SMN
18	-47.20	-31.40	54.80	SMN
19	20.80	-48.20	66.10	SMN
20	16.50	-32.80	67.70	SMN
21	4.80	-27.10	64.80	SMN
22	11.90	-40.70	67.00	SMN
23	5.10	-17.10	51.60	SMN
24	6.80	-8.10	50.90	SMN
25	38.10	-22.40	60.30	SMN
26	19.70	-25.00	65.20	SMN
27	12.40	-28.30	69.60	SMN
28	29.20	-13.50	64.20	SMN
29	17.00	-16.90	70.90	SMN
30	20.90	-6.40	65.00	SMN
31	29.50	-42.50	60.40	SMN
32	34.20	-40.60	51.60	SMN
33	39.60	-31.50	39.70	SMN
34	28.00	-34.80	63.10	SMN
35	39.20	-34.60	57.50	SMN
36	37.30	-25.90	50.90	SMN

TOPIC 2: Large-scale Network Integration in the Human Brain  
Tracks Temporal Fluctuations in Memory Encoding Performance

---

37	48.70	-26.10	52.20	SMN
38	53.00	-22.70	39.10	SMN
39	-51.80	-7.80	38.50	SMN
40	-41.50	-12.50	50.40	SMN
41	-51.50	-11.90	29.70	SMN
42	-46.10	-17.80	52.70	SMN
43	49.60	-7.40	36.10	SMN
44	42.30	-11.00	47.30	SMN
45	53.90	-8.30	26.10	SMN
46	47.80	-15.10	49.30	SMN
47	-16.60	-36.10	42.70	CON
48	-9.40	-0.10	42.90	CON
49	-8.40	14.60	33.80	CON
50	-9.00	25.30	27.70	CON
51	-8.00	-8.70	62.90	CON
52	-42.10	-4.50	47.30	CON
53	-57.70	-40.60	35.80	CON
54	-38.70	-16.00	-5.30	CON
55	-39.10	-1.60	-12.20	CON
56	-37.70	2.90	11.70	CON
57	-36.60	1.40	6.40	CON

Chapter 3

---

58	-37.30	8.90	-0.90	CON
59	-28.80	23.70	8.40	CON
60	-59.80	-4.10	8.80	CON
61	-55.10	-32.30	23.00	CON
62	-58.80	-23.90	31.00	CON
63	-51.80	-0.60	5.00	CON
64	-48.60	7.50	11.10	CON
65	-26.60	46.80	20.90	CON
66	-28.80	38.30	28.20	CON
67	16.20	-33.10	43.20	CON
68	6.70	5.00	55.90	CON
69	8.60	4.20	40.10	CON
70	8.80	10.80	45.90	CON
71	6.00	21.80	32.40	CON
72	16.20	0.80	67.50	CON
73	8.00	-6.20	63.70	CON
74	42.50	-2.30	47.20	CON
75	57.50	-40.30	34.70	CON
76	54.90	-27.00	29.60	CON
77	38.80	-14.40	-5.00	CON
78	39.70	1.20	-13.10	CON

TOPIC 2: Large-scale Network Integration in the Human Brain  
Tracks Temporal Fluctuations in Memory Encoding Performance

---

79	36.70	5.20	12.70	CON
80	39.60	10.40	-1.60	CON
81	36.50	5.70	6.00	CON
82	33.70	22.60	3.70	CON
83	34.00	24.40	10.00	CON
84	50.10	3.00	3.90	CON
85	24.40	50.80	24.30	CON
86	31.30	39.70	25.60	CON
87	-6.10	-26.00	28.50	CON
88	-12.70	-64.90	31.80	CON
89	-10.90	-73.40	42.90	CON
90	7.60	-27.00	28.40	CON
91	15.60	-69.50	39.60	CON
92	-32.00	-29.30	15.60	AUD
93	-46.30	-41.40	25.90	AUD
94	-35.80	-33.50	19.90	AUD
95	-52.70	-20.60	5.40	AUD
96	-59.60	-38.50	16.50	AUD
97	-58.70	-29.90	11.10	AUD
98	-40.60	-38.30	14.50	AUD
99	-33.70	-21.80	9.90	AUD

Chapter 3

---

100	-37.20	-14.00	19.40	AUD
101	-52.20	-14.10	15.20	AUD
102	-50.60	-22.40	19.20	AUD
103	-54.40	-1.40	-0.70	AUD
104	33.60	-22.30	13.00	AUD
105	36.40	-30.70	19.40	AUD
106	53.80	-15.80	5.20	AUD
107	59.20	-38.60	14.60	AUD
108	61.70	-24.00	1.30	AUD
109	60.00	-25.20	10.20	AUD
110	38.40	-12.20	20.00	AUD
111	36.60	-10.00	12.40	AUD
112	60.90	-2.20	10.70	AUD
113	54.20	-13.60	16.90	AUD
114	39.70	-22.50	2.60	AUD
115	55.80	2.00	-2.00	AUD
116	-11.20	-52.40	36.50	DMN
117	-11.70	26.70	57.00	DMN
118	-47.20	-58.00	30.80	DMN
119	-5.60	42.20	35.10	DMN
120	-1.70	-17.70	39.10	DMN

TOPIC 2: Large-scale Network Integration in the Human Brain  
Tracks Temporal Fluctuations in Memory Encoding Performance

---

121	-19.50	30.10	45.50	DMN
122	-39.30	-73.90	38.30	DMN
123	-27.50	53.60	0.00	DMN
124	-5.90	54.80	-11.30	DMN
125	-6.80	38.20	-9.40	DMN
126	-63.20	-28.70	-7.20	DMN
127	-53.10	-11.40	-16.00	DMN
128	-15.90	48.60	37.20	DMN
129	-19.50	56.30	27.50	DMN
130	-6.50	54.70	18.10	DMN
131	-15.70	64.70	13.70	DMN
132	-6.00	44.90	6.30	DMN
133	-26.20	26.60	38.80	DMN
134	-29.30	16.80	50.70	DMN
135	-41.70	16.10	47.50	DMN
136	12.30	-51.60	34.50	DMN
137	11.90	21.90	59.90	DMN
138	7.70	44.10	5.50	DMN
139	3.00	-19.60	37.90	DMN
140	21.90	21.00	46.20	DMN
141	48.90	-53.00	28.60	DMN



Chapter 3

---

142	62.50	-25.60	-5.50	DMN
143	7.40	-69.30	49.90	DMN
144	46.50	-67.30	36.20	DMN
145	7.20	48.40	-10.10	DMN
146	57.50	-7.40	-16.40	DMN
147	21.00	32.80	42.10	DMN
148	21.40	42.80	35.10	DMN
149	16.00	61.00	19.80	DMN
150	8.20	53.80	14.00	DMN
151	5.90	54.90	29.40	DMN
152	13.80	46.70	42.10	DMN
153	6.80	44.50	34.80	DMN
154	30.60	18.90	48.70	DMN
155	54.40	1.10	-12.90	DMN
156	-18.40	-85.50	21.60	VIN
157	-16.80	-60.10	-5.40	VIN
158	-11.30	-83.20	3.90	VIN
159	-22.00	-58.10	1.50	VIN
160	-9.60	-58.00	3.00	VIN
161	-16.70	-46.00	-3.70	VIN
162	-13.70	-77.40	26.60	VIN

TOPIC 2: Large-scale Network Integration in the Human Brain  
Tracks Temporal Fluctuations in Memory Encoding Performance

---

163	-31.30	-84.20	9.00	VIN
164	-34.20	-86.60	-0.50	VIN
165	-43.40	-67.60	9.70	VIN
166	-28.80	-58.80	-9.10	VIN
167	-34.40	-63.90	-15.70	VIN
168	-34.30	-43.80	-21.60	VIN
169	-5.40	-88.00	18.60	VIN
170	-8.60	-77.50	-3.50	VIN
171	-41.20	-72.10	-5.90	VIN
172	-25.20	-97.20	-7.90	VIN
173	-22.60	-81.70	-11.70	VIN
174	22.00	-84.60	23.70	VIN
175	22.30	-46.50	-9.90	VIN
176	15.50	-74.10	9.40	VIN
177	19.60	-45.30	-4.40	VIN
178	15.60	-59.60	-5.00	VIN
179	26.80	-55.00	54.20	VIN
180	17.60	-78.30	34.00	VIN
181	7.70	-85.60	31.60	VIN
182	35.40	-77.10	21.10	VIN
183	31.70	-85.70	2.40	VIN

Chapter 3

---

184	43.80	-67.20	2.00	VIN
185	47.30	-52.40	-11.70	VIN
186	49.00	-54.50	8.80	VIN
187	31.20	-45.60	-5.80	VIN
188	26.90	-69.10	-6.60	VIN
189	34.90	-44.00	-20.00	VIN
190	13.80	-92.30	14.70	VIN
191	10.50	-73.80	-1.50	VIN
192	20.40	-87.30	-6.60	VIN
193	5.10	-80.20	23.10	VIN
194	14.60	-70.30	23.30	VIN
195	-38.10	48.80	10.50	FPN
196	-55.90	-47.70	-9.30	FPN
197	-5.50	29.30	44.00	FPN
198	-40.30	50.40	-4.80	FPN
199	-34.10	-61.00	42.40	FPN
200	-43.00	19.40	33.50	FPN
201	-40.20	23.60	23.30	FPN
202	-21.30	63.10	1.90	FPN
203	-28.60	50.90	10.10	FPN
204	47.90	-42.50	41.50	FPN

TOPIC 2: Large-scale Network Integration in the Human Brain  
Tracks Temporal Fluctuations in Memory Encoding Performance

---

205	38.10	45.90	7.70	FPN
206	59.70	-41.00	-10.90	FPN
207	7.00	25.70	47.30	FPN
208	42.80	48.30	-5.10	FPN
209	41.50	-53.50	44.00	FPN
210	35.70	-56.70	45.20	FPN
211	37.80	28.70	35.60	FPN
212	41.80	29.10	21.60	FPN
213	38.60	18.80	25.50	FPN
214	28.40	57.00	-5.10	FPN
215	23.50	59.10	4.90	FPN
216	30.90	52.20	9.90	FPN
217	42.40	19.50	48.20	FPN
218	38.90	9.60	42.70	FPN
219	-10.00	33.90	21.50	SAN
220	-32.50	17.20	-7.80	SAN
221	8.40	34.70	22.60	SAN
222	30.60	22.80	-4.70	SAN
223	-3.80	12.10	64.60	VAT
224	-44.80	-54.00	14.60	VAT
225	-51.60	-55.90	11.40	VAT

Chapter 3

226	-48.10	-40.00	2.40	VAT
227	-50.00	20.80	10.60	VAT
228	-47.20	39.00	-9.10	VAT
229	-29.10	20.50	-14.00	VAT
230	-44.30	33.20	-7.20	VAT
231	-45.40	28.80	0.80	VAT
232	-38.70	4.80	48.40	VAT
233	-59.00	-18.00	-3.00	VAT
234	57.50	-45.30	9.00	VAT
235	60.90	-38.70	1.70	VAT
236	57.10	-17.00	-2.60	VAT
237	47.40	-39.60	13.20	VAT
238	45.50	-37.30	3.40	VAT
239	48.50	-26.50	-0.10	VAT
240	52.50	23.70	10.30	VAT
241	48.10	38.30	-9.20	VAT
242	45.20	30.70	-5.60	VAT
243	27.40	19.70	-14.90	VAT
244	57.10	-6.30	-7.70	VAT
245	46.60	-21.50	-8.50	VAT
246	-27.30	-6.80	46.30	DAT

TOPIC 2: Large-scale Network Integration in the Human Brain  
Tracks Temporal Fluctuations in Memory Encoding Performance

---

247	-27.30	1.90	52.90	DAT
248	-19.80	6.40	55.70	DAT
249	-21.30	-0.20	62.70	DAT
250	-31.10	-48.90	47.10	DAT
251	-42.90	-45.00	43.00	DAT
252	-51.70	-30.90	39.90	DAT
253	-43.60	36.30	8.50	DAT
254	-20.40	-64.60	51.40	DAT
255	-25.80	-65.00	32.20	DAT
256	-9.90	-56.90	59.80	DAT
257	-7.10	-63.70	54.90	DAT
258	-30.00	-74.10	36.10	DAT
259	-46.20	-57.70	-7.90	DAT
260	-45.20	2.70	32.40	DAT
261	-34.70	5.60	34.00	DAT
262	-37.60	38.40	17.20	DAT
263	-41.60	8.70	22.20	DAT
264	-35.70	33.10	32.00	DAT
265	10.30	-57.30	58.30	DAT
266	29.20	1.90	52.40	DAT
267	29.90	-7.80	47.40	DAT

### Chapter 3

---

268	22.60	5.60	57.60	DAT
269	38.80	-42.60	40.40	DAT
270	36.80	37.80	13.10	DAT
271	48.10	38.40	2.40	DAT
272	23.00	-66.40	51.80	DAT
273	32.30	-63.60	33.80	DAT
274	33.50	-48.20	49.40	DAT
275	57.00	-53.80	-1.10	DAT
276	47.30	2.00	37.60	DAT
277	46.60	7.80	19.30	DAT
278	-14.40	-57.80	18.40	RST
279	-8.80	-49.80	4.20	RST
280	-33.80	-33.20	-15.40	RST
281	-22.50	-37.10	-15.00	RST
282	13.80	-54.10	10.90	RST
283	34.60	-35.60	-12.30	RST
284	34.60	-23.90	-20.40	RST
285	24.50	-36.20	-13.20	RST

*Note.* SMN, sensorimotor networks; CON, cingulo-opercular network; CPN: Cingulo-Parietal network; AUD, auditory network; DMN, default mode network; VIN, visual network; FPN, fronto-parietal network; SAN, salience network; VAN, ventral attention network; DAN, dorsal attention network; RST: Retrosplenial temporal network.

**Supplementary file 1Q. Graph-analysis results using 285 ROIs from the Gordon atlas.**

Duration of time window	Threshold	$E_g$		$E_{loc}$		PC		Modularity	
		$z$	$P$	$z$	$P$	$z$	$P$	$z$	$P$
41TR (30 s)	0.10	3.9150	0.0001	0.5516	0.5812	2.5427	0.0110	2.1122	0.0347
	0.15	3.8880	0.0001	-1.0628	0.2879	2.7849	0.0054	1.8162	0.0693
	0.20	3.9419	0.0001	-3.6997	0.0002	2.0853	0.0370	1.4664	0.1425
	0.25	3.9688	0.0001	-3.8073	0.0001	2.4351	0.0149	1.1166	0.2641
50TR (36 s)	0.10	3.8342	0.0001	-0.4978	0.6186	3.1616	0.0016	1.6548	0.0980
	0.15	3.8611	0.0001	-3.1077	0.0019	2.6772	0.0074	1.1705	0.2418
	0.20	3.8342	0.0001	-3.8611	0.0001	3.1616	0.0016	0.2556	0.7982
	0.25	3.8880	0.0001	-3.9419	0.0001	3.4037	0.0007	-0.2018	0.8401
62TR (45 s)	0.10	3.7804	0.0002	1.3857	0.1658	3.5383	0.0004	3.1885	0.0014
	0.15	3.9419	0.0001	-2.2736	0.0230	3.1616	0.0016	2.8118	0.0049
	0.20	3.9957	0.0001	-3.6190	0.0003	3.3230	0.0009	1.8969	0.0578
	0.25	4.0226	0.0001	-3.7535	0.0002	2.4351	0.0149	1.6817	0.0926
83TR (60 s)	0.10	3.8073	0.0001	0.4709	0.6377	2.3813	0.0173	3.0808	0.0021
	0.15	3.6190	0.0003	-2.7311	0.0063	2.8387	0.0045	2.5696	0.0102
	0.20	3.6728	0.0002	-3.5114	0.0004	2.8925	0.0038	1.9508	0.0511



### Chapter 3

---

	0.25	3.5652	0.0004	-3.7535	0.0002	3.1616	0.0016	0.9821	0.3260
--	------	--------	--------	---------	--------	--------	--------	--------	--------

*Notes.* Statistics are derived from Wilcoxon signed-rank tests. Graph metrics ( $E_g$ : global efficiency;  $E_{loc}$ : local efficiency; PC: participation coefficient; Modularity) were computed at the entire-network level.

**Supplementary file 1R. Graph-analysis results using 226 ROIs from the Power atlas combining with the bilateral hippocampus ROIs derived from Kim's meta-analysis.**

Duration of time window	Threshold	$E_g$		$E_{loc}$		PC		Modularity	
		$z$	$P$	$z$	$P$	$z$	$P$	$z$	$P$
41TR (30 s)	0.10	3.8611	0.0001	-0.2018	0.8401	3.2154	0.0013	1.6817	0.0926
	0.15	4.0495	0.0001	-2.1929	0.0283	3.5652	0.0004	1.2781	0.2012
	0.20	4.0764	0.0000	-3.6997	0.0002	2.7849	0.0054	0.5785	0.5629
	0.25	3.9957	0.0001	-3.9419	0.0001	2.8118	0.0049	-0.0135	0.9893
50TR (36 s)	0.10	3.8880	0.0001	-1.4126	0.1578	3.4844	0.0005	1.1435	0.2528
	0.15	3.8611	0.0001	-3.1077	0.0019	3.1077	0.0019	0.2825	0.7775
	0.20	3.8880	0.0001	-3.5921	0.0003	2.5965	0.0094	-0.7399	0.4593
	0.25	3.6728	0.0002	-3.6728	0.0002	3.0270	0.0025	-1.2512	0.2109
62TR (45 s)	0.10	4.0226	0.0001	1.1974	0.2312	3.5652	0.0004	2.1660	0.0303
	0.15	4.0495	0.0001	-2.5965	0.0094	4.0495	0.0001	1.8700	0.0615
	0.20	4.0226	0.0001	-3.4844	0.0005	2.9732	0.0029	1.3588	0.1742
	0.25	4.0226	0.0001	-3.8073	0.0001	3.1347	0.0017	0.2556	0.7982
83TR (60 s)	0.10	3.3768	0.0007	-0.5785	0.5629	2.9463	0.0032	2.4889	0.0128
	0.15	3.4306	0.0006	-2.5696	0.0102	3.5383	0.0004	1.9508	0.0511
	0.20	3.5652	0.0004	-3.2692	0.0011	2.2736	0.0230	1.0897	0.2758

### Chapter 3

---

	0.25	3.4306	0.0006	-3.6459	0.0003	2.2736	0.0230	0.3632	0.7164
--	------	--------	--------	---------	--------	--------	--------	--------	--------

*Notes.* Statistics are derived from Wilcoxon signed-rank tests. Graph metrics ( $E_g$ : global efficiency;  $E_{loc}$ : local efficiency; PC: participation coefficient; Modularity) were computed at the entire-network level.

**Supplementary file 1S. Edge stability analysis.**

Threshold	High encoding state (Real vs. Randomized)		Low encoding state (Real vs. Randomized)		High vs. low encoding states	
	<i>z</i>	<i>P</i>	<i>z</i>	<i>P</i>	<i>z</i>	<i>P</i>
0.1	4.3724	0.00001	4.3724	0.00001	0.0042	2.8656
0.15	4.3726	0.00001	4.3724	0.00001	0.0926	1.6817
0.2	4.3724	0.00001	4.3724	0.00001	0.2699	1.1033
0.25	4.3724	0.00001	4.3724	0.00001	0.0455	2.0000

*Notes.* Statistics are derived from Wilcoxon signed-rank tests. Comparisons between the real and randomized networks gave the same results in most cases because the signed ranks were identical.

**Supplementary file 1T. Results of additional analysis using adjusted graph metrics.** We computed “adjusted” graph metrics by regressing out overall FC on a window-by-window basis.

Duration of time window	Threshold	$E_g$		$E_{loc}$		PC		Modularity	
		$z$	$P$	$z$	$P$	$z$	$P$	$z$	$P$
36 s	0.10	0.2825	0.7775	-0.3094	0.7570	1.4126	0.1578	0.8745	0.3819
	0.15	0.0942	0.9250	-0.7130	0.4758	0.0673	0.9464	0.4171	0.6766
	0.20	-1.0090	0.3130	-0.0942	0.9250	-0.1211	0.9036	0.2018	0.8401
	0.25	-1.0090	0.3130	-0.0404	0.9678	0.4440	0.6571	-0.2018	0.8401

*Notes.* Statistics are derived from Wilcoxon signed-rank tests. Graph metrics ( $E_g$ : global efficiency;  $E_{loc}$ : local efficiency; PC: participation coefficient; Modularity) were computed at the entire-network level.

**Supplementary file 1U. Graph-analysis results from the group of 13 subjects showing the minimal difference in FD between high and low encoding states.**

Duration of time window	Threshold	$E_g$		$E_{loc}$		PC		Modularity	
		Signed rank	$p$	Signed rank	$p$	Signed rank	$p$	Signed rank	$p$
41TR (30 s)	0.10	87	0.0017	46	1.0000	74	0.0479	65	0.1909
	0.15	90	0.0005	29	0.2734	78	0.0215	57	0.4548
	0.20	90	0.0005	7	0.0046	73	0.0574	53	0.6355
	0.25	89	0.0007	1	0.0005	63	0.2439	46	1.0000
50TR (36 s)	0.10	90	0.0005	49	0.8394	72	0.0681	53	0.6355
	0.15	89	0.0007	24	0.1465	84	0.0046	44	0.9460
	0.20	90	0.0005	6	0.0034	69	0.1099	38	0.6355
	0.25	85	0.0034	9	0.0081	70	0.0942	30	0.3054
62TR (45 s)	0.10	90	0.0005	67	0.1465	91	0.0002	69	0.1099
	0.15	91	0.0002	17	0.0479	87	0.0017	63	0.2439
	0.20	91	0.0002	10	0.0105	85	0.0034	64	0.2163
	0.25	91	0.0002	0	0.0002	87	0.0017	52	0.6848
83TR (60 s)	0.10	76	0.0327	60	0.3396	68	0.1272	74	0.0479
	0.15	74	0.0479	38	0.6355	82	0.0081	76	0.0327

### Chapter 3

---

	0.20	80	0.0134	24	0.1465	48	0.8926	72	0.0681
	0.25	77	0.0266	10	0.0105	50	0.7869	71	0.0803

*Notes.* Statistics are derived from Wilcoxon signed-rank tests. Graph metrics ( $E_g$ : global efficiency;  $E_{loc}$ : local efficiency; PC: participation coefficient; Modularity) were computed at the entire-network level.

**Supplementary file 1V. Graph-analysis results using 32P+scrubbing denosing.**

Duration of time window	Threshold	$E_g$		$E_{loc}$		PC		Modularity	
		$z$	$P$	$z$	$P$	$z$	$P$	$z$	$P$
41TR (30 s)	0.10	4.1302	0.00004	0.2287	0.8191	2.3544	0.0186	2.7041	0.0068
	0.15	4.2917	0.00002	-1.2781	0.2012	1.1705	0.2418	2.5965	0.0094
	0.20	4.2647	0.00002	-3.1077	0.0019	1.6279	0.1036	2.1660	0.0303
	0.25	4.2917	0.00002	-3.9419	0.0001	1.0628	0.2879	1.7355	0.0827
50TR (36 s)	0.10	3.8342	0.00013	1.1705	0.2418	2.5965	0.0094	2.9732	0.0029
	0.15	4.0495	0.00005	-1.1435	0.2528	3.1616	0.0016	2.4620	0.0138
	0.20	4.0495	0.00005	-2.7580	0.0058	2.5965	0.0094	2.1122	0.0347
	0.25	4.2109	0.00003	-3.8611	0.0001	3.0808	0.0021	1.5471	0.1218
62TR (45 s)	0.10	4.1840	0.00003	1.6817	0.0926	2.3274	0.0199	3.2154	0.0013
	0.15	4.2917	0.00002	-0.9014	0.3674	2.5696	0.0102	3.1616	0.0016
	0.20	4.2647	0.00002	-3.0001	0.0027	3.2154	0.0013	2.5427	0.0110
	0.25	4.2647	0.00002	-3.9957	0.0001	3.3768	0.0007	2.0315	0.0422
83TR (60 s)	0.10	3.1885	0.00143	-0.1749	0.8612	0.0404	0.9678	3.0270	0.0025
	0.15	3.6728	0.00024	-1.3588	0.1742	1.6548	0.0980	2.8656	0.0042
	0.20	3.6728	0.00024	-2.4082	0.0160	1.2512	0.2109	2.6234	0.0087



### Chapter 3

---

	0.25	3.7266	0.00019	-3.9957	0.0001	2.0584	0.0396	2.4620	0.0138
--	------	--------	---------	---------	--------	--------	--------	--------	--------

*Notes.* Statistics are derived from Wilcoxon signed-rank tests. Graph metrics ( $E_g$ : global efficiency;  $E_{loc}$ : local efficiency; PC: participation coefficient; Modularity) were computed at the entire-network level.

## **CHAPTER 4**

### **CONCLUSION**

In the topic 1, we investigated whether the intrinsic fluctuations (here we defined as LFFs) can account for subsequent memory performance. Our findings demonstrate that prestimulus LFFs in the SME related regions can predict whether the encoding trial will be remembered. Specifically, the higher LFFs amplitude was observed before the stimulus later remembered indicating that LFFs in these brain regions benefit for memory encoding. In contrast, before the stimulus later forgotten, we observed stronger LFFs functional connectivity from the fusiform gyrus to the brain regions inside the CO network. Together, our findings indicate the effect of LFFs to memory encoding processes providing compelling evidence to support the view that LFFs (independent from task-evoked responses) can account for the variability in task performances and later observed behaviors.

In the topic 2, we analyzed time-varying FC patterns during an incidental encoding task, and found that dynamic reconfiguration of a large-scale functional brain network was associated with encoding performance. The periods of high encoding performance were characterized by greater network integration, mainly driven by inter-subnetwork integration between the subcortical, default mode, and visual networks. Our findings provide a better understanding of the neural mechanisms of memory encoding, highlighting the importance of orchestration across many distinct brain systems.

## LISTS OF PUBLICATIONS AND CONFERENCES

### 1. Peered review journals/Proceedings (2)

- 1.1 **R. Keerativittayayut**, R. Aoki, M. T. Sarabi, K. Jimura K. Nakahara, “Large-scale network integration in the human brain tracks temporal fluctuations in memory encoding performance”. eLIFE, under revision. This journal included in WOS, IF: 7.725, Q1.
- 1.2 **R. Keerativittayayut**, R. Aoki, M. T. Sarabi, and K. Nakahara, “Low frequency fluctuations and its functional connectivity before memory encoding predict subsequent memory performances”. Scientific Reports, preparing to submit. This journal included in WOS, IF: 4.259, Q1.

### 2. International conferences (5)

- 2.1 **R. Keerativittatayut**, R. Aoki, M. Taghizadeh, and K. Nakahara, “Dynamic integration of large-scale brain network predicts incidental memory encoding performance”, The Annual Meeting of Organization for Human Brain Mapping (OHBM 2018), Singapore. (Oral)
- 2.2 **R. Keerativittatayut**, R. Aoki, and K. Nakahara, “Dynamic functional connectivity during incidental memory encoding: a functional magnetic resonance imaging (fMRI) study”, The Society for Neuroscience's Annual Meeting (SFN 2017), Washington, D.C., USA. (Poster)

- 2.3 **R. Keerativittatayut**, R. Aoki, K. Nakahara, “Functionally coupled intrinsic fluctuations in fMRI signals predict subsequent memory performance”, OHBM 2017, Vancouver, Canada. (Poster)
- 2.4 **R. Keerativittatayut**, R. Aoki, M. Taghizadeh, and K. Nakahara, “Relationships between ongoing activity fluctuation in the medial temporal lobe and subsequent memory performance”, SFN 2016, San Diego, USA, November, 2016. (Poster)
- 2.5 R. Aoki, M. Taghizadeh, **R. Keerativittatayut**, K. Nakahara, “Measuring reward-related brain activations with multiband EPI”, The Japan Neuroscience Society international conference, Yagohama, Japan, July, 2016. (Poster)
- 2.6 M. Taghizadeh, R. Aoki, **R. Keerativittatayut**, and K. Nakahara, “Feasibility of multiband EPI for detection of brain activation in the reward system”, SFN 2016, San Diego, USA, November, 2016. (Poster)

### **3. Publications before enrolling Kochi University of Technology (1)**

**R. Keerativittatayut**, B Kaewkamnerdpong, J Laothamatas, O. Tritanon, and W. Sungkarat, “Dynamic causal model of fMRI images for early detection in people at risk of Alzheimer’s disease”, International Journal of Applied Biomedical Engineering, Vol.7, pp. 29-39, 2014.

### **4. International conferences before enrolling Kochi University of Technology**

4.1 **R. Keerativittatayut**, B. Kaewkamnerdpong, J. Laothamatas, and W. Sungkarat, Mirror neuron system study on elderly using dynamic causal modeling fMRI analysis,

International Conference on Bioinformatics and Biomedicine, Bali, Indonesia, October 2011 (Oral presentation)

- 4.2 **R. Keerativittayayut**, J. Laothamatas, T. Pulkes, P. Boonkongchuen, S. Tunlayadechanont, C. Prasartsakulchai, S. Pongpakdee, T. Supharatpayakorn, J. Praditsilpachote, and W. Sungkarat, Whole brain voxel wise study of iron deposits with MRI R2\* in Parkinson's disease, The 4th Asian and Oceanian Parkinson's and Movement Disorders Congress, Chonburi, Thailand, November 2014. (Oral presentation)
- 4.3 J. Laothamatas, T. Pulkes, J. Sirasarn, P. Boonkongchuen, S. Tunlayadechanont, C. Prasartsakulchai, S. Pongpakdee, **R. Keerativittayayut**, T. Supharatpayakorn, J. Praditsilpachote, and W. Sungkarat, "Diffusion tensor imaging of the brain in Parkinson's disease: a whole-brain voxel-wise approach", The 4th Asian and Oceanian Parkinson's and Movement Disorders Congress, Chonburi, Thailand, November 2014. (Poster)
- 4.4 W. Sungkarat, T. Pulkes, P. Boonkongchuen, S. Tunlayadechanont, C. Prasartsakulchai, S. Pongpakdee, **R. Keerativittayayut**, R., T. Supharatpayakorn, J. Praditsilpachote, and J. Laothamatas, "Functional MRI studies in Parkinson's Disease: complex motor and modified stroop tasks", the 4th Asian and Oceanian Parkinson's and Movement Disorders Congress, Chonburi, Thailand, November 2014. (Poster)
- 4.5 J. Laothamatas, O. Sangfai, A. Plitponkarnpim, P. Patputtipong, T. Sudsang, **R. Keerativittayayut**, T. Suparatpriyakon, and W. Sungkarat, "Diffusion tensor imaging of the brain in pediatric boxers: voxel-wise whole brain analyses, OHBM 2015, Hawaii, USA, June 2015, #1318. (Poster)

- 4.6 J. Laothamatas, M. Oonsivilai, A. Plitponkarnpim, P. Patputtipong, T. Sudsang, T. Suparatpriyakon, **R. Keerativittayayut**, J. Praditsilpachote, V. Sakulsaengprapha, and W. Sungkarat, “Whole brain voxel-wise study of iron deposits with MRI R2\* in pediatric boxers, OHBM 2015, Hawaii, USA, June 2015. (Poster)
- 4.7 W. Sungkarat, C. Madla, P. Cheecharoen, **R. Keerativittayayut**, T. Suparatpriyakon, A. Plitponkarnpim, and J. Laothamatas, “Memory and motor task fMRI changes in pediatric semi-professional boxers, OHBM 2015, Hawaii, USA. (Poster)

## **BIOGRAPHY**

**NAME:** Ruedeerat Keerativittayayut

**DATE OF BIRTH:** March 22<sup>th</sup>, 1988

**PLACE OF BIRTH:** Takuapa, Phang-nga, Thailand

**INSTITUTION ATTENDED:** 1. King Mongkut's University of Technology Thonburi,  
2009-2011, Master of Engineering in Biological  
Engineering (M.Eng.)  
2. Prince of Songkla University, 2005-2009, Bachelor of  
Engineering in Computer Engineering (B.Eng.)

**STUDY GRANT:** Special Scholarship Program (SSP) from Kochi University  
of Technology, Japan

**HOME ADDRESS** 13 moo 3, Kogkian, Takuapa, Phang-nga, Thailand 82110

**OFFICE ADDRESS** -

**E-MAIL** ruadeerat321@gmail.com